

# Optimization-driven set-based design for dynamic design requirements

Khalil Al Handawi

Doctor of Philosophy

Department of Mechanical Engineering

McGill University

Montreal, Quebec

December 2020

A thesis submitted to McGill University in partial fulfilment of the requirements of the  
degree of Doctor of Philosophy

© Khalil Al Handawi 2020

## **Dedication**

My effort, I dedicate to my sweet and loving  
*mother, father, and sister,*  
whose love, encouragement, and prays of day and night make me able to attain the  
highest and most honorable of professions.

## **Acknowledgements**

I would like to thank my supervisor, Prof. Michael Kokkolaras, for providing me with the opportunity and limitless freedom to innovate and pursue my research interests. He was an invaluable resource and mentor that has molded me into a professional and adept researcher and engineer. He always stressed the importance of quality research and responsible academic practices making them a part of my identity as a researcher. He made me realize my full potential and capabilities through his encouragement and vision. Thank you for being available even outside of office hours and providing me with access to knowledge and resources that is unprecedented in all my years of education.

I also wish to thank my committee members Prof. Damiano Pasini and Prof. Mathias Le-grand for their advice and guidance throughout my graduate studies at McGill University. I would like to express my most profound appreciation to my collaborators at Chalmers University of Technology at Gothenburg, Sweden for providing me with the resources and connections to contextualize my contributions and better bring them to the engineering design community. I wish to particularly thank Prof. Ola Isaksson and Dr. Massimo Panarotto for their constant guidance and suggestions for improving the relevance of my work to the industry in which it will be applied.

I am very grateful to GKN Aerospace, Engine Systems at Trollhättan, Sweden for giving me the opportunity to implement my work on challenging engineering applications. I wish to thank Dr. Petter Andersson for his steadfast support, advice, and guidance throughout my work.

I am grateful for the partial support of this work by grants NSERC CRDPJ 479630-15 X-243027 and CARIC CRDPJ479630-15 X-243067. I am also very grateful for the partial support of FRQNT through the *Bourses de doctorat en recherche* program (file 273486). I am grateful to the Faculty of Engineering at McGill University for its partial support through a McGill Engineering Doctoral Award.

To my mother Chaza, thank you for your persistent encouragement and support. Your belief in me and my abilities propels me ever further in my educational journey. To my father Bassam, thank you for everything you gave and taught me and for instilling a sense of curiosity and love for discovery and learning ever since I was a child by taking me to your chemistry lab. To my sister Marieh, thank you for your continuous steady support. Whenever I fall, I always find you by my side helping me to stand back up again. I would like to acknowledge my pet cat Daboos for his emotional support that meant a lot to me. I hope you are in a better place now.

I would like to show appreciation for my fellow graduate students at McGill for making this a memorable experience. We have forged lifelong friendships through the experiences we shared. Finally, I would like to thank my friend Dr. Ahmed Saleh Dalaq for being there for me since day one of this academic journey and showing me the ropes. Our intellectual discussions were truly eye-opening and have broadened my horizons.

## **Contributions to original knowledge**

The thesis presents a number of design methods for addressing uncertain and dynamic design requirements. They are listed as follows.

1. A set-based design framework for identifying sets of parametric optimal designs and scalable optimal designs.

The following were developed as part of this framework.

- (a) A surrogate-enabled parametric optimization method using rigorous derivative-free algorithms for obtaining parametric optimal designs.
- (b) A response surface method for performing post-optimality analysis on the parametric optimal designs and evaluating their scalability.
- (c) A quantitative scalability transition rule formulated in the parameter space.
- (d) A method for mapping scalable optimal designs from the parameter space to the design space using random sampling techniques.

2. A design margin quantification and allocation framework for addressing changing requirements throughout a product's lifecycle or development process.

The following were developed as part of this framework.

- (a) A method for computing reliability and excess of a particular design and requirement using Monte Carlo integration.
- (b) A method for generating different product development or lifecycle scenarios using Monte Carlo simulation and importance sampling.
- (c) A method for obtaining sets of optimal designs.
- (d) A set-based design method for obtaining flexible and robust sets of solutions.

- (e) A tradespace exploration strategy for visualizing and comparing flexible, robust, and optimal sets of solutions.

### **Contribution of Authors**

The author of this thesis is the sole contributor to the entire material of each chapter presented in this thesis; he has developed all of the ideas and their implementation under the guidance of his supervisor.

Some of the material presented in this thesis has appeared in conference and journal papers that include additional co-authors who contributed to discussion and exchange of ideas (during the author's summer visit stays at Chalmers University of Technology and collaboration with GKN Aerospace Engine Systems Sweden), review of manuscript drafts, and practical interpretation of case study results. None of the material presented in this thesis has been developed by any of these co-authors.

## **Abstract**

This thesis presents novel design methods for obtaining a set of design solutions to address design requirements that may change during the design process or over a system's lifetime. These methods aim at supporting design engineers quantitatively so they can make informed decisions in the early phases of product development when uncertainty is high. The applications used in this thesis demonstrate the efficacy of these methods and are centered around product remanufacturing by means of directed energy deposition, an additive manufacturing technique. Specifically, they aim at providing design solutions in the form of geometry of the deposit and the remanufacturing process parameters. The first method considers remanufacturing as a strategy to address changing requirements in optimal design problems. Sets of optimal design solutions, as opposed to single-point designs, are obtained using numerical optimization. The optimization objective is to maximize structural performance subject to design and process constraints. Since optimality and feasibility depend on varying design parameters, parametric studies are conducted to obtain optimal solutions for different parameter values. A response surface of the optimization solutions captures the effect of changing one or more parameters on the optimal solution and provides a method to map designs from the design space to the parameter space. A manufacturing transition rule is formulated in the parameter space to identify sets of design solutions that are scalable by additive manufacturing. The transition rule is based on the physical limitations of the manufacturing method. Scalable design solutions are mapped back to the design space to obtain the corresponding design variable values. This method draws inspiration from set-based design principles used to generate sets of

design solutions rather than converging to a single design solution early in the product development process. The first method focuses on making decisions using information that is available to the designer. Since product development involves several design iterations and stages, a second method for making decisions based on information from past iterations is presented in this thesis. It focuses on additive manufacturing problems where design requirements remain constant throughout a time interval referred to as an epoch and only change at discrete times in between epochs. This results in a series of design decisions that must be made at the end of each epoch referred to as a decision arc. This method considers selecting the best combination of design decisions from a set of discrete design choices. A combinatorial optimization problem is formulated to minimize the level of overdesign subject to reliability constraints. The reliability constraints are computed by evaluating the probability that a design will satisfy a design requirement given by a joint probability density function. Several design requirements are chained together and defined at the end of each epoch to form a requirement arc. Several requirement arc samples are generated using importance sampling. The optimization problem is solved for each requirement arc to obtain a set of corresponding decision arcs. This set of optimal decision arcs is compared against sets of robust and flexible design arcs. A tradespace is used to visualize the design sets and identify the relative degree of flexibility and robustness in the set of optimal decision arcs. The remanufacturing of a turbine rear structure, an aeroengine structural component is used to test the proposed methods. A stiffener is deposited on the outer casing of the turbine rear structure to increase its stiffness when subjected to thermal loads due to the exhaust gases. The first method is used to determine the sets of optimal and scalable stiffener designs by optimizing the geometry and laser power used

to deposit the stiffener. The second method is used to identify the set of optimal design arcs by chaining together several discrete stiffener designs to minimize the overall level of overdesign while maintaining a threshold reliability throughout the design process or the product's lifecycle. The two methods form a complete set-based design framework for addressing changing requirements in design problems featuring continuous and discrete design variables for instantaneous or progressive change in the design requirements.

## Résumé

Cette thèse présente de nouvelles méthodes de conception pour obtenir un ensemble de solutions de conception pour répondre aux exigences de conception qui peuvent changer au cours du processus de conception ou au cours de la durée de vie d'un système. Ces méthodes visent à aider les ingénieurs de conception quantitativement afin qu'ils puissent prendre des décisions éclairées dans les premières phases du développement de produits lorsque l'incertitude est élevée. Les applications utilisées dans cette thèse démontrent l'efficacité de ces méthodes et sont centrées sur la refabrication de produits au moyen d'un dépôt d'énergie dirigé, une technique de fabrication additive. Plus précisément, ils visent à fournir des solutions de conception sous la forme de la géométrie du gisement et des paramètres du processus de reconditionnement. La première méthode considère le reconditionnement comme une stratégie pour répondre aux exigences changeantes dans des problèmes de conception optimaux. Des ensembles de solutions de conception optimales, par opposition aux conceptions à un seul point, sont obtenus à l'aide de l'optimisation numérique. L'objectif d'optimisation est de maximiser les performances structurelles soumises aux contraintes de conception et de processus. Étant donné que l'optimalité et la faisabilité dépendent de paramètres de conception variables, des études paramétriques sont menées pour obtenir des solutions optimales pour différentes valeurs de paramètres. Une surface de réponse des solutions d'optimisation capture l'effet de la modification d'un ou plusieurs paramètres sur la solution optimale et fournit une méthode pour mapper des conceptions de l'espace de conception à l'espace de paramètres. Une règle de transition de fabrication est formulée dans l'espace des paramètres pour identifier des ensembles

de solutions de conception qui sont évolutives par fabrication additive. La règle de transition est basée sur les limites physiques de la méthode de fabrication. Les solutions de conception évolutives sont mappées vers l'espace de conception pour obtenir les valeurs des variables de conception correspondantes. Cette méthode s'inspire des principes de conception basés sur des ensembles utilisés pour générer des ensembles de solutions de conception plutôt que de converger vers une solution de conception unique au début du processus de développement du produit. La première méthodologie se concentre sur la prise de décisions en utilisant les informations dont dispose le concepteur. Étant donné que le développement de produits implique plusieurs itérations et étapes de conception, une deuxième méthodologie pour prendre des décisions basées sur les informations des itérations passées est introduite dans cette thèse. Il se concentre sur les problèmes de fabrication additive où les exigences de conception restent constantes tout au long d'un intervalle de temps appelé époque et ne changent qu'à des moments discrets entre les époques. Il en résulte une série de décisions de conception qui doivent être prises à la fin de chaque époque, appelées arc de décision. Cette méthodologie considère la sélection de la meilleure combinaison de décisions de conception à partir d'un ensemble de choix de conception discrets. Un problème d'optimisation combinatoire est formulé pour minimiser le niveau de sur-conception soumis à des contraintes de fiabilité. Les contraintes de fiabilité sont calculées en évaluant la probabilité qu'une conception satisfasse à une exigence de conception donnée par une fonction de densité de probabilité conjointe. Plusieurs exigences de conception sont enchaînées et définies à la fin de chaque époque pour former un arc d'exigences. Plusieurs échantillons d'arc d'exigence sont générés en utilisant un échantillonnage d'importance. Le problème d'optimisation combinatoire est résolu pour

chaque arc d'exigence pour obtenir un ensemble d'arcs de décision correspondants. Cet ensemble d'arcs de décision optimaux est comparé à des ensembles d'arcs de conception robustes et flexibles. Un espace commercial est utilisé pour visualiser les ensembles de conception et identifier le degré relatif de flexibilité et de robustesse dans l'ensemble des arcs de décision optimaux. La remise à neuf d'une structure arrière de turbine, un composant structurel de moteur d'avion est utilisé pour tester les méthodes proposées. Un raidisseur est déposé sur le carter extérieur de la structure arrière de la turbine pour augmenter sa rigidité lorsqu'elle est soumise à des charges thermiques dues aux gaz d'échappement. La première méthode est utilisée pour déterminer les ensembles de conceptions de raidisseurs optimales et évolutives en optimisant la géométrie et la puissance laser utilisées pour déposer le raidisseur. La deuxième méthode est utilisée pour identifier l'ensemble des arcs de conception optimaux en enchaînant plusieurs conceptions de raidisseurs discrets pour minimiser le niveau global de sur-conception tout en maintenant un seuil de fiabilité tout au long du processus de conception ou du cycle de vie du produit. Les deux méthodes forment un cadre de conception complet basé sur un ensemble pour répondre aux exigences changeantes dans les problèmes de conception comportant des variables de conception continues et discrètes pour un changement instantané ou progressif des exigences de conception.

## Table of Contents

Dedication . . . . .	ii
Acknowledgements . . . . .	iii
Contributions to original knowledge . . . . .	v
Abstract . . . . .	vii
Résumé . . . . .	x
List of Tables . . . . .	xvi
List of Figures . . . . .	xviii
1 Introduction . . . . .	1
1.1 Motivation . . . . .	3
1.1.1 Circular economy and product recovery . . . . .	3
1.1.2 Designing for changing requirements . . . . .	4
1.1.3 A thought experiment . . . . .	5
1.2 Objectives . . . . .	8
1.3 Outline . . . . .	10
2 Background . . . . .	12
2.1 Product design for remanufacturing . . . . .	12
2.2 Quantifying changeability in product design . . . . .	14
2.3 The use of design margins for managing uncertain requirements . . . . .	23
2.4 Set-based design principles and applications . . . . .	28
2.5 The use of tradespace exploration for quantifying design margins and flexibility . . . . .	35
2.6 Research gaps and opportunities . . . . .	36
2.7 Optimization algorithms for model-based design optimization . . . . .	40

3	Thermomechanical models for product remanufacturing of a turbine rear structure . . . . .	44
3.1	Thermomechanical modeling . . . . .	45
3.2	Load cases applied to turbine rear structure . . . . .	50
3.2.1	Pressure load case . . . . .	51
3.2.2	Thermal load case . . . . .	51
3.2.3	Low-cycle fatigue analysis . . . . .	53
3.3	Summary . . . . .	54
4	Scalable set based design optimization . . . . .	56
4.1	Method . . . . .	56
4.1.1	Surrogate modeling . . . . .	57
4.1.2	Parametric optimal designs . . . . .	58
4.1.3	Reduction to set of scalable optimal designs . . . . .	62
4.1.4	Numerical example for determining the scalable design set . . . . .	68
4.2	Application example: aeroengine component remanufacturing . . . . .	70
4.2.1	Problem formulation . . . . .	72
4.2.2	Parametric optimal design results . . . . .	72
4.2.3	Scalable optimal design results . . . . .	74
4.2.4	Design set variability and comparison . . . . .	77
4.3	Computational cost . . . . .	79
4.4	Summary . . . . .	80
5	Design margin quantification and optimization . . . . .	83
5.1	Method . . . . .	84
5.1.1	Relevant design metrics . . . . .	84
5.1.2	Epoch-era analysis for product redesign . . . . .	89
5.1.3	Set-based design to mitigate changing requirements . . . . .	95
5.1.4	Tradespace exploration for comparing solution sets . . . . .	102
5.2	Application . . . . .	102
5.2.1	Stiffener deposition on turbine rear structure (TRS) outercasing . . . . .	102
5.2.2	Loadcase description . . . . .	104
5.2.3	Loadcase requirements . . . . .	105
5.3	Results and discussion . . . . .	107
5.3.1	Example for calculating the design properties of a given design arc . . . . .	108
5.3.2	Combinatorial optimization with respect to a requirement arc . . . . .	111

5.3.3	Set-based design and tradespace exploration . . . . .	112
5.4	Computational cost . . . . .	121
5.5	Summary . . . . .	123
6	Managing uncertain requirements by means of stochastic optimization . . . . .	125
6.1	Method . . . . .	125
6.2	Example . . . . .	126
6.2.1	Monte Carlo simulation of stochastic objective function . . . . .	128
6.2.2	StoMADS results for stochastic optimization problem . . . . .	128
6.3	Summary . . . . .	132
7	Conclusions . . . . .	134
7.1	Recommendations for future work . . . . .	136
	Bibliography . . . . .	138

## List of Tables

<u>Table</u>		<u>page</u>
2–1	Summary of changeability aspects considered in the literature . . . . .	23
2–2	Summary of design margin aspects considered in the literature . . . . .	27
2–3	Summary of set-based approaches considered in the literature . . . . .	35
3–1	Comparison of transient and static models: parameter values . . . . .	49
3–2	Relevant model inputs . . . . .	54
3–3	Relevant model outputs . . . . .	55
4–1	Design variables $\mathbf{x}$ . . . . .	71
4–2	Design parameters $\mathbf{p}$ . . . . .	72
4–3	Sample optimization problem results . . . . .	74
4–4	Design space comparison results . . . . .	78
4–5	Breakdown of total computational cost . . . . .	80
5–1	Example sets, parameters, and constants . . . . .	108
5–2	Results obtained for example design arcs . . . . .	109
5–3	Requirement arc $\mathbf{R}_w$ . . . . .	111
5–4	Results obtained for example decision arcs . . . . .	113
5–5	Set-based solution comparison . . . . .	116
5–6	Top performing design arcs in $S_E$ . . . . .	119
5–7	Top performing design arcs in $S_W$ . . . . .	120
5–8	Breakdown of total computational cost for obtaining surrogate models . . .	122

5–9 Breakdown of total computational cost for Chapter 5 algorithms . . . . .	123
6–1 Design variables $\mathbf{x}$ . . . . .	127
6–2 Relevant model parameters and constants . . . . .	127
6–3 turbine rear structure (TRS) optimization problem results . . . . .	131

## List of Figures

<u>Figure</u>		
1–1 Example product development project showcasing different decision arcs . . . . .	7	
3–1 TRS stiffener example . . . . .	45	
3–2 Heat conduction for a moving Gaussian heat source . . . . .	46	
3–3 Deposition load . . . . .	48	
3–4 Spatial distribution of principle residual stresses along the circumference of the turbine rear structure (TRS) obtained using transient and static models . . . . .	50	
3–5 turbine rear structure (TRS) pressure load case . . . . .	51	
3–6 turbine rear structure (TRS) thermal load case . . . . .	52	
3–7 Modified Goodman criterion . . . . .	53	
4–1 Isocontours of the response surface $x_1^*(\mathbf{p})$ and transition rule $\mathbf{N} \mathbf{J}^T(\mathbf{p}) \mathbf{M} \geq \mathbf{0}$ in a two-dimensional parameter space . . . . .	66	
4–2 Effect of number of training points and kernel bandwidth on order-based error . . . . .	68	
4–3 Approximation of scalable set using kernel smoothing (KS) with non-scalable regions of the parameter space hatched . . . . .	68	
4–4 Set-based design space reduction method . . . . .	71	
4–5 Three sample parametric optimal designs; $x_0$ denotes the baseline design . . . . .	73	
4–6 Projections of the optimal width design variable $\hat{x}_3^*$ with non-scalable regions of the parameter space hatched . . . . .	75	
4–7 Effect of number of training points and kernel bandwidth on order-based error . . . . .	75	

4–8 Safety factor in the feasible design space as a function of design variables for different monotonicity vectors . . . . .	76
5–1 Contours of feasibility constraint $g_{f1}(\mathbf{p})$ in the two-dimensional parameter space for uniform (left) and Gaussian (right) probability density functions (PDFs) . . . . .	87
5–2 Buffer and excess relative to a feasibility constraint $g_{f1}(\mathbf{p})$ in the two-dimensional parameter space for uniform (left) and Gaussian (right) probability density functions (PDFs) . . . . .	88
5–3 Contours of feasibility constraint $g_{f1}(\mathbf{p})$ in the 2 dimensional parameter space for different types of requirement probability density functions (PDFs) . . . . .	95
5–4 Flowdiagram of method for generating set-based solutions . . . . .	101
5–5 Illustration of possible concepts and redesign choices for turbine rear structure (TRS) stiffener . . . . .	104
5–6 2D projections of isocontours of safety factor in the parameter space . . . . .	110
5–7 Visualization of decision arcs . . . . .	112
5–8 Distribution of design arcs in optimization driven set-based solutions . . . . .	114
5–9 Distribution of design arcs in set-based solutions . . . . .	114
5–10 Tradespace of set-based design arcs . . . . .	115
5–11 Reduced tradespace of solutions in sets $S_E$ and $S_W$ . . . . .	117
5–12 Distribution of concepts in sets $S_E$ and $S_W$ . . . . .	118
5–13 Distribution of first deposit $D_1$ when concept $c = 1$ is selected in sets $S_E$ and $S_W$ . . . . .	121
6–1 Monte Carlo simulation of $\hat{f}_{\mathbf{P}}(\mathbf{x})$ using 1000 samples . . . . .	130
6–2 Monte Carlo simulation results of StoMADS–PB and NOMAD solutions . . . . .	131

## **Chapter 1**

### **Introduction**

The development of engineering systems relies on the definition and communication of design requirements from stakeholders to original equipment manufacturers (OEMs), who then define and communicate design requirements to suppliers of components. In this context, design requirements specify what the components shall achieve to provide value to stakeholders once integrated as part of a system [1]. While requirements are supposed to be clear and well-defined, they are subject to changes during a product development project [2].

In the aerospace industry, requirement changes can occur for a variety of reasons [3, 4]. For example, the temperature loads a structural component must sustain in operation may change during product development due to a shift in the engine architecture specified by the engine OEM. Furthermore, requirements may change during the in-service phase due to changes in the market or in the legislation that governs the industry. There is an inherent uncertainty in design requirements at the beginning of a product development project, which reduces when the project advances and decisions are made. At the beginning of product development, where the innovation potential is high, such uncertainty can be very large [5]. In the early phases, design requirements are usually communicated through ranges, and the final requirement (e.g., temperature load) may lie anywhere within a range (in some cases, even outside).

If the product's specifications fall short of the requirements during development or product lifecycle, an upgrade to the specifications is warranted to maintain functionality. This may involve a complete redesign of the product depending on the severity of the required changes. Complete redesign involves discarding the current iteration of the product and starting a new development cycle with the changed requirements as inputs. This cradle-to-grave approach is extremely inefficient when considering a circular economy (CE) where value is generated from each unit of resource by recovering and regenerating products and materials at the end of each service life [6]. In order to increase the recoverability of the product, and avoid loss in value due to disposal, products should be designed for such activities in order to increase their relevance in a CE and extract as much value from them as possible. Recovering a product involves returning its specifications to its pre-disposal levels. However, requirements are seldom the same after a product's lifecycle has run its course. As a result, the product's specifications have to be upgraded to meet the set of requirements expected of current generation products. Designing products for such unforeseeable requirements is the main subject of this thesis.

This thesis utilizes numerical methods for addressing the problem of designing products for remanufacturing activities where requirements are expected to be highly dynamic. In this chapter, Section 1.1 provides motivation for implementing the design paradigms introduced in this thesis to mitigate the challenges that arise due to changing product requirements. The research objectives of this thesis are then discussed in the context of product remanufacturing design problems. The chapter concludes by outlining the remainder of the thesis in Section 1.3.

## 1.1 Motivation

The increasing environmental impact of industrial activities is changing the perception of legislators and business enterprises towards the importance of recovering value from products that have reached the end of their useful lifecycles, especially if this end is brought about by an unforeseen change in requirements or specifications. As a result, a new paradigm for product design has become increasingly relevant in modern economies.

### 1.1.1 Circular economy and product recovery

A CE can be used to return products that have reached the end of their useful lifecycles into service and extract as much value from them as possible. CE helps achieve both economic growth and environmental protection. Since resources are limited, legislation has been put forth so that business enterprises bear responsibility for the environmental, social and economic impacts their products have on society [7]. This caused business enterprises to adopt sustainable development practices when designing their products.

A closed-loop supply chain (CLSC) can return used or discarded products to working condition. This enables sustainable development by reducing the environmental impact of products [8]. A CLSC includes a forward supply chain where products are used normally until the end of their life and a reverse supply chain that returns the discarded products to a previous stage in its lifecycle. Examples of recovery activities in a reverse supply chain include remanufacturing, reuse, and recycling [9, 10]. Since CE encompasses products as well as their forward and reverse supply chains, businesses must design their products for closed-loop product recovery activities [9]. This includes design for remanufacturing, recycling, and reuse. In this thesis, we focus on remanufacturing since it is more sustainable than recycling and recovers more value across the supply chain due to increased

virgin material substitution and retention of the embodied energy used to manufacture the original product from the raw materials [10, 11].

There is a number of studies that consider product design for remanufacturing [12, 13]. However, the majority focus on closed-loop supply chain logistics of remanufacturing [14–18]. Product remanufacturing design problems are more challenging to address due to the variable design requirements encountered during product design. Studies that focus on remanufacturing design are reviewed in Section 2.1.

Design for remanufacturing rules found in the literature specify that a product's components should allow room for modifications to meet design requirements [19]. Furthermore, it is important to distinguish refurbishment from remanufacturing: the former is used to satisfy original specifications, whereas the latter allows for considering changed requirements. As a result, products should be designed for changing requirements to enable product recovery by remanufacturing.

### 1.1.2 Designing for changing requirements

Design requirements are subject to change during a product's lifecycle [11, 20–22]. Variable parameters such as customer requirements and loading conditions influence design requirements such as cost and product life requirements [23] and can be unpredictable despite the best efforts of forecasters and analysts [24].

Design *changeability* enables designs to change through a number of change mechanisms whose aspects can include flexibility, agility, robustness, and adaptability. A number of basic and extended principles have been identified as enablers of design changeability [23]. In this thesis we focus on two aspects of changeability, flexibility and robustness

in product design for accommodating uncertain requirements. Advances in incorporating design changeability in product design are reviewed in Section 2.2.

The first contribution of this thesis provides a rigorous formulation for flexibility in terms of *scalability*. Scalability is an aspect of flexibility which is defined in the literature and expanded upon in Section 2.2. Scalability is highly relevant to remanufacturing design problems as will be explained in Chapter 2. Decisions regarding the scalability of a remanufacturing design are made based on current information that is available to the designer. The issue of designing a product based on the current state of the product and its corresponding requirements has been addressed by Alhandawi et al. [25].

However, requirements change over the course of a product development project or lifecycle. A decision-making tool based on past and current information is required [26]. The second contribution of this thesis formulates and quantifies design flexibility and robustness over the course of a remanufacturing design process. Decisions about the desired amount of flexibility and robustness are made based on current and past information from the design process or the product lifecycle.

The motivation for such a decision-making tool stems from conventional design practices with regards to changing requirements. We use a thought experiment to provide motivation for the research presented in this thesis.

### 1.1.3 A thought experiment

Manufacturers introduce substantial design margins in the early phases to cope with changes in requirements. Design margins accommodate changing requirements by providing a buffer before any change to the product is required. For example, consider a book shelf designed to sustain 90 N of load instead of the required 50 N to accommodate future

changes in the operative load [26]. This strategy may result in overdesign if the 90 N load is never realized, which negatively impacts performance (e.g., through increased weight) [27, 5].

An alternative approach is to design a component based on a preliminary requirement (aiming for minimal capability) and to modify it when higher requirements arise. In the previous example, this is the equivalent of designing the shelf to sustain 50 N, and modify the shelf for a 90 N load requirement should it arise. This alternative can be made possible using additive manufacturing (AM), which enables geometry modification on existing components through material deposition [19, 12, 15]. However, this strategy has drawbacks. If the changes in requirements are too many or unforeseen, the cost of such modifications could overcome the cost of overdesigning the product.

We show an example of our own that is inspired by the industry to illustrate these challenges. A turbine rear structure (TRS) is a static aeroengine structural component that must sustain temperature loads as a result of the hot engine exhaust gases. These temperature loads can change during the design or in-service phases as is shown in Figure 1–1.

These changes are represented by the red line, hereafter defined as the requirement arc. The temperature requirement is assumed to change five times as a result of critical design reviews [28] and negotiations between the OEM and the manufacturer of the TRS. These five points are referred to as *epochs*, to resonate with tradespace exploration literature [29].

The manufacturer uses AM to cope with this requirement change in the above example. In particular, the manufacturer starts working on two different designs, A and B (hereafter defined as decision arcs). With AM, the geometry of the TRS can be initially

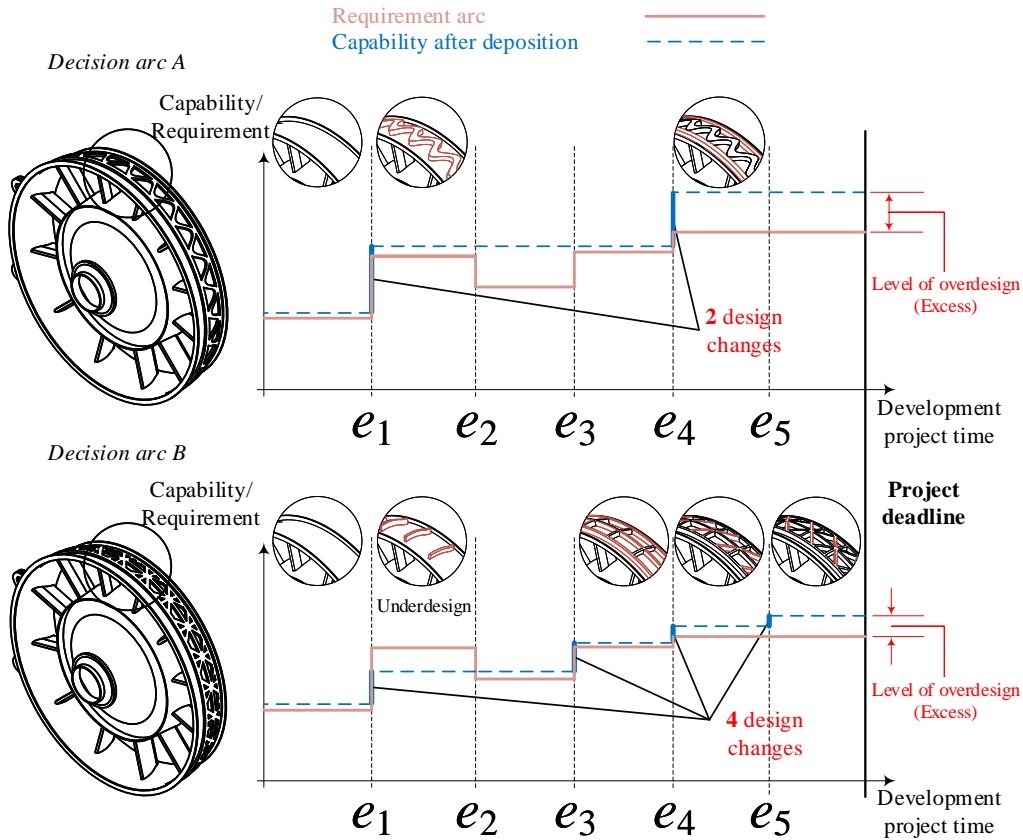


Figure 1–1: Example product development project showcasing different decision arcs

designed to meet the lower bound of the temperature range, while depositing a stiffener on the structure as the temperature requirement changes (first epoch). However, the decisions made during the design of the stiffener's geometry may impact the capability of coping with changes without resulting in overdesign.

For instance, choosing the geometry of the deposition as decision arc A (wavy design concept) will allow for a design with a capability that fulfills the new requirement at the second epoch. However, further changes of this geometry (such as the one made at epoch 5) do not allow for close tracking of the requirement arc, resulting in overdesign (blue line).

On the other hand, decision arc B (hatched design concept) allows for better tracking of the requirement arc. This reduces the risk for overdesign at the end of the process. However, this comes with the cost and effort of performing more depositions during the course of the development (4 instead of 2), outweighing the benefits given by this more *flexible* decision arc. There is a trade-off between the flexibility that can be enabled by AM deposition and other attributes of the design (such as weight and manufacturing costs).

This example draws inspiration from the contrast in longevity observed in the B-52 stratofortress bomber when compared to the F/A-18 hornet. The B-52 enjoyed a longer service cycle and was able to cope with the needed modifications due to technological advancements as opposed to the F/A-18 hornet. This was due to the embedded design margins (in the form of excess) during initial production of the B-52. The F/A-18 hornet had more *modularity* (a form of design changeability) to counteract the reduced margins that were available for upgrade. However, the F/A-18 still suffered greatly once the margins were consumed during its service life requiring a complete redesign [27]. This case study underscores the necessity for quantifying and strategically allocating design margins and changeability in product design.

We aim to address the shortcomings of either design strategy that were identified in this thought experiment. We formulate the thesis objectives accordingly.

## **1.2 Objectives**

The goal of this thesis is to develop several design frameworks for managing changing design requirements during the product development process or throughout its lifecycle.

The frameworks developed in this thesis follow the principles of set-based design (SBD) by providing a set of feasible design solutions in order to leverage the added design changeability from our frameworks.

Feasibility is assessed using engineering models which can be computationally intensive. Specifically, remanufacturing design problems involving AM feature thermomechanical models with coupled thermal and structural analyses of the deposition process. These thermomechanical models are developed for the TRS described earlier as it will be used as a remanufacturing design problem to demonstrate our methods. The thermomechanical models are evaluated prior to assessing the feasibility of the design in terms of its structural performance. In order to navigate the design space with relative ease in search of the solution sets respective of each framework, a surrogate model is obtained by training a response surface model with data obtained from the thermomechanical/engineering model.

Decisions are rendered in each framework using rigorous derivative-free optimization algorithms. This is due to the non-smooth response that can be exhibited by the thermomechanical/engineering models and their surrogates.

The first framework provides decisions about the design variables in order to maintain scalability in the set of design solutions given current information about the state of the design problem. Parametric design optimization is used to assess feasibility while maximizing structural performance to obtain a set of parametric optimal designs in the design space. A response surface of the optimization solutions with respect to the parameters governing the design requirements is constructed in the parameter space. A scalability

constraint based on the manufacturing process used is formulated in the parameter space and used to identify scalable design solutions that can be mapped back to the design space.

The second design framework provides decisions regarding design variables such that overdesign (excess) is minimized throughout the different stages of the development process or the product lifecycle while maintaining a threshold reliability level with respect to uncertain requirements. Monte Carlo integration is used at each stage where decisions are made to quantify the reliability (probability of satisfying a requirement governed by a joint probability density function) and excess. Additionally, metrics for quantifying flexibility and *robustness* are developed as part of this framework. Monte Carlo simulation is used to generate and chain together different requirements. Corresponding design decisions are obtained by solving a combinatorial optimization problem. This results in sets of optimal, flexible, and robust design solutions. The effect of minimizing excess on robustness and flexibility is investigated via tradespace exploration.

The objectives are summarized as follows.

- Develop a framework for identifying design solutions that have the greatest potential for remanufacturing.
- Strategically quantify and allocate the aspects of design flexibility and robustness to address changing requirements during remanufacturing.
- Provide a sufficiently diverse set of equally reamnufacturable solutions to provide designers with alternatives after committing to a particular solution.

### **1.3 Outline**

The thesis is organized through the following chapters. Chapter 2 presents a detailed literature review of the main aspects featured in our contributions. We review literature

related to remanufacturing design, design changeability, design margins, SBD, and tradespace exploration. Chapter 3 presents the thermomechanical models used to model the AM remanufacturing process of a TRS used in both frameworks as described in subsequent chapters. Chapter 4 describes a SBD framework for identifying scalable optimal designs during an instant in the product development process or lifecycle. An example based on the remanufacturing of a TRS subject to varying requirements and loads is used to demonstrate the framework. Chapter 5 presents a framework for minimizing design excess throughout the product development process or lifecycle while maintaining a threshold reliability given uncertain requirements. The TRS example used for demonstrating this framework is modified to feature multiple epochs at which design decisions must be made. SBD results are obtained using the described framework for minimizing excess and are compared against flexible and robust design sets using tradespace exploration. Chapter 6 discusses the application of stochastic optimization algorithms for providing sets of design solutions when requirements are uncertain. Based on the results of stochastic optimization, recommendations for improving the frameworks in Chapters 4 and 5 are made. The conclusion and thesis contributions are presented in Chapter 7.

## Chapter 2 Background

In this chapter, Section 2.1 reviews remanufacturing design problems to identify the key enablers of this product recovery route. Section 2.2 introduces changeable design principles which are necessary to enable remanufacturing design. Section 2.3 introduces metrics for quantifying the level of overdesign in a product which is impacted by the amount of embedded changeability in a product. Section 2.4 discusses advances in SBD for providing sets of design solutions to leverage the added product changeability. Section 2.5 introduces a useful design space exploration tool for visualizing and comparing sets of design solutions throughout a product's lifecycle or development process.

### 2.1 Product design for remanufacturing

The effectiveness of AM for remanufacturing end-of-life (EoL) components is reported by [Van-Thao et al.](#) and [Wilson et al.](#) [16, 30]. They consider replacement strategies and EoL decisions regarding reuse, recycling or remanufacturing. However, there are some notable studies that have introduced remanufacturing considerations into component design.

Level set topology optimization was used by [Liu and Ma](#) to optimize a structural component considering subtractive remanufacturing [13]. A containment constraint is formulated and used to ensure that a remanufactured design is contained within the material

domain of the parent design. This method yields designs that can be scaled down by remanufacturing. However, it does not consider the reverse operation of remanufacturing by additive methods. Furthermore, variable loading requirements are not considered.

Environmental impact was considered as an optimization objective for a topology optimization problem of a structural component [31]. Additive manufacturing was accommodated by incorporating life cycle analysis (LCA) considerations into the design problem. Although this is not a remanufacturing study, the ability of AM to enable remanufacturing is underlined.

An important feature of a product's lifecycle is upgrade, defined as an improvement at the specifications level [32]. The upgrade levels for remanufacturing of a product are usually predetermined and are not adjusted based on required specifications at the EoL. Based on this, a strategy for determining the optimal market position in terms of pricing and remanufacturing costs can be developed [33]. **Kwak and Kim** address the major activities of remanufacturing which include product takeback (the process of collecting EoL products for the activity of remanufacturing, modeled using several scenarios where the remanufacturer either passively accepts all EoL products or selectively purchases them), remanufacturing operations, and remarketing [33]. Decisions are then made regarding the reusability of the EoL product's components. The target specifications for components in need of an upgrade are optimized to maximize revenue from resale of the remanufactured product. The upgrade levels for remanufacturing are captured using generational differences defined as the amount of discrepancy between the current component's specifications and those of components in recent cutting edge products.

The previous study describes the importance of designing remanufactured products for variable markets and requirements. There are additional sources of uncertainty in remanufacturing design problems due to the condition of the recovered product prior to remanufacturing and the specification levels its components should meet in order to function within the product system.

Prior research suggests that successful remanufacturing requires a product's components to be designed for variable requirements to maximize environmental benefits. The main principle governing the ease of upgrading component specifications involves design changeability [34]. As a result, a review of changeable design practices is warranted.

## **2.2 Quantifying changeability in product design**

Design changeability is defined as the ability of a system to undergo specified classes of changes with relative ease and efficiency. A design change is effected when the cost of the change is below a specified threshold. This definition was used by Lawand et al. to make decisions regarding different end-of-life scenarios [35]. However, cost is not the only factor that governs the changeability of a component.

Design changeability addresses the challenges of modern product development which include dynamic marketplaces, rapid technological evolution, and changing operating environments. Design flexibility and robustness are two aspects of design changeability that directly address these challenges.

A product and its operating environment undergo change during design and operation in order to stay relevant in dynamic markets. Change events are characterized by three elements: i) the agent of change, ii) the mechanism of change, and iii) the effect of change.

The change agent is the instigator for change in the product and is specified in the form of product requirements. The nature of the change agent helps identify the type of change the system must undergo. If the change is external to the product system (e.g., environmental operational conditions) then the change is of a flexible type. If the change agent is internal to the system (e.g., sizing and tolerance requirements) then it is of an *adaptable* type.

The change effect is the difference between the states of a product before and after the change. Based on the nature of change effects, three more changeability aspects are defined. Robustness is defined as the insensitivity of the design to internal or external change (e.g., stability of a vehicle despite changes in road conditions and grade). Scalability is the ability of the design to change to meet a different level of a specification (e.g., reinforce a structural member to carry a larger load than originally intended). *Modifiability* is the ability of the design to change in order to accommodate unforeseen requirements not native to the original design (e.g., ability of a cargo plane to be repurposed for reconnaissance missions) [36]. This term is also referred to as *evolvability* in the literature [37].

A system may undergo some or all types of change. Several works in the literature have attempted to quantify and capture the changeability of a product system for embedding this principle in product design.

**Tackett et al.** use the product system's capability of meeting design requirements to quantify the available excess capacity for evolving [37]. Based on the excess available in a product, an evolvability metric based on the principle of stored elastic energy in a system

is computed. The evolvability metric is a relative metric that is useful for comparative design studies.

Other studies focus on quantifying flexibility as a result of predictable and unpredictable changes in the operating environment [38, 39]. In one study, the tradeoff between various requirements (referred to as design objectives and performances) is captured by a Pareto set. Movement along the shortest path from one end of the Pareto set to the other is penalized by a change cost. Flexible designs are identified as a ranged set between the extremes of the Pareto set such that the overall change costs are minimized [38].

The notion of flexible ranged sets is also investigated by other researchers [39]. Candidate target sets of solutions that maximize a flexibility metric over the set are identified in the design space by mapping flexible designs identified in the requirements space. The design and requirements spaces are defined as the set of possible values the design variables or requirements can assume respectively. The process begins by producing a number of design alternatives through probing the design space. The design alternatives are mapped on the requirements space (referred to as the attribute space). Design alternatives are partitioned into ranged sets in the requirements space. A flexibility metric for each set is calculated by integration of an influence function over the set. Sets that maximize flexibility are preferred as possible design solutions.

Suh et al. considered modularity of product platforms as a means for achieving changeability [34]. Requirement bandwidths (referred to as product attributes) are computed based on the market conditions for the product platform. Optimization is used to position product platforms in the market (similar to Kwak and Kim [33]) and compute design bandwidths. Monte Carlo simulation is used to evaluate the effect of uncertainty in the

market on the net present value of the product platform. The sensitivity of flexible and inflexible product platforms to uncertainty is compared via the expected net present value. In this study, only predetermined product variants are considered as part of the product platform. As explained earlier, in a remanufacturing context it is important to adjust the upgrade levels of the product based on changes in the requirements [33].

A quantification of flexibility is shown to be the filtered outdegree of a design within a networked tradespace [36]. A tradespace is a design exploration tool that assesses the tradeoff between utility of a given design and its associated costs. The utility and cost functions are defined based on the designer's preferences and experience.

In addition to defining metrics for design capability and capacity, Rehn et al. use the filtered outdegree to quantify the flexibility of enumerated designs in the tradespace [40]. The tradeoff between a multi-attribute utility function containing capability, capacity, operability, and flexibility and the acquisition cost is quantified by generating Pareto-optimal designs. The change path taken between several design instantiations is referred to as an arc and governs the rules regarding changeability between different designs [40, 41, 36, 42]. Rehn et al. count the number of end-states when quantifying the filtered outdegree [40].

More advanced representations of the filtered outdegree are defined and used in the literature. Viscito and Ross use the value weighted filtered outdegree as a proxy for quantifying flexibility [41]. This metric captures the utility difference between an originating design and its possible destination designs such that the best flexible designs that generate an increase in utility during transition are considered during tradespace exploration.

In other studies, flexibility is defined as the ability of a system to be modified to do its basic job or jobs not originally included in the definition of the system's requirements in changing environments. This can be conceptualized as actively minimizing the set of infeasible designs across different requirement scenarios [43]. Although this may be confused with other aspects of design changeability such as adaptability, the main commonality with the filtered outdegree definition is the ability of a design to be modified.

Other studies look at flexibility from a cost of change perspective which is important to realize the needed design changes. Rapp et al. quantify design flexibility in terms of development and integration costs associated with adding a subsystem option to a set of design solutions [42].

Cardin et al. explore alternative flexible design scenarios by solving a multistage stochastic programming problem to minimize a cost function [44]. The authors solve a waste-to-energy system design problem to determine the appropriate upgrade capacities and times. The cost function for flexibility is formulated in terms of net present value of the system in previous work [45]. Several waste demand (requirements) scenarios are generated via Monte Carlo simulation. The average profit of all the scenarios for a given system design (upgrade levels and times) is maximized subject to a number of constraints. The most important constraint governing the behavior of the decision maker is the nonanticipativity constraint. It implies that decisions made up to a certain time period during the lifecycle are made solely based on previous and current knowledge of the system demands (requirements). This approach simulates a realistic design problem that progresses over the course of a product's lifecycle. Furthermore, a set of solutions can be obtained simply

by minimizing the cost function of each Monte Carlo sample to obtain a corresponding solution.

Flexibility can be considered in both the design and requirements spaces [46]. When reviewing the available literature, it appears that quantifying changeability is performed largely in the requirements space rather than the design space and a method for mapping between the two spaces is required to identify the most flexible designs [37–39, 47]. Furthermore, when considering changeability due to changes in the operating environment and the product, it is important to consider a set of solutions that are changeable in order to leverage the added flexibility of the design solutions [38, 39, 34]. A single point design that is flexible would not be justified if no alternatives are offered. Finally, among the mentioned aspects of changeability, scalability appears to be of relevance to remanufacturing since it involves upgrading the specifications of a product’s components to achieve the required change. As a result, we will focus on set-based design principles while considering a metric for identifying scalable solution sets for remanufacturing purposes in Chapter 4.

Another important aspect of design changeability is robustness. Robustness characterizes a product’s ability to be insensitive towards changing operational environments without the need for change or modification in contrast to flexibility. In the literature, robustness is usually associated with resilience, survivability, adaptability, and reliability depending on the design application being considered.

For example, military products tend to incorporate resilience into their designs. Resilience has been defined as the capacity to cope with unanticipated dangers after they have become manifest; having the generic ability to cope with unforeseen challenges such as

compromised performance during missions or changes to the mission objectives (requirements). This is an example where a resilient design can cope with changing operating environments and requirements [43, 48]. On the other hand, a robust design addresses changing requirements only [43].

Survivability is used in the literature and draws a lot of parallels with the definition of resilience. It defines the ability of the design to cope with changing requirements (referred to as needs) and operational environments (referred to as operating context) [29].

Resilience is not explicitly defined by [Rehn et al.](#) but appears to be a measure of the ability of a set-based solution to accommodate variabilities in the requirements [40].

Reliability is defined in terms of the probability that the system will operate within or above the failure threshold for a nominal-is-better and a less-is-better objective function respectively [43].

Adaptability differs from robustness and resilience in the sense that the design modifies itself whilst in operation to accomplish its function in changing environments [43]. An example of this would be active spoilers on sports vehicles that dynamically adjust while the vehicle is in operation based on conditions presented.

[Mcmanus et al.](#) attempted to quantify robustness [29]. In this study, changing needs and contexts are represented as discrete time periods, called epochs, during which the context and needs are stable. The tradespace for each epoch differs as the utility and cost of designs changes with changing requirements. Robustness is related to maintaining performance (capability) given changing operational environments (referred to as context) and requirements (referred to as needs). Value robustness is a special type of robustness

related to value delivery which is the ability of the design to maintain Pareto efficiency on the tradespace across epochs.

Another study has quantified resilience and some of its aspects including survivability using a probability tree [48]. E.g., the reliability of an unmanned aerial vehicle is calculated by multiplying the reliability of the system during the mission with the probability that the system is available (availability). This is a measure of the ability of the system to perform reliably provided that the system is available to perform during the mission. The probability value for each resilience metric is computed based on design decisions and mission requirements. Monte Carlo simulation is used to investigate model uncertainty. Parameter uncertainty is then investigated in the tradespace by randomly sampling different parameter samples that drive the requirements and performances from a normal distribution [48].

Chen et al. introduce the concept of capability indices for use in robust design optimization [49]. Design requirements are modeled using ranged sets while system performances are assumed to follow a uniform or normal distribution when subjected to noise variables (referred to as changing parameters in this thesis). The probability that the system performance will satisfy the required range is computed as the capability index and is the subject of a multi-objective optimization problem. A capability index of unity implies that the system's performance satisfies the requirement by a probability of 99.7%. Any value greater than or equal to unity is considered satisfactory.

In summary, design flexibility is associated with the ease of modifying the design to meet changing requirements outside the operational context. Robustness is associated with

passively accommodating changing requirements outside the operational context. Resilience is an umbrella term for robustness and adaptability and describes the ability of the design to passively or actively cope with changing requirements and operational contexts. In this thesis, we will focus on quantifying and designing for flexibility and robustness as we are concerned with changes to requirements both during the product development cycle and its operational lifetime.

Since flexibility is usually defined in the tradespace via the filtered outdegree, we review some tradespace exploration studies in the context of flexible design in Section 2.5. In order to check robustness, the probability of meeting a requirement can be used to impose reliability constraints on the design solution under consideration. These design practices are showcased as part of our design framework for a product development problem where requirements change progressively in Chapter 5.

The studies reviewed in this section are summarized in Table 2–1 and classified based on the changeability aspects considered and the metrics used to quantify them. We also position our contributions in Chapters 4 and 5 relative to some of the most notable studies that have been reviewed in this section.

Table 2–1 shows that our contributions focus entirely on external changes in requirements (such as changes in the operational context or the customer requirements). We focus specifically on scalability and robustness when considering changeability aspects. This is because in remanufacturing, a component is expected to adapt to increased requirement levels as opposed to new unforeseen requirements. Finally, both our contributions provide a method for determining the upgrade levels needed to accommodate the changing requirements by using design optimization.

The amount of design changeability embedded in a product is derived from its flexibility and robustness. Robustness is usually associated with design margins that are embedded in a design to absorb change. Metrics for quantifying these design margins are reviewed in the following section.

Table 2–1: Summary of changeability aspects considered in the literature

Feature		Contribution(s)										Chapter 4	Chapter 5	
		[37]	[38]	[39]	[34]	[40]	[41]	[42]	†	[29]	[48]	[49]		
Change type	Internal		✓				✓			✓	✓		✓	✓
	External	✓	✓	✓	✓	✓	✓	✓	✓	✓	✓	✓		
Change effect	Robust		✓	✓		✓	✓	✓	✓	✓	✓	✓	✓	✓
	Modifiable	✓					✓							
	Scalable	✓	✓	✓	✓	✓	✓	✓	✓	✓	✓	✓		
Upgrade levels	Predetermined	✓		✓	✓	✓	✓	✓					✓	✓
	Computed		✓	✓				✓		✓	✓	✓		
Flexibility metric	Cost function	✓		✓	✓	✓	✓	✓	✓				✓	✓
	Set size	✓												
	FO				✓	✓								
Change type	Environment	✓				✓			✓	✓	✓	✓	✓	✓
	Change													
	Requirement change	✓	✓	✓	✓	✓	✓	✓	✓	✓	✓	✓		
Robustness metric	Reliability										✓		✓	✓
	Capability								✓	✓	✓			
	Probability chain								✓	✓	✓			
Set-based		✓	✓	✓	✓	✓	✓	✓	✓	✓	✓	✓	✓	

† Cardin et al. [44], Cardin and Hu [45]

## 2.3 The use of design margins for managing uncertain requirements

Design margins accommodate changing requirements by providing a buffer before any change to the product is required. They are measured as a portion of a product’s capability. Capability is defined as the set of possible values for a design parameter for which feasibility is maintained [26].

Quantifying design margins involves measuring the constituents of margins: buffer and excess. Buffer is defined as the portion of a design's capability reserved for meeting variations in a requirement. Excess is the portion of a design's capability beyond the limits within which a requirement may vary [37].

Design margins are incorporated into product design by augmenting the capability of a product to include parameter values beyond the initial ones that were intended to satisfy the requirements resulting in more excess. This can be referred to as overdesign [26].

Design margins can be managed by quantifying them explicitly to assess the cost and risk of moving to a new design solution later in a product's lifecycle or development process.

Few studies in the literature have focused on quantifying buffer and excess for use as metrics in product design.

Tackett et al. use the product system's capability of meeting design requirements to quantify the available excess capacity for evolving [37]. Evolvability depends on the product's capacity for upgrade which in turn depends on the available excess for upgrading the product's capabilities. Product capability is defined as a weighted sum of multiple excess values for each requirement that the product must meet. Requirements depend on changing parameters and are usually defined in the parameter space which encompasses all the possible parameter values. Excess values are obtained by finding the range of changing parameters that the product satisfies in addition to the product's design requirements.

Tackett et al. present an interesting perspective for computing capability and excess, however, they assume independence of the requirements from one another [37]. The example used in Chapter 5 shows that design problems could feature requirements that are

dependant on multiple changing parameters. A change in one of the changing parameters could impact several requirements simultaneously. As a result, a linear combination of the excess values obtained by calculating the range of the parameters satisfied by the design in excess of the requirements would overestimate their quantities.

Other studies define application specific capability and capacity measures [40, 44]. In the context of ship design, capability is defined as a function of the specifications of the equipment that the ship can be upgraded with. Capacity, on the other hand, is defined in terms of the available excess for transport and storage [40]. In the context of a waste-to-energy system, capability is defined in terms of the volume of the anaerobic digestion and gasifier tanks [44]. Such definitions are characterized by an interval bounded by the minimum and maximum carrying capacity (changing parameters) of the design and suffer from the same issues described above when using ranged sets to describe a design's capability and excess.

Design margins are also used as an umbrella term defined as the amount by which system specifications exceed requirements [50]. [Cross and Mulford](#) do not distinguish margins in terms of buffer and excess. The distribution of the changing parameters driving the requirements is known for a particular design problem defined at the current design stage. Buffer and excess are defined based on future changes to the distribution of the changing parameters such that the requirement spans a different range of values. However, for design purposes, [Cross and Mulford](#) present a method for allocating design margins such that design performance is maximized via multidisciplinary design optimization (MDO)

[50]. So-called reliability levels are defined by the probability of satisfying the requirements must be maintained in the solution. This is one of the few studies that utilize design margins as a design metric that can be optimized.

In another study, the performance of the design (the surface temperature of a thermal protection system) is subject to variabilities due to random fluctuations associated with the computational model used to calculate the temperature on the bottom surface of the system [51]. Taking one sample from the calculated temperature distribution, capacity is defined as the maximum allowable temperature that may be reached by the system. Safety margins that are less than the capacity (maximum allowable temperature) are also defined and optimized in the study to minimize weight while maintaining a threshold probability of failure. In this study, there is only one requirement on the temperature of the bottom surface of the system. For such a problem, the description of capacity and safety margins is sufficient.

Capability indices provide a useful tool for estimating reliability in the presence of changing parameters in multi-dimensional spaces. However, they do not provide a method for quantifying excess and buffer [49]. The work can be extended to include such definitions by considering design capability indices greater than unity to be a form of overdesign. However, system performance is assumed to follow a normal distribution when subject to noise variables. This does not always hold when considering a variety of design problems.

The need for scaling up the dimensionality of design problems in terms of number of requirements has been partially addressed by Chen et al. [49]. Majority of the reviewed studies use intervals to represent design margins and capabilities which are not accurate

representations of the sets of designs that satisfy them. Finally, possible changes in the requirements should also be considered in order to incorporate the needed design flexibility.

Methods for quantifying the degree of flexibility were reviewed in Section 2.2.

We summarize the methods reviewed for computing design margins in Table 2–2 in terms of the dimensionality of the requirements considered and the numerical method used for calculating them. They are also compared to the methods used as part of our framework in Chapter 5.

Table 2–2 shows that we present a novel method for quantifying and distinguishing the excess and buffer components of design margins. We use Monte Carlo integration to compute the size of the excess and buffer sets defined in a multi-dimensional parameter space.

A set of equally changeable solutions is needed to leverage the added design changeability. We review the most recent advances in SBD in the following section to use them as part of our frameworks.

Table 2–2: Summary of design margin aspects considered in the literature

Feature	Contribution(s)						Chapter 4	Chapter 5
	[37]	[52]	[40]	[50]	[51]	[49]		
Margins	Excess	✓	✓	✓			✓	
	Buffer						✓	
	Excess + buffer			✓	✓			
Calculation method	Interval-based		✓	✓	✓	✓		
	Integral-based	✓				✓		✓
Used for design optimization			✓	✓	✓		✓	
Multi-dimensional interactions					✓		✓	

## 2.4 Set-based design principles and applications

Due to the high level of uncertainty at the early phases of the product development process, designers have adopted iterative product design methods. Traditionally, the design problem is solved by selecting an initial design based on existing knowledge or expert opinion as an initial “seed” in the design space. The initial seed design is improved iteratively until a satisfactory design that meets the design requirements is reached. This paradigm is known as point-based design (PBD) [53–55]. PBD allows the design engineers to arrive at a solution in a short time frame. However, once the design engineers commit to a solution in the design phase, it becomes difficult to modify the design should the system requirements change during the later stages of the product development process [56, 57].

A possible remedy to the above shortcomings is to delay commitment to a single design early in the design stage. Set-based design (SBD) is another design paradigm that addresses this by exploring alternative designs in the early stages of product development and delay commitment to a single design. The set of alternative designs is developed simultaneously until the variable parameters driving the requirements have been refined. Only the set of designs that has been refined by the updated requirements is developed further. This results in several designs rather than a single design that are gradually refined over the course of the product development process.

Sobek II et al. identify three principles to be observed during SBD [55]. 1) The design space is explored to identify feasible designs comprising the feasible design set (FDS) with respect to each design requirement and quantify trade-offs between possible design solutions. 2) The intersection of the FDSs is identified in 1) while still maintaining

flexibility in the offered design solutions. 3) The FDS is gradually narrowed down by eliminating undesirable solutions as design requirements become more well-defined and constraints are tightened. It can be concluded that an SBD method should feature (i) design maps of the FDSs that are transferable to ease communication between different engineering teams, (ii) must capture arbitrarily shaped FDSs, (iii) assess feasibility of design solutions efficiently to offset the longer lead time associated with SBD, and (iv) have the ability to incorporate designer preferences as a means for eliminating designs.

There are several works that address the SBD principles introduced by Sobek II et al. quantitatively. They can be classified into works that focus on either design feasibility assessment or design space reduction based on performance and designer preferences.

Interval arithmetic has been used to map the FDS [53, 58]. Qureshi et al. partition the design space into hyper-rectangle domains in which feasibility is assessed [53]. If feasibility is not established throughout the hyper-rectangle, the domain is further subdivided and feasibility is checked in each subdivision until all feasible hyper-rectangles are identified. *Noise* variables associated with uncertain parameters in the set-based context are quantified by means of intervals. Hyper-rectangles that lie within noise variable intervals are considered a subset of the robust design space. The method is intuitive and effective at reducing the design space to a manageable subspace. However, design spaces cannot always be captured by hyper-rectangles due to their irregular shapes. This is because uncertain parameters and design variables may affect several requirements simultaneously. This often causes the feasible regions that satisfy the requirements to assume highly irregular shapes including disconnected regions. Moreover, design requirements are often not given as analytic expressions of the design variables and parameters, but are obtained

from simulation models. Fuzzy set theory has been used to accommodate design variable uncertainties in the context of SBD [59]. However, fuzzy sets describe the membership of a quantity over an interval or a hyper-rectangle just like classical sets which may be inadequate for capturing arbitrarily shaped design spaces. The SBD approach is similar to the notion of ranged sets described earlier [39].

Convex hulls have been used to identify the feasible sets while design constraints have been used to treat design requirements [60]. The constraints are perturbed to represent variability of the design requirements, resampling in proximity of the constraint is used to refine the convex hull and redefine the FDS. The method can capture irregularly shaped design spaces and is intuitive. However, this method is computationally intensive due to the need for constant resampling as the design problem evolves (especially if expensive engineering models are used to calculate the constraints).

Another feasibility assessment tool is formulated using Bayesian network classifiers (BNCs) [61–63]. The motivation of this work comes from using constraint programming (CP) to identify feasible solution sets [47]. CP requires analytical expressions of the system constraints to map the feasible regions. As mentioned above, such analytical expressions are not always available in simulation-based design problems. In these cases, metamodels can be used as surrogates of the constraint functions. BNCs use a set of training data generated by engineering models to train a kernel density estimate (KDE) for estimating a posterior probability distribution for feasible and infeasible design events. The decision surface is computed from the intersection of the two probability distributions and a threshold probability (typically 0.5) is used to render feasibility decisions [61]. The method is systematic and can accommodate a constant stream of data from the designer.

Furthermore, the BNC approach can render decision boundaries for irregularly shaped design spaces and produces a KDE that can be communicated with other design teams for visualizing the feasible set of each subsystem in question. Finally, Monte Carlo simulation can be used to calculate the volume of the reduced design space for comparative studies [47].

Ge et al. introduced a surrogate-based SBD method to facilitate interactive negotiations in design engineering groups who are responsible for design tasks at different hierarchical levels, i.e., at the system, subsystem, and component levels [64]. Surrogate models are used to capture the interactions and the dynamics of the engineering systems and subsystems and are used to map feasible design regions (FDRs) and effective design regions (EDRs) to satisfy design requirements and performances respectively. Finally, robustness is evaluated using the hypervolume of the EDRs as a metric. The larger the hypervolume, the more robust is the EDR [65].

SBD principles have also been extended to platform development [66, 34] and conceptual design [67]. Platform assessment processes have been used to ensure feasibility of the narrowed-down set-based solutions in platform development of product variants. The process blocks are integrated in a product lifecycle management (PLM) architecture to facilitate information exchange between the platform assessment blocks [66]. Wang and Terpenny employ a design synthesis technique to generate concepts using an agent-based modeling approach to conceptual design [67]. The generated concepts embody the FDS for conceptual design.

So far, the studies reviewed provide means for identifying set-based solutions. SBD principles involve narrowing down the FDS to a handful of acceptable designs for further investigation and detailed design. Several works have presented a design or concept elimination method for narrowing down feasible sets by eliminating undesirable designs in terms of performance or designer preferences.

A diversity metric can be used to develop a representative cost for configurations within the FDS of the design space associated with the risk of violating feasibility [68]. [Malak et al.](#) use utility theory to make set-based decisions. Interval dominance criterion was used to eliminate designs when there is no overlap in their uncertainty ranges [69]. The maximality criterion was used to make decisions involving design variables with overlapping uncertainty intervals. [Nahm and Ishikawa](#) accommodate designer preferences in the form of “preference numbers” and functions [58]. The designer’s preference structure spans design variables and requirements which may be a product of multidisciplinary analyses. However, as with fuzzy sets, the approach may not span arbitrarily shaped design spaces.

In most design problems, a number of competing objectives or attributes often arise. This is the case with SBD problems. [Wang and Terpenny](#) used a genetic algorithm to evaluate alternative design trade-offs in a component-based system synthesis problem [67]. A generalized weighted aggregate of fuzzy-set preferences was used as an optimization objective. [Avigad and Moshaiov](#) solved a trade-off problem based on the optimality & variability (OAV) of each conceptual design in the design space [70]. The two metrics are extracted from the Pareto sets associated with each set-based concept [70]. Trade-off

rules are subjective to designer preferences and are a good approach for accommodating designer preferences during design elimination.

[Miller et al.](#) investigated a multi-fidelity approach to SBD, where increasing levels of fidelity are concurrently met with increasing level of detail in the set-based solutions [71]. The refinement is carried out over a modeling sequence to minimize the cost associated with modeling effort. Interval dominance is used to gradually narrow down the solution set for each model used.

[Hannapel and Vlahopoulos](#) present an MDO approach to set-based design by treating the design space boundaries as design variables for the system-level optimization problem [72]. The discipline problems are solved individually for a specific objective and are coordinated by the system-level optimization problem. The objective of the system-level problem is an aggregate of design space hypervolume, weighted sum of individual discipline objectives and relaxable constraint violation. By solving the MDO problem, the design space is narrowed down. Design performance is accommodated in the discipline-level optimization problems. The method assumed a design space in the form of a hyper-rectangle as prescribed by the design variable intervals. However, practical engineering design problems feature irregularly shaped design spaces [61]. Furthermore, the utilized weighted method assumes a convex attainable set for the objectives considered in the system-level optimization problem, which is not necessarily the case [73].

We classify the SBD methods based on how sets of design solutions are represented. The two distinct representations that emerge are ranged sets [53, 58, 38, 39, 34] and response surfaces [60, 61, 47, 64]. Response surfaces have the advantage of being able to capture irregularly shaped design spaces and are more conservative in comparison to

hyper-rectangular sets. [Shahan and Seepersad](#) and [Yannou et al.](#) accommodate nonlinear design requirements through various metamodels such as BNCs and polynomial response surfaces (PRSs) used as surrogates of feasibility models [61, 47].

SBD methods consider predominantly computational design engineering problems. However, the surrogate models used by [Shahan and Seepersad](#) and [Yannou et al.](#) can be used with experimental, testing, and operational data from the component being remanufactured [61, 47]. This makes surrogate models useful for a wide range of engineering design problems.

Finally, a number of techniques for narrowing down the set-based solution has been proposed. These techniques include Pareto set membership [38, 71], optimality of a ranged set with respect to an objective function (design performance or flexibility) [72, 39, 34], and interval dominance for ranged sets [69, 71].

A summary of these findings is given in Table 2–3 with respect to the principles of set-based design established by [Sobek II et al.](#) [55]. Our contributions in Chapters 4 and 5 are also compared against the most recent advances in SBD.

Table 2–3 shows that we address the limitation of using ranged sets to represent the solution set. We use response surfaces to identify set-based solutions in Chapter 4. In Chapter 5 we used a convex hull to represent our set-based solutions due to the finiteness and discreteness of the design space being considered. This is because the application example used in that chapter featured categorical and discrete design variables. However, as explained in Chapter 7 response surfaces should be used when adapting the method in Chapter 5 for continuous or mixed variable problems.

Table 2–3: Summary of set-based approaches considered in the literature

Features of reported sets	Contribution(s)										Chapter 4	Chapter 5	
	[53]	[58]	[38]	[39]	[59]	[60]	†	[71]	[72]	[34]	[69]		
<b>Set representation</b>	Interval	✓	✓	✓				✓	✓	✓	✓		
	Fuzzy set		✓		✓								
	Convex hull				✓								✓
	Metamodel				✓		✓					✓	
<b>Update ease</b>	Resampling	✓	✓	✓	✓	✓		✓	✓	✓	✓		✓
	No resampling				✓		✓					✓	
<b>Reduction method</b>	Pareto optimality			✓									✓
	MDO				✓							✓	✓
	Interval dominance						✓					✓	
	Flexibility criteria				✓				✓			✓	✓
<b>Shape</b>	Hyper-rectangle	✓	✓	✓	✓	✓		✓	✓	✓	✓		
	Arbitrary					✓	✓					✓	✓

† Shahani and Seepersad [61], Yannou et al. [47], Ge et al. [64]

Studies that utilize tradespace exploration will be reviewed in order to quantitatively compare sets of design solutions in Chapter 5.

## 2.5 The use of tradespace exploration for quantifying design margins and flexibility

Several studies reviewed thus far have incorporated tradespace exploration strategies to quantify their design metrics and visualize their design solutions [40, 29, 41, 48]. Other studies generate Pareto-optimal solutions exclusively in their analyses which is a form of tradespace exploration that focuses on designs that dominate the tradespace in terms of utility and cost [51, 50].

Viscito and Ross and Rehn et al. considered quantifying flexibility in terms of the filtered outdegree [41, 40]. Mcmanus et al. quantify survivability as a multi-attribute function for the tradespace [29]. Another study similarly uses survivability among other aspects of resilience as the utility metric for tradespace exploration [48].

Most studies focus on quantifying a robustness or resilience metric for use as a utility during tradespace exploration. This tends to lead to costly overdesigns in some cases, especially if solution sets are derived from the Pareto front on the tradespace. On the other hand, maximizing design flexibility derived from the filtered outdegree could lead to designs that do not meet requirement thresholds. It is worth investigating designs in the tradespace that are dominated by the Pareto front when considering robustness or reliability as a utility to avoid overdesign.

Furthermore, the design margin components reviewed in Section 2.3 such as buffer and excess could be used as part of the multi-attribute function governing our tradespace exploration strategy since they impact robustness.

The main utility of tradespace exploration lies in its ability to visualize and categorize designs into sets of solutions. Viscito and Ross use Pareto optimality to extract flexible cost-efficient designs from the tradespace and plot a reduced tradespace to further analyze this reduced set [41]. Small et al. categorize solutions into sets by allocating design solutions into bins based on the value of the decision variable governing each solution [48]. Combining tradespace exploration with a robustness metric as the utility while investigating flexibility via filtered outdegree should prove useful for helping designers understand the tradeoff between these design metrics.

The gaps in the studies reviewed so far will be identified in order to position our contributions relative to the literature.

## **2.6 Research gaps and opportunities**

The literature reviewed on this subject featured several studies that have attempted to quantify the aspects of changeability related to modifiability, robustness, and scalability of

the design. We narrow down these studies to those that report set-based solutions. Among those studies, several research gaps in the field are evident.

- None of the set-based representations featured a metamodel to represent the arbitrarily-shaped solutions sets. Intervals were used for reporting set-based solutions.
- Only one study used MDO to reduce the feasible design space to a flexible design set by narrowing down the intervals on design variables [72].
- Studies that used metamodels for reporting set-based solutions focused on identifying the feasible design space without further reduction [61, 47].

We aim to address these research gaps in our first contribution. Our objective is to generate a set of changeable component designs that can be upgraded as necessary through remanufacturing to meet changing requirements that may arise at a product or system's EoL.

We propose a systematic design space reduction method using optimization and response surfaces. An optimization problem is formulated to include parameters reflecting the requirements at the current stage of the product development process or its lifecycle. We then obtain a set of parametric optimal solutions to maximize the performance of the remanufactured products.

Since designers must commit to a solution eventually, it is important to consider the changeability of a product throughout its lifecycle and not just at the current stage to allow products to retain most of their economic value [23]. We therefore incorporate a scalability constraint in our SBD method to further reduce our solutions set to readily changeable designs. The scalability constraint is evaluated in the requirements space since changeability and scalability by proxy are defined in the requirements space. The set of

possible parameter values related to performance requirements are used as a proxy for the requirements space. We provide a mapping between the design space and the parameter space to transfer scalable designs identified in the parameter space back to the design space.

The proposed method is based on:

- surrogates of the computational models for rapid evaluations during optimization,
- numerical optimization for identifying the best performing feasible designs for different design parameter values, i.e., a set of *parametric* optimal designs,
- response surfaces of the parametric optimal design solutions that provide a mapping of design solutions between the design and parameter spaces,
- sensitivity analysis of design variables with respect to design parameters,
- a remanufacturing constraint based on the sensitivity of design variables to design parameters and manufacturing process capabilities that reduces the set of parametric optimal designs to a set of scalable optimal designs in the parameter space.

The reviewed literature suggests that the study of excess is relatively nascent. A method on where to place excess strategically in the design is required. The successful implementation of such a method requires a metric for quantifying design excess while providing a means to manage the change in requirements likely to be encountered throughout a product's lifetime or development process. Finally, the value of excess must be estimated and traded against during system design [27]. In this field, the following research gaps have been identified.

- There appears to be no attempt to quantify design margins (or its constituents: buffer and excess) in a multi-dimensional space by means other than intervals.

- Although there is an abundance of studies on quantifying design robustness and flexibility, the tradeoff between these important aspects of design for changing requirements has not been investigated within a tradespace exploration framework.
- Little work has been done to examine the evolutionary path of products in response to changes in their environment or requirements hence the need for an epoch-based analysis that explores product changes in a progressive manner as requirements change [27, 44].

In our second contribution, we propose a method where we compute design reliability, capability, buffer, and excess in a multi-dimensional parameter space. We use Monte Carlo simulation to chain multiple requirements (given by their probability density functions (PDFs)) together to generate a requirement arc across multiple epochs. This formulation of the requirements captures the progressive nature of a product’s development process and lifetime. A corresponding design arc is found by optimization such that excess is minimized while reliability is maintained above a threshold. In this manner, Monte Carlo simulation is used to generate multiple requirement arcs to obtain a set of solutions that balances robustness with flexibility by minimizing excess.

Our approach differs from the one in [44] in that we obtain set-based solutions by minimizing a cost function in terms of excess. Furthermore, categorical design variables are considered during the progressive upgrade of the design. Our method features the following elements.

- We determine design capability relative to a feasibility constraint in the parameter space using Monte Carlo simulation.
- We model requirements using PDFs.

- We compute buffer and excess relative to requirements in the parameter space using Monte Carlo simulation.
- We use epochs for chaining multiple requirement PDFs to generate requirement arcs.
- We formulate and solve an optimization problem [42] for determining the design arc that minimizes excess while satisfying reliability constraints for a corresponding requirement arc.
- We use Monte Carlo simulation to generate a set of optimal design arcs with respect to excess.
- We generate a tradespace for visualizing the set of optimal design arcs and positioning it relative to sets that maximize filtered outdegree (flexible design set) and sets that satisfy the largest number of requirement arcs without regards to minimizing excess (robust design sets).

## 2.7 Optimization algorithms for model-based design optimization

Our approach necessitates a rigorous algorithm that can solve blackbox optimization problems. A blackbox is defined as a computational model or process that when provided an input, returns an output with no analytical knowledge of its inner workings [74]. Blackboxes can be computationally expensive, which poses a practical challenge to optimization. In addition, the functions underlying these models are not necessarily smooth, continuous, or differentiable. Therefore, derivatives of such blackbox models are difficult to approximate numerically.

Genetic algorithms (GAs) are a popular choice for blackbox optimization problems since they do not require derivative information. However, convergence of GAs is highly dependant on tuning the hyperparameters, encoding, and crossover techniques for the

problem considered [74]. We attempt to qualify our methods for a wide variety of design problems and do not consider such algorithms as a result.

Nelder-Mead (NM) is another popular heuristic method based on simplices. Convergence analysis for such algorithms does not provide much insight on when the algorithm converges to a solution. In practice, NM is effective, as it converges to a solution when the problem is nicely behaved. However, counter examples such as the McKinnon example show that NM may converge to a non-minimizer for a convex function [74].

Mesh adaptive direct search (MADS) is a pattern search algorithm with rigorous convergence properties. It is based on advancement of the coordinate search (CS) and generalised pattern search (GPS) algorithms and features an optional search step and a poll step. The search step allows the algorithm to apply heuristics to break free of local minimizers while the poll step performs a localized search around the incumbent solution. This algorithm is shown to converge for constrained blackbox optimization problems. This advancement in direct search strategies is enabled by the use a richer set of polling directions as defined by two distinct parameters that control the mesh and frame size in which polling is done. As with all direct search methods, MADS does not require derivative information.

The previous direct search methods can be used with surrogate models of the expensive simulation model. In such frameworks a list of trail points such as those generated during the poll step of MADS are evaluated using the surrogate to rank them in terms of decreasing the objective function. The blackbox is then exercised at trail points in the same order opportunistically to avoid evaluating trail points that will be discarded by the algorithm. The surrogate model can be updated dynamically by the algorithm to improve

its accuracy around the incumbent solution. The use of such methods is strongly recommended when surrogates for the expensive blackbox are available. This is the case with examples used in the thesis. However, such methods still involve evaluations of the expensive blackbox. This would result in an immense computational cost when executing the set-based approaches in this thesis by solving many parametric optimization problems. Instead, we use a static surrogate model based on an ensemble of response surfaces to obtain the best possible estimates of the objective and constraints functions. Since the derivatives of this ensemble of surrogates are also difficult to estimate, we resort to MADS for obtaining solutions to the optimization problems in this thesis.

We also consider reliability-based design optimization (RBDO) methods since the subject of this thesis is to design products for changing requirements. In the application example, a reliability constraint must be satisfied subject to a changing requirement defined by a random joint PDF. Most probable point (MPP) methods are used for solving problems where the objective and constraints are functions of random variables. However, MPP methods can suffer in terms of accuracy when estimating reliability for constraints that are highly nonlinear [75]. Monte Carlo simulation (MCS) is shown to provide good accuracy for estimating reliability when used with Latin hypercube (LH) sampling [76]. This allows MCS to scale proportionally with the dimensionality of the problem.

The application example in this thesis involves optimization problems with mixed variables that lend themselves to multistage stochastic programming. In the literature, Lagrange relaxation methods are used for decomposing an integer programming problem into several scenarios corresponding to the different requirements that can occur. Constraints such as nonanticipativity are penalized with Lagrange multipliers in the objective

function. Since the variables considered are discrete, a duality gap exists and the search algorithm is terminated when the gap is lower than a certain value. This approach is useful for determining a single series of decisions that are insensitive to the different requirement scenarios that can arise. To leverage the added flexibility of our designs, we aim to solve several such problems for many different scenarios to obtain a set of solutions. Since our reliability constraints are expensive to compute, we resort to a mixed variable extension of MADS that is suited for such problems [77]. It is worth noting that heuristics can solve mixed variable programming problems. However, they suffer from the same drawbacks when used for continuous variables due to their obscure convergence properties.

The algorithms in this thesis are developed such that different optimization algorithms can be used interchangeably depending on the problem being solved.

In the following chapter, we describe an application example from the industry to demonstrate the efficacy of our frameworks. In this example, we consider the remanufacturing of an aeroengine structural component that is subject to changing load requirements. The details of our contributions are outlined in the following chapters.

## Chapter 3

### Thermomechanical models for product remanufacturing of a turbine rear structure

In this chapter, we introduce the industrial application example used to demonstrate our methods in Chapters 4, 5, and 6. We define the thermomechanical model used to analyze the deposition process used to remanufacture the product. The product considered in this thesis is the TRS. The models developed in this section are specific to the deposition of various stiffener geometries on the turbine rear structure (TRS). However, the simplifications to the thermomechanical analysis used to compute the residual effects of directed energy deposition on the substrate are generalizable to any deposit and substrate.

A TRS is a structural aeroengine component at the turbine exhaust. It must sustain thermal and structural loads during flight due to exhaust gases while mounting the engine to the wing structure. Analysis of the component in the industry involves multiple disciplines (aerodynamic, structural, and thermal).

We consider the deposition of a stiffener on the TRS to support higher loading requirements. The first step of the analysis involves a thermomechanical model to compute the residual stresses in the structure ( $\sigma_{v1}$ ).

Any subsequent loading of the TRS during operation results in a new stress state ( $\sigma_{v2}$ ). The mean and amplitude of the initial and final stress states are used to compute the safety factor against low-cycle fatigue as a structural performance metric. We consider two different load cases in Chapters 4 and 5. However, the calculation of the safety factor against low-cycle fatigue is independent of the load case used in the analysis.

The following section outlines the thermomechanical models used to predict the residual stresses that result from the AM deposition process. All the loadcases presented in this thesis take advantage of the cyclic symmetry of the TRS by restricting the analysis to one sector.

### 3.1 Thermomechanical modeling

The directed energy deposition (DED) of the stiffener increases the thickness of the outer casing as shown in Figure 3–1.

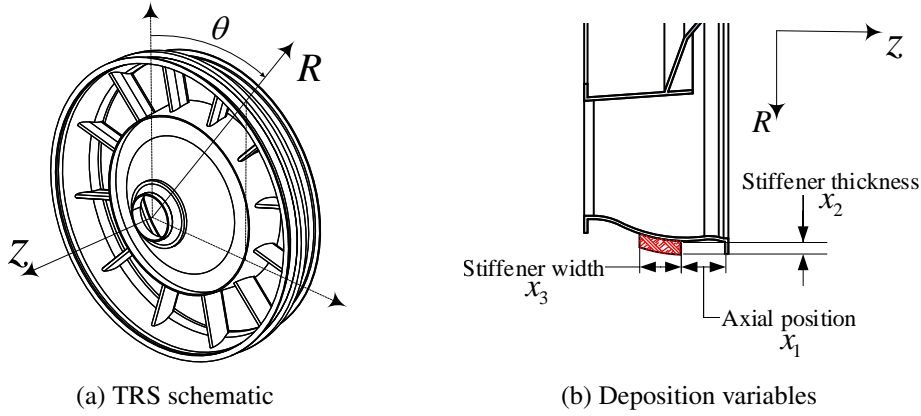


Figure 3–1: TRS stiffener example

Comprehensive thermomechanical models feature a coupled transient heat transfer and fluid flow model to accurately calculate the transient temperature field. The temperature field is used for residual stress and distortion modeling [78]. Complex physical processes govern the temperature field making its computation intensive. Computations of the temperature field involve various simplifications and assumptions to make the calculations tractable. [Manvatkar et al.](#) consider a finite element analysis (FEA) conduction model for calculating the transient temperature field due to a moving Gaussian heat source

on the substrate [79]. The problem of a moving heat source on an infinite plate was formulated and solved analytically by Rosenthal [80]. The Rosenthal model is used for cases where there is limited heat conduction in the through thickness dimension typical of thin plates [81]. The TRS outer casing where the stiffener is to be deposited has a through thickness dimension considerably smaller than its width and circumference allowing us to approximate the heat source by a Gaussian heat source as in the Rosenthal model.

The melt pool dimensions are estimated from the transient thermal model to determine the deposit width and depth. Figure 3–2 shows the details of the thermomechanical simulations for determining deposit size. A Gaussian heat source scanning the surface of a substrate at a constant speed  $V$  has a heat flux distribution given by

$$Q(r, \theta, t) = \frac{P_{\text{laser}}}{\pi r_l^2 D_p} e^{-2\left(\frac{r-Vt}{r_l}\right)^2}, \quad (3.1)$$

where  $r_l$  is the laser beam radius,  $P_{\text{laser}}$  is the laser power, and  $D_p$  is the depth of penetration of the laser source [80]. The coordinates  $r$  and  $\theta$  are defined on the surface of the deposit as shown in Figure 3–2a.

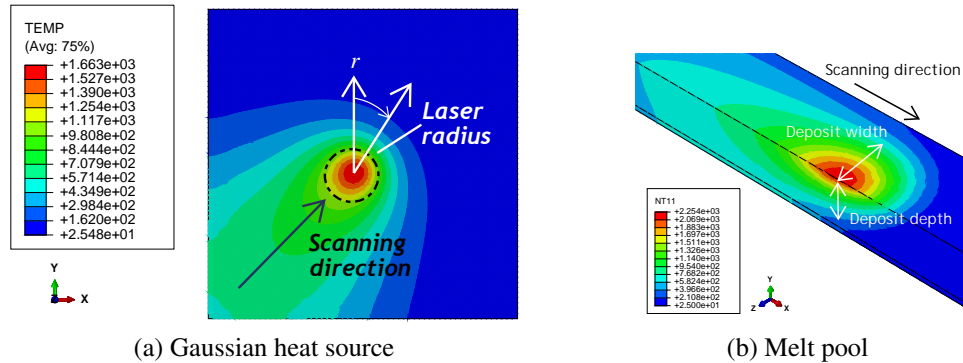


Figure 3–2: Heat conduction for a moving Gaussian heat source

The resulting deposit width  $D_w$  and depth  $D_d$  are used to partition the stiffener geometry into  $n_l$  by  $n_d$  deposits in the axial and radial directions, respectively, where  $n_l = \lfloor x_3/D_w \rfloor$  and  $n_d = \lfloor x_2/D_d \rfloor$ .

For deposition on the TRS outercasing, a further simplification of the transient conduction model can be made by applying the heat flux uniformly on the surface of the deposit [82]. We use a static model with a uniformly distributed heat flux to compute residual stresses. This idealization (relative to using a transient heat transfer model) reduces the number of variables and parameters involved and alleviates computational cost by exploiting TRS symmetry without sacrificing accuracy excessively.

Each deposit is heated uniformly by an equivalent heat flux that supplies the same energy as a moving Gaussian heat source scanning the entire deposit surface. The power at  $t = 0$  is given by the surface integral of the heat flux over an infinite plane

$$P(t = 0) = \frac{P_{\text{laser}}}{\pi r_l^2 D_p} \int_0^{2\pi} \int_0^{\infty} e^{-2\left(\frac{r}{r_l}\right)^2} r dr d\theta = \frac{P_{\text{laser}}}{\pi r_l^2 D_p} \frac{\pi r_l^2}{2} = \frac{P_{\text{laser}}}{2D_p}. \quad (3.2)$$

The power per unit depth  $P(t = 0)$  is multiplied by the scanning time  $t_{\text{scan}}$  to obtain the heat energy input to the deposit. The scanning time is calculated for each stiffener by dividing total distance traveled by the heat source (stiffener length) by the scanning speed  $t_{\text{scan}} = L/V$ .  $A_{\text{stiff}}$  is the surface area of the stiffener where heat is applied. These values are obtained from the geometry of the stiffener using computer aided design (CAD) tools.

The energy is divided by an equivalent step time  $t_{\text{step}}$  used for static thermal analysis in lieu of a transient thermal analysis to obtain the equivalent uniformly distributed power per unit depth  $P_{\text{eqv}}$ .  $P_{\text{eqv}}$  is divided by the area of the deposit  $A_{\text{stiff}}$  to yield the equivalent

heat flux per unit depth

$$Q_{\text{eqv}} = \frac{P_{\text{laser}}}{2D_p} \frac{t_{\text{scan}}}{t_{\text{step}}} \frac{1}{A_{\text{stiff}}}. \quad (3.3)$$

A special case of stiffener is the circumferential stiffener shown in Figure 3–1. For this type of stiffener, Equation (3.3) can be simplified by setting  $L = 2\pi R_{\text{outer}}$ , where  $R_{\text{outer}} = 0.5$  m is the radius of the outer casing of the TRS. This results in  $t_{\text{scan}} = 2\pi R_{\text{outer}}/V$ . The deposit surface area becomes  $A_{\text{deposit}} = 2\pi R_{\text{outer}} D_w$  to yield the equivalent heat flux per unit depth

$$Q_{\text{eqv}} = P(t=0) \frac{2\pi R_{\text{outer}}}{V} \frac{1}{t_{\text{step}}} \frac{1}{2\pi R_{\text{outer}} D_w} = P(t=0) \frac{1}{V t_{\text{step}} D_w} = \frac{P_{\text{laser}}}{2V t_{\text{step}} D_w D_p}. \quad (3.4)$$

Here, we assume that the radius of the deposit is equal to the radius of the outer casing  $R_{\text{outer}}$  since the thickness of the deposit is small relative to the outer casing.

An example of the application of  $Q_{\text{eqv}}$  to the surface of a circumferential deposit layer is shown in Figure 3–3.

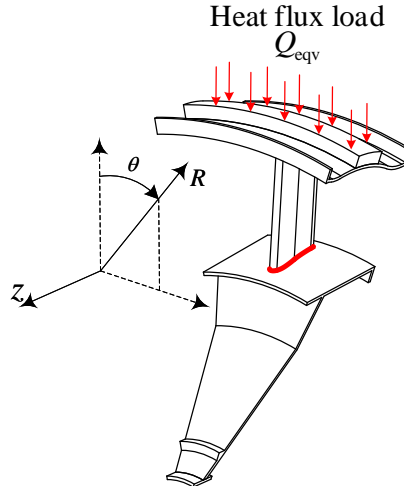


Figure 3–3: Deposition load

After obtaining the thermal gradients due to the application of the heat flux load, the corresponding thermal stresses are computed. The stresses that persist after removal of the heat flux load are the residual stresses. These residual stresses are inherent in the structure and affect the structural performance of the TRS during subsequent operational loads.

The maximum and minimum residual principal stresses along the circumference of the TRS outer casing are shown in Figure 3–4 for both static and transient models. Table 3–1 summarizes the utilized parameter values for this comparative study.

Table 3–1: Comparison of transient and static models: parameter values

Parameter	Notation	Units	Value
Stiffener axial position	$x_1$	mm	80.0
Stiffener thickness	$x_2$	mm	4.0
Stiffener width	$x_3$	mm	23.5
Laser Power	$P_{\text{laser}}$	W	3,889.13
Laser beam radius	$r_l$	mm	13.63
Scanning speed	$V$	mm/s	5.0
Number of layers	$n_l$	-	2
Number of deposits (transverse)	$n_d$	-	1
Deposit depth	$D_d$	mm	2.01
Deposit width	$D_w$	mm	25.0
Deposit surface area	$A_{\text{deposit}}$	mm <sup>2</sup>	$8.304 \times 10^4$
Equivalent heat flux per unit depth	$Q_{\text{eqv}}$	W/mm <sup>3</sup>	0.8138

In all our analyses throughout the thesis, the scanning speed is considered constant at a nominal value of  $V = 5$  mm/s.

The principal stresses provide an indication of the compressive or tensile nature of the stress state and will be used in subsequent failure analysis to determine the safety factor. There is a general agreement in the value of the predicted stresses with lower values recorded for the transient model due to the time taken by the substrate to reach

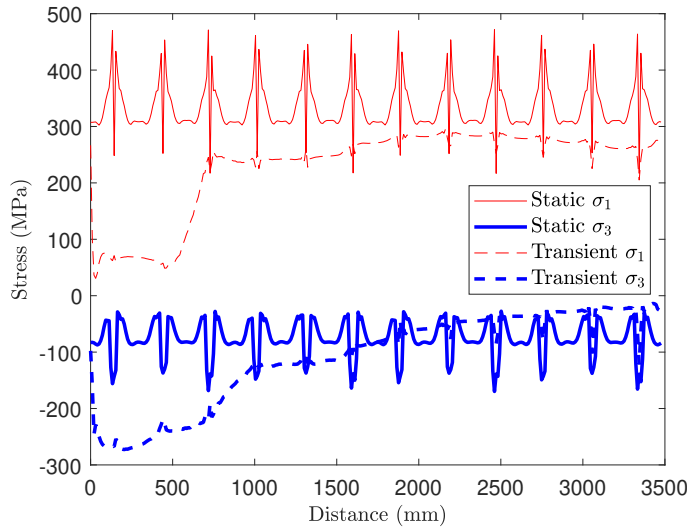


Figure 3–4: Spatial distribution of principle residual stresses along the circumference of the TRS obtained using transient and static models

steady state temperatures as the heat source scans its surface. Furthermore, the static model overpredicts the maximum principal stress making it a more conservative choice for thermomechanical modeling.

In the following section we describe the different load cases that the TRS may experience in operation.

### 3.2 Load cases applied to turbine rear structure

The TRS experiences a number of thermal and mechanical loads due to the exhaust gases it directs while providing structural support to the engine. Two significant load cases are used for the analyses in this thesis to address the effect of changing parameters on the functionality of the TRS.

We describe the first load case in the following section.

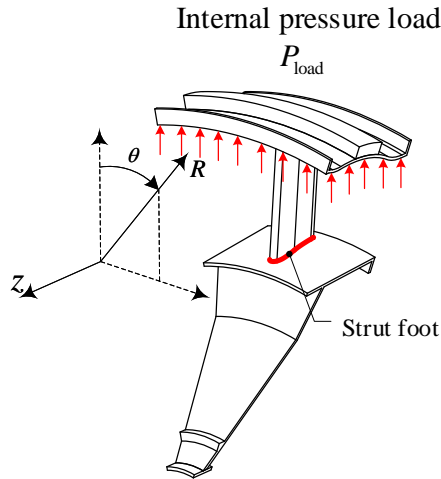


Figure 3–5: TRS pressure load case

### 3.2.1 Pressure load case

The first load case is due to the internal pressure  $P_{\text{load}}$  applied on the outer casing of the TRS by the hot exhaust gases. A pressurization/depressurization cycle on a sector of the TRS is shown in Figure 3–5. The load case is cycled and is used to compute the expected fatigue life of the TRS using low-cycle fatigue calculations. The stress state at the foot of a strut (shown in Figure 3–5) is monitored before and after the load case to obtain the initial and final Von Mises stresses  $\sigma_{v1}$  and  $\sigma_{v2}$ , respectively. Note that  $\sigma_{v1} \neq 0$  due to the residual stress state in the structure from prior thermomechanical loads.

We now describe the thermal loadcase due to the temperature of the exhaust gases.

### 3.2.2 Thermal load case

The TRS shown in Figure 3–1a is subject to thermal loads due to temperature gradients experienced during operation. The temperature profile of a TRS during operation is

shown in Figure 3–6b. These temperature loads are specified by the OEM engine architect to the TRS component supplier in the form of changing parameters.

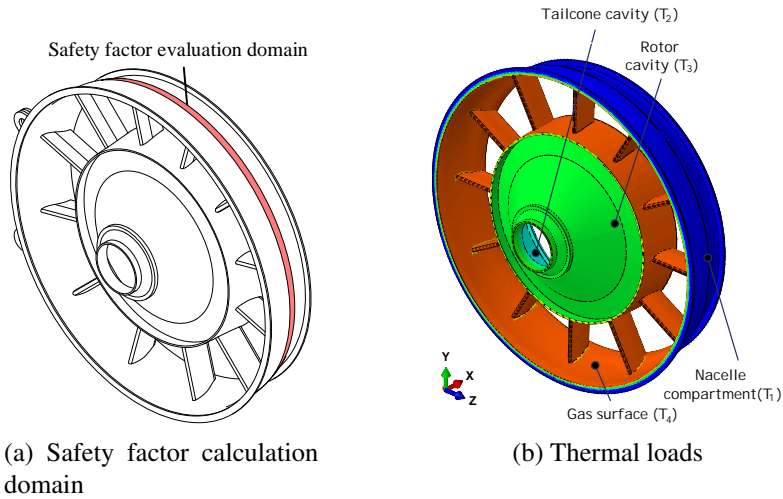


Figure 3–6: TRS thermal load case

The thermal load case is cycled and is used to compute the expected fatigue life of the TRS using low-cycle fatigue calculations. The stress state at the midsection of the outer casing is recorded before and after the load case to obtain the initial and final Von Mises stresses  $\sigma_{v1}$  and  $\sigma_{v2}$ , respectively.

The structural analyses presented for the thermomechanical, pressure, and thermal load cases are performed using a finite element (FE) simulation model which is computationally expensive. As a result, we will construct surrogates for these models in Chapters 4, 5, and 6 to alleviate the computational effort involved in exploring the design and parameter spaces for these application examples.

We explain how the safety factor  $n_{\text{safety}}$  is computed for these load cases in the following section.

### 3.2.3 Low-cycle fatigue analysis

We use the initial and final Von Mises stresses  $\sigma_{v1}$  and  $\sigma_{v2}$  obtained before and after the application of either load case described earlier to compute the safety factor against low-cycle fatigue.

The midrange stress ( $\sigma_m = -\text{sign}(\sigma_P)(\sigma_{v1} + \sigma_{v2})/2$ ) and the amplitude stress ( $\sigma_a = |\sigma_{v1} - \sigma_{v2}|/2$ ) are calculated, where  $\text{sign}(\sigma_P)$  is the sign of the pressure given by the sum of the principle stresses ( $\sigma_P = -(1/3)(\sigma_1 + \sigma_2 + \sigma_3)$ ) and provides of measure of the compressive or tensile state of the stress. A negative  $\sigma_P$  implies tension while a positive value implies compression. The failure locus is determined by the modified Goodman criterion for low-cycle fatigue as shown in Figure 3–7. The endurance limit ( $S_e$ ), yield stress ( $\sigma_y$ ), and ultimate strength ( $S_{ut}$ ) are defined as parameters and are obtained from mechanical design handbooks [83]. The number of lifecycles to failure is estimated from Wöhler's relation ( $N_f = (\sigma_{\text{rev}}/a)^b$ ), where  $a$  and  $b$  are empirical constants. The safety factor is calculated as  $n_{\text{safety}} = 1 / \left( \frac{\sigma_a}{S_e} + \frac{\sigma_m}{S_{ut}} \right)$  for each load case.

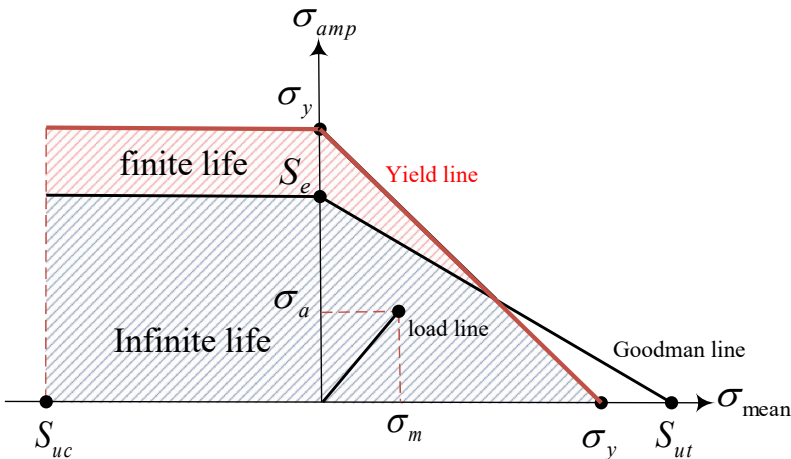


Figure 3–7: Modified Goodman criterion

The safety factor  $n_{\text{safety}}$  is used as a structural performance metric throughout this thesis. We now summarize all the relevant model inputs and outputs for the thermomechanical models and loadcases.

### 3.3 Summary

This chapter presented the industrial application example that will be used throughout the thesis to demonstrate the developed frameworks. The chapter defined the thermo-mechanical model and two loadcases that the TRS experiences in operation. The loadcase parameters and outputs are summarized in Tables 3–2 and 3–3 respectively. Some parameters in Table 3–2 can change and are denoted by ranges. They will be elaborated on during the analyses in the following chapters.

Table 3–2: Relevant model inputs

<b>Parameter</b>	<b>Notation</b>	<b>Units</b>	<b>Value</b>
Stiffener axial position	$x_1$	mm	$91 \pm 54$
Stiffener thickness	$x_2$	mm	$6 \pm 4$
Stiffener width	$x_3$	mm	$25 \pm 15$
Laser Power	$P_{\text{laser}}$	W	$3750 \pm 250$
Internal pressure load	$P_{\text{load}}$	MPa	$2 \pm 0.5$
Deposit melting point	$T_m$	°C	$1,500 \pm 100$
Substrate base width	$W_{\text{total}}$	mm	$137.5 \pm 17.5$
Nacelle temperature	$T_1$	°C	$300 \pm 100$
Tailcone temperature	$T_2$	°C	$400 \pm 100$
Rotor temperature	$T_3$	°C	$450 \pm 100$
Gas surface temperature	$T_4$	°C	$600 \pm 100$
Laser beam radius	$r_l$	mm	14.2
Scanning speed	$V$	mm/s	5.0
Laser penetration depth	$D_p$	mm	5.0

Table 3–3: Relevant model outputs

Output	Notation	Units
Number of layers	$n_l$	-
Number of deposits (transverse)	$n_d$	-
Deposit depth	$D_d$	mm
Deposit length	$D_l$	mm
Deposit width	$D_w$	mm
Deposit surface area	$A_{\text{stiff}}$	mm <sup>2</sup>
Deposit length	$L$	mm
Scanning time	$t_{\text{scan}}$	s
Equivalent heat flux	$Q_{\text{eqv}}$	W/mm <sup>2</sup>
Safety factor against low-cycle fatigue	$n_{\text{safety}}$	-
Number of lifecycles to failure ( $P_{\text{load}}$ )	$N_f$	-
Deposition temperature	$T_{\text{deposit}}$	°C

We describe the method for obtaining scalable design solutions for product remanufacturing in the following chapter. The internal pressure loadcase described in Section 3.2.1 will be used to demonstrate this framework. The thermal loadcase described in Section 3.2.2 will be used for demonstrating the design margin allocation tool developed in Chapter 5.

## Chapter 4

### Scalable set based design optimization

This chapter describes a novel design tool for identifying a set of scalable designs for product remanufacturing using parametric design optimization. Scalability is an enabler for product remanufacturing since it provides components with the flexibility to have their specifications upgraded to meet higher requirement levels.

The method in this chapter is demonstrated using an industrial application example for the remanufacturing design of a TRS. The thermomechanical model described in Section 3.1 along with the load case in Section 3.2.1 is used to define the design variables and uncertain parameters involved in the remanufacturing design problem. Remanufacturing is performed by AM using laser DED. However, our method can be extended to remanufacturing problems where subtractive manufacturing is used.

We begin by defining the method for obtaining the set-based solutions for arbitrary design and parameter spaces in Section 4.1. We then demonstrate the method for the remanufacturing of the TRS in Section 4.2. We provide some insights and conclusions about the uses and limitations of the developed framework in Section 4.4.

#### 4.1 Method

Engineering design optimization problems involve decision variables  $\mathbf{x} \in \mathbb{R}^n$  and design parameters  $\mathbf{p} \in \mathbb{R}^m$ . Objective ( $f(\mathbf{x}; \mathbf{p})$ ) and constraint ( $\mathbf{g}(\mathbf{x}; \mathbf{p})$ ) functions are used to reflect design requirements. Given bounded design optimization variables and parameters  $\mathbf{L} \leq \mathbf{x} \leq \mathbf{U}$  and  $\mathbf{L}_p \leq \mathbf{p} \leq \mathbf{U}_p$ , respectively, we define the design space  $D$  and the

parameter space  $P$ . We also consider constraint sets  $C_u$  for  $u = 1, 2, \dots, q$  where  $q$  is the number of constraints. In a product design context, constraints are part of the design requirements and are driven by the parameters  $\mathbf{p}$ . Finally, the feasible set  $F$  is defined as the intersection of all constraint sets and contains designs that meet all design requirements. The set  $F$  is the FDS and represents the outcome of SBD before elimination of potential designs.

Design parameters may affect the optimal solution of the optimization problem due to their influence on design requirements. As a result, designs that are optimal throughout the parameter space  $P$  and satisfy the design requirements comprise the set of parametric optimal designs which is a reduction of the FDS. Since practical SBD methods require solutions sets that can be easily communicated across design teams, response surfaces are used as a surrogate model to evaluate feasibility and performance and to classify membership of each design to the feasible set and the set of parametric optimal designs.

#### 4.1.1 Surrogate modeling

The objective and constraint functions used to represent design requirements are evaluated using computer-aided engineering (CAE) tools that model the repair/remanufacturing process. These computational models are computationally expensive. Any SBD method requires a large number of function evaluations to investigate not only the design but also the parameter space. Therefore, we resort to building less expensive response surfaces to be used as surrogate models.

We conduct designs of experiments to sample the aggregate design and parameter spaces and then exercise the computational models at these sample points to generate adequate training data. An ensemble of surrogate models is then constructed and denoted by

$\hat{f}(\mathbf{x}; \mathbf{p})$  and  $\hat{\mathbf{g}}(\mathbf{x}; \mathbf{p})$ . An open source surrogate model library is used to build the surrogates [84, 85].

An order-based metric is used to assess the predictive capability of the surrogates [86]. This metric ensures the consistency between the computationally expensive and surrogate model predictions. The order-based metric is also used for constructing response surfaces of the parametric optimal solutions with respect to varying design parameters in subsequent sections and is discussed using a numerical example in Section 4.1.4.

#### 4.1.2 Parametric optimal designs

We use numerical optimization to provide a set of design solutions that can address a range of requirements. Specifically, we solve the optimization problem for different parameter values. This can be seen as a form of post-optimality analysis (POA) that provides the sensitivity of optimal design variable values with respect to varying parameter values [87].

The surrogate optimization problem is formulated as

$$\begin{aligned} & \underset{\mathbf{x}}{\text{minimize}} \quad \hat{f}(\mathbf{x}; \mathbf{p}) \\ & \text{subject to} \quad \hat{\mathbf{g}}(\mathbf{x}; \mathbf{p}) \leq \mathbf{0} \end{aligned} \tag{4.1}$$

and solved to obtain the solution  $\mathbf{x}^*(\mathbf{p})$ . Given intervals for the parameters  $\mathbf{p}$ , sampling techniques can be used to obtain a set of  $m$  combinations. Here, we use LH sampling

which produces a uniform random distribution over the parameter space [88]

$$\mathbf{P} = \begin{bmatrix} \mathbf{p}_1^T \\ \mathbf{p}_2^T \\ \vdots \\ \mathbf{p}_w^T \end{bmatrix} = \begin{bmatrix} p_{11} & p_{12} & \cdots & p_{1m} \\ p_{21} & p_{22} & \cdots & p_{2m} \\ \vdots & \vdots & \ddots & \vdots \\ p_{w1} & p_{w2} & \cdots & p_{wm} \end{bmatrix}. \quad (4.2)$$

LH sampling is used since the number of samples needed to fit an adequate response surface scales better with dimensionality relative to uniform sampling techniques such as full factorial sampling. Once we have obtained a solution  $\mathbf{x}^*(\mathbf{p})$  for each of the  $w$  parameter vectors, a response surface  $\hat{\mathbf{x}}^*(\mathbf{p})$  is built using the set of parametric optimal designs  $\mathbf{X}^* = \{\mathbf{x}^*(\mathbf{p}_1), \mathbf{x}^*(\mathbf{p}_2), \dots, \mathbf{x}^*(\mathbf{p}_w)\}$ . A rule of thumb indicates that the initial sample size should be about an order of magnitude larger than the dimensionality of the problem, i.e.,  $w \approx 10m$  [89]. To potentially save computational cost, we also monitor the convergence rate of the order-based error proposed in [86] as more samples are added and accept the response surface as adequate once it has reached an appropriate threshold. It does not rely on comparisons with the true scalable set (which is not available in real problems). It is computed by checking how accurately the response surface model orders the validation points. It is calculated as

$$\varepsilon_{OE} = \frac{1}{n_{cv}^2} \sum_{i=1}^{n_{cv}} \sum_{l=1}^{n_{cv}} \theta(\mathbf{x}^*(\mathbf{p}_i) - \mathbf{x}^*(\mathbf{p}_l), \hat{\mathbf{x}}^*(\mathbf{p}_i) - \hat{\mathbf{x}}^*(\mathbf{p}_l)), \quad (4.3)$$

where  $n_{cv}$  is the number of validation points. In our work,  $n_{cv}$  is set equal to the number of samples used for training the response surface. The function  $\theta$  is defined as

$$\theta(a, b) = (a \leq 0) \text{ xor } (b \leq 0), \quad (4.4)$$

where xor is the logical *exclusive or* operator. An example of this procedure is provided in Section 4.1.4. The response surface  $\hat{\mathbf{x}}^*(\mathbf{p})$  is used to predict parametric optimal designs throughout the parameter space.

Sensitivity gradients of the design variables with respect to the parameters allow designers to understand the effect of requirement changes to optimal designs. The Jacobian of  $\hat{\mathbf{x}}^*(\mathbf{p})$  is

$$\mathbf{J}(\mathbf{p}) = \nabla \hat{\mathbf{x}}^*(\mathbf{p}) = \begin{bmatrix} \nabla \hat{x}_1^*{}^T(\mathbf{p}) \\ \nabla \hat{x}_2^*{}^T(\mathbf{p}) \\ \vdots \\ \nabla \hat{x}_n^*{}^T(\mathbf{p}) \end{bmatrix} = \begin{bmatrix} \frac{\partial \hat{x}_1^*}{\partial p_1} & \frac{\partial \hat{x}_1^*}{\partial p_2} & \cdots & \frac{\partial \hat{x}_1^*}{\partial p_m} \\ \frac{\partial \hat{x}_2^*}{\partial p_1} & \frac{\partial \hat{x}_2^*}{\partial p_2} & \cdots & \frac{\partial \hat{x}_2^*}{\partial p_m} \\ \vdots & \vdots & \ddots & \vdots \\ \frac{\partial \hat{x}_n^*}{\partial p_1} & \frac{\partial \hat{x}_n^*}{\partial p_2} & \cdots & \frac{\partial \hat{x}_n^*}{\partial p_m} \end{bmatrix}. \quad (4.5)$$

It can be estimated using the derivatives of the basis functions used to construct the response surface. Differentiation of the response surface is possible because it is based on a linear combination of basis functions. The ability of a response surface to accurately predict the Jacobian is described by the order-based error metric which determines the computational expense for obtaining the necessary number of training samples to achieve the threshold error value. The type of surrogate model used to obtain the response surface should feature differentiable basis functions such as the correlation function used in Kriging metamodels or the kernel function used in kernel smoothing metamodels.

We use a kernel smoothing (KS) model to build  $\hat{\mathbf{x}}^*(\mathbf{p})$  and estimate the Jacobian  $\mathbf{J}(\mathbf{p})$  using the linear combination of the gradient of the kernel functions. KS was used to construct the response surface due to their immediate computation since it does not require matrix inversions. Furthermore, KS models typically respect the order of the output which

reflects its ability to predict the correct order of values of any two evaluation points. This is very important for this application since it relies on differentiating the KS model [86].

For the remainder of this subsection, let us use the typical notation between an independent variable  $x$  and a dependent variable  $y$  recalling however, that in our context  $\hat{\mathbf{x}}^*(\mathbf{p})$  is corresponding to  $y$  (dependent variable) while  $\mathbf{p}$  is corresponding to  $x$  (independent variable).

KS models consist of a weighted sum of training points where the weight for each training point decreases as the distance from the prediction point increases. KS predictions are given by

$$\begin{aligned}\hat{y}(\mathbf{x}) &= \frac{\sum_{j=1}^w \phi_j(\mathbf{x})y_j}{\sum_{j=1}^k \phi_j(\mathbf{x})} = \frac{\phi_1(\mathbf{x})y_1 + \phi_2(\mathbf{x})y_2 + \cdots + \phi_w(\mathbf{x})y_w}{\phi_1(\mathbf{x}) + \phi_2(\mathbf{x}) + \cdots + \phi_w(\mathbf{x})} = \\ &\quad \frac{\phi_1(\mathbf{x})y_1}{\phi_1(\mathbf{x}) + \phi_2(\mathbf{x}) + \cdots + \phi_w(\mathbf{x})} + \frac{\phi_2(\mathbf{x})y_2}{\phi_1(\mathbf{x}) + \phi_2(\mathbf{x}) + \cdots + \phi_w(\mathbf{x})} + \\ &\quad \cdots + \frac{\phi_w(\mathbf{x})y_w}{\phi_1(\mathbf{x}) + \phi_2(\mathbf{x}) + \cdots + \phi_w(\mathbf{x})}, \quad (4.6)\end{aligned}$$

where  $\phi_j$  is the kernel function for the  $j$ th training point,  $y_j$  is the output at the  $j$ th training point, and  $\mathbf{x}$  is the prediction point. To determine the gradient of  $\hat{y}(\mathbf{x})$ , the quotient rule of differentiation is applied to each term in Equation (4.6) and the common terms are factored out to yield

$$\begin{aligned}\nabla \hat{y}(\mathbf{x}) &= \frac{\phi_1(\mathbf{x}) + \phi_2(\mathbf{x}) + \cdots + \phi_w(\mathbf{x})}{[\phi_1(\mathbf{x}) + \phi_2(\mathbf{x}) + \cdots + \phi_w(\mathbf{x})]^2} \times [\nabla \phi_1(\mathbf{x})y_1 + \nabla \phi_2(\mathbf{x})y_2 + \cdots + \nabla \phi_w(\mathbf{x})y_w] - \\ &\quad \frac{\nabla \phi_1(\mathbf{x}) + \nabla \phi_2(\mathbf{x}) + \cdots + \nabla \phi_w(\mathbf{x})}{[\phi_1(\mathbf{x}) + \phi_2(\mathbf{x}) + \cdots + \phi_w(\mathbf{x})]^2} \times [\phi_1(\mathbf{x})y_1 + \phi_2(\mathbf{x})y_2 + \cdots + \phi_w(\mathbf{x})y_w] = \\ &\quad \frac{\sum_{j=1}^w \phi_j(\mathbf{x}) \sum_{j=1}^w \nabla \phi_j(\mathbf{x})y_j - \sum_{j=1}^w \nabla \phi_j(\mathbf{x}) \sum_{j=1}^w \phi_j(\mathbf{x})y_j}{\left[ \sum_{j=1}^w \phi_j(\mathbf{x}) \right]^2}. \quad (4.7)\end{aligned}$$

We used the Gaussian kernel function (and its gradient) defined as

$$\phi_j(\mathbf{x}) = e^{-\pi\lambda\|\mathbf{x}-\mathbf{x}_j\|_2} \quad (4.8)$$

$$\nabla\phi_j(\mathbf{x}) = -\frac{\pi\lambda(\mathbf{x}-\mathbf{x}_j)}{\|\mathbf{x}-\mathbf{x}_j\|_2}e^{-\pi\lambda\|\mathbf{x}-\mathbf{x}_j\|_2}, \quad (4.9)$$

where  $\lambda$  is the bandwidth of the kernel function. The bandwidth parameter's effect on the order-based error is also used to determine the optimal bandwidth for adequately capturing the Jacobian of the KS model.

Equations (4.8) and (4.9) are substituted into Equation (4.7) to provide the gradient of the prediction function  $\hat{y}(\mathbf{x})$ . This process is repeated for each of the design variables  $\hat{x}_1^*(\mathbf{p}), \hat{x}_2^*(\mathbf{p}), \dots, \hat{x}_n^*(\mathbf{p})$  to populate the Jacobian in Equation (4.5). The Jacobian is used to formulate a transition rule in the parameter space to obtain the set of scalable optimal designs.

Algorithm 1 presents the method followed to obtain the set of parametric optimal designs. The procedure including the calculation of the order-based error is demonstrated by means of a numerical example in Section 4.1.4.

#### 4.1.3 Reduction to set of scalable optimal designs

We adopt the terminology used by Ross et al. [36] for defining the aspects of design changeability. Varying design parameters as proxies of requirements is a *change agent* that provides motivation for changing the design. Scalability represents the ability of the design to adapt to changing requirements by means of scaling. For example, a design that is in service must now sustain a higher static load than originally intended during the design phase. This change can be accommodated by reinforcing the structure using AM techniques. Transition rules may govern changes. For example, the reinforcement can

---

**Algorithm 1:** Pseudo-algorithm for obtaining the set of parametric optimal designs  $\mathbf{X}^*$  and KS response surface of parameter space  $\hat{\mathbf{x}}^*(\mathbf{p})$

---

**Input:** Surrogate model  $\hat{f}(\mathbf{x}; \mathbf{p})$  and  $\hat{\mathbf{g}}(\mathbf{x}; \mathbf{p})$ , number of parameter space samples  $w$ , number of cross-validation samples  $n_{cv}$

**Output:**  $\mathbf{X}^*, \hat{\mathbf{x}}^*(\mathbf{p}), \nabla \hat{\mathbf{x}}^*(\mathbf{p})$

- 1 Initialize  $\mathbf{X}^* = \emptyset$  and  $\mathbf{X}_{cv}^* = \emptyset$
- 2 Generate LH samples of parameter space  $[\mathbf{p}_1, \mathbf{p}_2, \dots, \mathbf{p}_w]^T$  and  $[\mathbf{p}_1, \mathbf{p}_2, \dots, \mathbf{p}_{n_{cv}}]^T$
- 3 **for**  $k \leftarrow 1$  to  $n_{cv}$  **do**
  - 4     Solve the parametric optimization problem in Equation (4.1) to obtain  $\mathbf{x}^*(\mathbf{p}_k)$
  - 5     Augment cross-validation set  $\mathbf{X}_{cv}^* \leftarrow \mathbf{X}_{cv}^* \cup \{\mathbf{x}^*(\mathbf{p}_k)\}$
- 6 **for**  $k \leftarrow 1$  to  $w$  **do**
  - 7     Solve the parametric optimization problem in Equation (4.1) to obtain  $\mathbf{x}^*(\mathbf{p}_k)$
  - 8     Augment  $\mathbf{X}^* \leftarrow \mathbf{X}^* \cup \{\mathbf{x}^*(\mathbf{p}_k)\}$
  - 9     Train response surface  $\hat{\mathbf{x}}^*(\mathbf{p})$  using  $\mathbf{X}^*$
  - 10    Compute order-based error up to and including  $k$ th sample  $\varepsilon_{OE}$  using Equation (4.3),  $\hat{\mathbf{x}}^*(\mathbf{p})$ , and  $\mathbf{X}_{cv}^*$
- 11 Find index  $k_{\min}$  that minimizes order-based error  $\varepsilon_{OE}$
- 12 Set  $k \leftarrow k_{\min}$
- 13 Set  $\mathbf{X}^* \leftarrow \mathbf{X}^* = \{\mathbf{x}^*(\mathbf{p}_1), \mathbf{x}^*(\mathbf{p}_2), \dots, \mathbf{x}^*(\mathbf{p}_k)\}$
- 14 Train response surface  $\hat{\mathbf{x}}^*(\mathbf{p})$  using  $\mathbf{X}^*$
- 15 Find bandwidth  $\lambda$  that minimizes order-based error of response surface  $\hat{\mathbf{x}}^*(\mathbf{p})$
- 16 Compute Jacobian of response surface  $\nabla \hat{\mathbf{x}}^*(\mathbf{p})$  using Equation (4.7)

---

only add material to the design and not subtract from it (analogous to the containment rule formulated by Liu and Ma [13] for subtractive remanufacturing). Furthermore, there is a cost and time associated with the change. As a result, designs that minimize the transition costs while maximizing the offered alternatives should be considered during SBD to add more value to the design. We focus here on *transition rules* that consider the ability of the manufacturing process to scale the design.

We derive transition rules pertaining to additive and subtractive manufacturing. AM processes can only add material to the substrate which results in an increase in the volume of the deposit. The opposite applies to subtractive manufacturing. The volume of the deposited part must be described in terms of the design variables pertaining to the geometry. The *monotonicity* of the volume with respect to each design variable is the basis for selecting designs that are scalable. For example, a variable such as the thickness of a beam has a positive monotonicity with respect to the beam volume. This is because an increase in the beam thickness leads to an increase in beam volume. Conversely, a variable such as hole diameter through the thickness of the beam has a negative monotonicity with respect to the beam volume. This is because a larger hole will subtract more material from the volume of the beam. This view of scalability is sufficient for problems where remanufacturing is used to alter the geometry of the component.

In this work we focus on variables where a strict monotonic increase or decrease with respect to volume can be determined. Variables that do not have a monotonic impact on volume are excluded from the analysis. We consider a problem involving four design variables denoted as  $x_1, x_2, x_3$ , and  $x_4$ . Equation (4.10)

$$V = f(x_2^+, x_3^+) \quad (4.10)$$

reflects the fact that only variables  $x_2$  and  $x_3$  have a monotonic impact on volume, where the superscripts + and – denote increasing and decreasing monotonicity, respectively. We define a monotonicity vector  $\mathbf{m}$  of  $n$  components;  $m_l = 1$  if the monotonicity of the volume with respect to variable  $x_l$  is increasing and  $m_l = -1$  if the monotonicity is decreasing, where  $l = 1, 2, \dots, n$ . Opposite signs for  $m_l$  should be used if subtractive manufacturing is considered. If the designer wishes to neglect the effect of variable  $x_l$  on the volume, then  $m_l = 0$ . For example, based on Equation (4.10),  $\mathbf{m} = [0 \ 1 \ 1 \ 0]^T$ . A diagonal matrix  $\mathbf{M}$  is then constructed as

$$\mathbf{M} = \begin{bmatrix} 0 & 0 & 0 & 0 \\ 0 & 1 & 0 & 0 \\ 0 & 0 & 1 & 0 \\ 0 & 0 & 0 & 0 \end{bmatrix}. \quad (4.11)$$

Similarly, a vector characterizing the change agent  $\mathbf{n}$  can be defined for the system parameters  $\mathbf{p}$  to describe the sign of the change:  $n_i = 1$  if parameter  $p_i$  is expected to increase and  $n_i = -1$  if the parameter is expected to decrease, where  $i = 1, 2, \dots, m$ . If, for example, the vector  $\mathbf{n}$  is defined as  $\mathbf{n} = [1 \ -1 \ -1]^T$  a diagonal matrix  $\mathbf{N}$

$$\mathbf{N} = \begin{bmatrix} 1 & 0 & 0 \\ 0 & -1 & 0 \\ 0 & 0 & -1 \end{bmatrix} \quad (4.12)$$

is constructed similar to above.

In order to select designs that are scalable, the required change in the variable must result in either an increase or no change in volume. This is expressed as

$$n_i m_l \frac{\partial \hat{x}_l^*}{\partial p_i} \geq 0. \quad (4.13)$$

The non-strict inequality includes zero-valued components to accommodate nonsensitive variables where  $m_l = 0$ . The transition rule can be formulated in matrix form as

$$\mathbf{N} \mathbf{J}^T(\mathbf{p}) \mathbf{M} \geq \mathbf{0}. \quad (4.14)$$

Every element of the resulting matrix must be greater than or equal to zero in order to satisfy the transition rule.

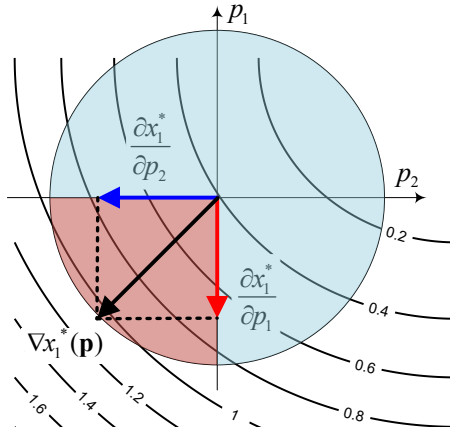


Figure 4–1: Isocontours of the response surface  $x_1^*(\mathbf{p})$  and transition rule  $\mathbf{N} \mathbf{J}^T(\mathbf{p}) \mathbf{M} \geq \mathbf{0}$  in a two-dimensional parameter space

To illustrate Equation (4.14), a two-dimensional parameter space example is shown in Figure 4–1.

The change agent vector  $\mathbf{n}$  describes a quadrant (or hyper-octant in higher dimensions) in the parameter space that should contain the gradient vector  $\nabla \hat{\mathbf{x}}^*(\mathbf{p})$ . The sign

of the gradient vector is modified by the monotonicity vector  $\mathbf{m}$ . Figure 4–1 shows an example when  $m_l \nabla \hat{x}_l^*(\mathbf{p}) \geq 0$  and lies within the quadrant defined by  $\mathbf{n}$ . Designs within the change agent quadrant and having gradients leading to an increase in their value are considered scalable.

In order to map scalable designs from the parameter space to the design space, the design space is resampled randomly and the transition rule (Equation (4.14)) is checked for every sample  $\mathbf{p}_o$ . If  $\mathbf{N} \mathbf{J}^T(\mathbf{p}_o) \mathbf{M} \geq \mathbf{0}$  is satisfied then the corresponding design  $\hat{\mathbf{x}}^*(\mathbf{p}_o)$  is retrieved and appended to a set of scalable solutions  $\mathbf{X}_s$ .

The procedure for obtaining the set of scalable optimal solutions is presented in Algorithm 2.

---

**Algorithm 2:** Pseudo-algorithm for obtaining the set of scalable optimal designs  $\mathbf{X}_s$

---

**Input:** KS response surface of parameter space  $\hat{\mathbf{x}}^*(\mathbf{p})$ , Jacobian of parameter space  $\nabla \hat{\mathbf{x}}^*(\mathbf{p})$ , Monotonicity matrix  $\mathbf{M}$ , Change agent matrix  $\mathbf{N}$ , number of parameter space LH samples  $o$

**Output:**  $\mathbf{X}_s$

```

1 Initialize  $\mathbf{X}_s = \emptyset$ 
2 Generate LH samples of parameter space  $[\mathbf{p}_1, \mathbf{p}_2, \dots, \mathbf{p}_o]^T$ 
3 for  $k \leftarrow 1$  to  $o$  do
4   if  $\mathbf{N} \mathbf{J}^T(\mathbf{p}_k) \mathbf{M} \geq \mathbf{0}$  then
5     Find design variables corresponding to parameters sample using response
      surface  $\mathbf{x}^*(\mathbf{p}_k) = \hat{\mathbf{x}}^*(\mathbf{p}_k)$ 
6     Augment  $\mathbf{X}_s \leftarrow \mathbf{X}_s \cup \{\mathbf{x}^*(\mathbf{p}_k)\}$ 
7   else
8      $\mathbf{X}_s \leftarrow \mathbf{X}_s$ 

```

---

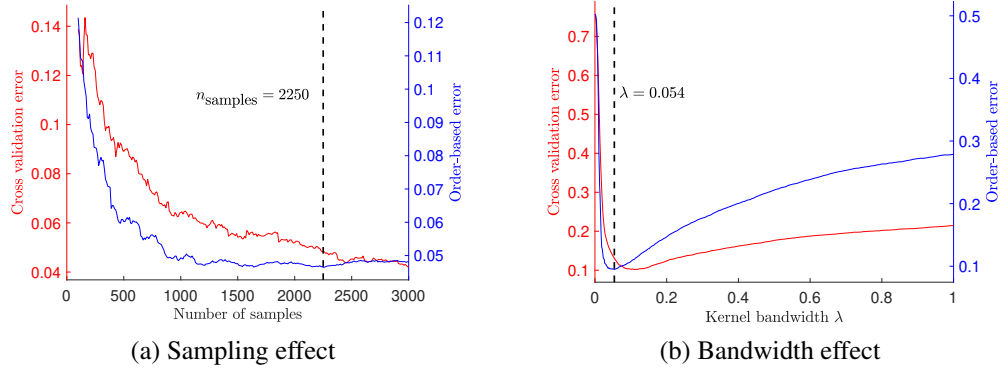


Figure 4–2: Effect of number of training points and kernel bandwidth on order-based error

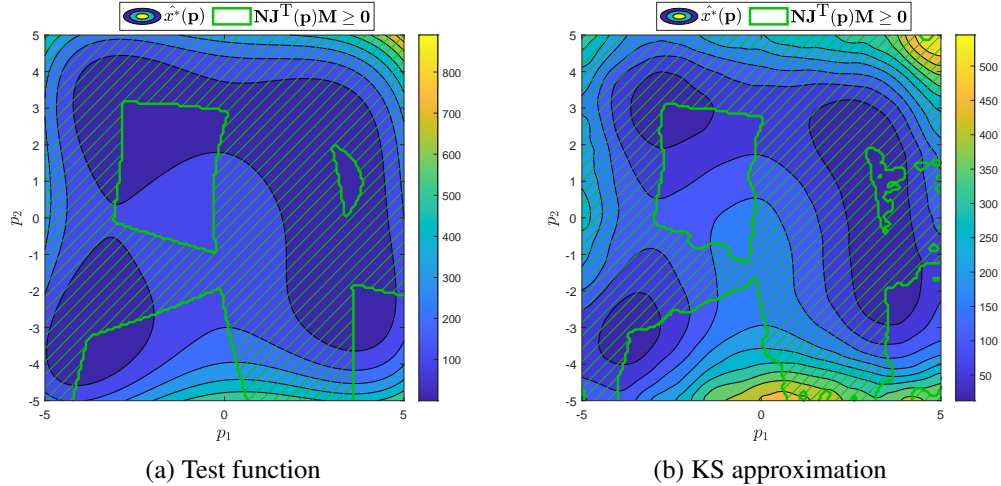


Figure 4–3: Approximation of scalable set using KS with non-scalable regions of the parameter space hatched

#### 4.1.4 Numerical example for determining the scalable design set

We demonstrate the concepts related to constructing a KS response surface to estimate the Jacobian using a numerical example. We also show how the estimated Jacobian can be used for identifying the scalable design set. Himmelblau’s test function is used as it features multiple local minima. This results in a discontinuous set of scalable optimal

designs which is not trivial to compute and has been identified as one of the challenges associated with set-based design [61]. The test function and its Jacobian are

$$x^*(p_1, p_2) = (p_1^2 + p_2 - 11)^2 + (p_1 + p_2^2 - 7)^2$$

and

$$\mathbf{J}(p_1, p_2) = \begin{bmatrix} 4p_1(p_1^2 + p_2 - 11) + 2(p_1 + p_2^2 - 7) \\ 2(p_1^2 + p_2 - 11) + 4p_2(p_1 + p_2^2 - 7) \end{bmatrix},$$

respectively.

We approximate the response surface for this function via KS to obtain  $\hat{x}^*(\mathbf{p})$ . For this example we set the change agent vector as  $\mathbf{n} = [1 \ -1]$  and the monotonicity vector as  $\mathbf{m} = [1]$ . The test function is sampled via LHs to create the training data for the KS model. We evaluate the transition rule  $\mathbf{N} \mathbf{J}^T(\mathbf{p}) \mathbf{M} \geq \mathbf{0}$  defining the scalable set using the analytical and estimated Jacobian. The estimated Jacobian was obtained by differentiation of the KS basis functions. A portion of the LH samples are reserved for use as a validation set and are not used to train the KS model. The cross-validation error reflects the classification accuracy of the KS response surface at the validation points as part of the true scalable set obtained from the analytical Jacobian.

Figure 4–2 shows the effect of the number of training points ( $n_{\text{samples}}$ ) and the bandwidth ( $\lambda$ ) on the cross validation and order-based errors.

It can be seen that there is a unique combination of  $n_{\text{samples}}$  and  $\lambda$  that yield the best response surface for assessing scalability in the parameter space. The true and estimated scalable sets are shown in Figure 4–3. The KS model used for the estimation is trained using 2305 training samples and a bandwidth of  $\lambda = 0.054$ . Figure 4–3 shows that KS

is capable of capturing the scalable set despite underestimating the magnitude of the test function. Figure 4–2 shows that the order-based error is a good indication of the prediction accuracy of the KS model for the scalable set. As a result, the KS parameters and number of training points can be determined by minimizing the order-based error.

In summary, the proposed method consists of two design filters that determine a set of scalable optimal designs to be considered for further development. The first filter retains designs that dominate in terms of performance throughout the parameter space (set of parametric optimal designs  $\mathbf{X}^*$ ). The second filter retains designs that are scalable by remanufacturing (scalable design set  $\mathbf{X}_s$ ). The number of samples for the KS response surface is chosen such that the order-based error is minimized with respect to a validation set. The methods developed in this section are demonstrated using the application example.

The proposed method, is presented as a flow diagram in Figure 4–4.

## 4.2 Application example: aeroengine component remanufacturing

The TRS structural aeroengine component described in Chapter 3 is used to demonstrate the method for obtaining scalable optimal designs when considering it for remanufacturing. The safety factor against low-cycle fatigue is computed using the model in Section 3.2.3 as a structural performance requirement. The design variables for the circumferential stiffener shown in Figure 3–1 are extracted from Table 3–2 and listed in Table 4–1 along with their monotonicity. Similarly, the design parameters relevant to the optimization problem in this chapter are extracted from Table 3–2 and are listed in Table 4–2 along with their change agent values.

## 4.2. APPLICATION EXAMPLE: AEROENGINE COMPONENT REMANUFACTURING

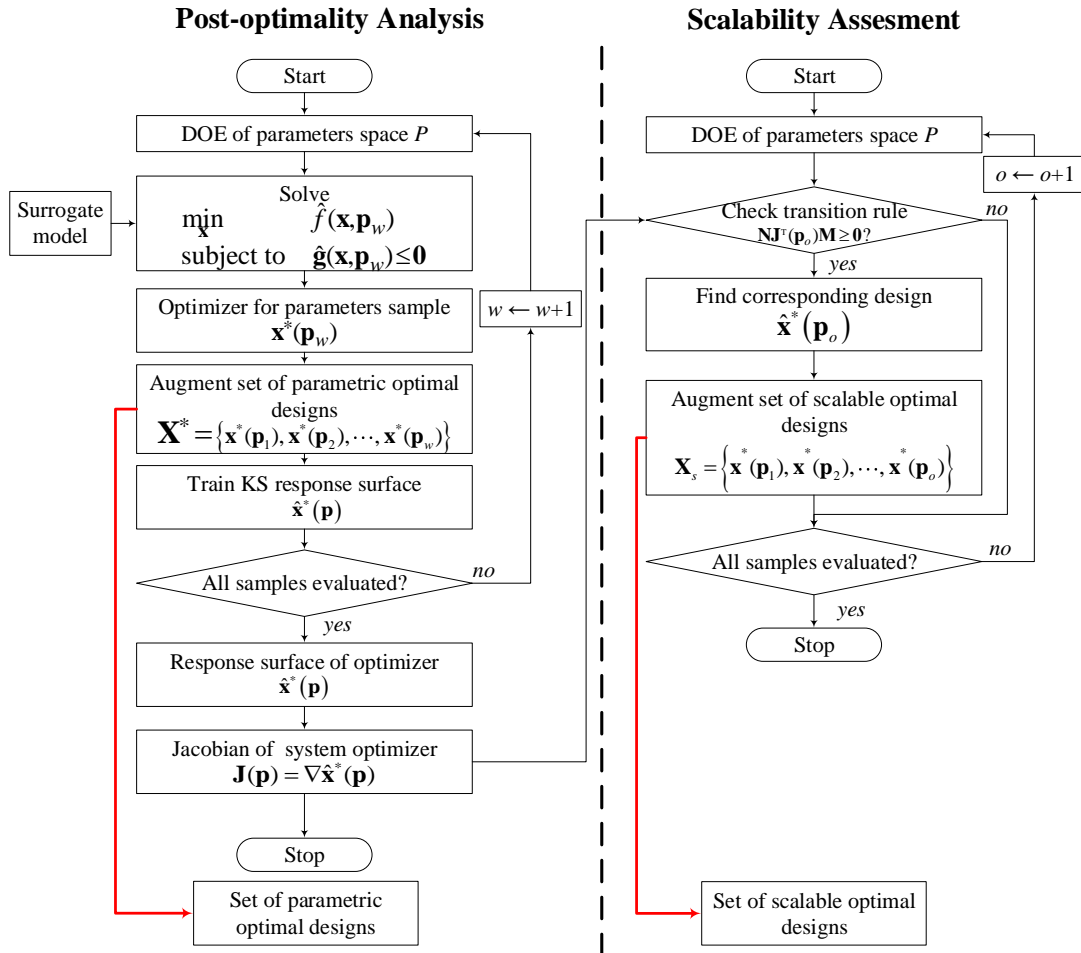


Figure 4–4: Set-based design space reduction method

Table 4–1: Design variables  $\mathbf{x}$

Design variable	Notation	Units	Lower bound	Upper bound	Mono-tonicity
Stiffener axial position	$x_1$	mm	37	145	0
Stiffener thickness	$x_2$	mm	2	10	1
Stiffener width	$x_3$	mm	10	40	1
Laser Power	$P_{\text{laser}}$	W	3,500	4,000	0

Table 4–2: Design parameters  $\mathbf{p}$ 

Parameter	Notation	Units	Range	Change agent
Internal pressure load	$P_{\text{load}}$	MPa	$2 \pm 0.5$	1
Deposit melting point	$T_m$	°C	$1,500 \pm 100$	-1
Substrate base width	$W_{\text{total}}$	mm	$137.5 \pm 17.5$	-1

The remanufacturing model variables and parameters given by Tables 4–1 and 4–2 respectively are used for the formulation of the optimization problem for SBD in the following section.

#### 4.2.1 Problem formulation

The design optimization problem is formulated as

$$\begin{aligned} & \min_{\mathbf{x}=[x_1, x_2, x_3, P_{\text{laser}}]^T} f(\mathbf{x}; \mathbf{p}) = -n_{\text{safety}}(P_{\text{load}}) \\ & \text{subject to} \quad g_1(\mathbf{x}; \mathbf{p}) = x_3 + x_1 - W_{\text{total}} \leq 0 \\ & \quad g_2(\mathbf{x}; \mathbf{p}) = T_m - T_{\text{deposit}} \leq 0, \end{aligned} \tag{4.15}$$

where  $n_{\text{safety}}$  is the safety factor against low cycle fatigue or first cycle yielding for the load case. The constraints pertain to the substrate width on the outer casing (the region where deposition is permitted) and the melting temperature of the deposit material needed to consolidate the material.

#### 4.2.2 Parametric optimal design results

The design optimization problem in Equation (4.15) is solved using the MADS algorithm. We use the OrthoMADS implementation provided by the NOMAD algorithm [90]. The termination criterion for MADS was the minimum mesh size (defined by Audet and Dennis [91]) reached in the virtually discretized design variable space. Non-opportunistic

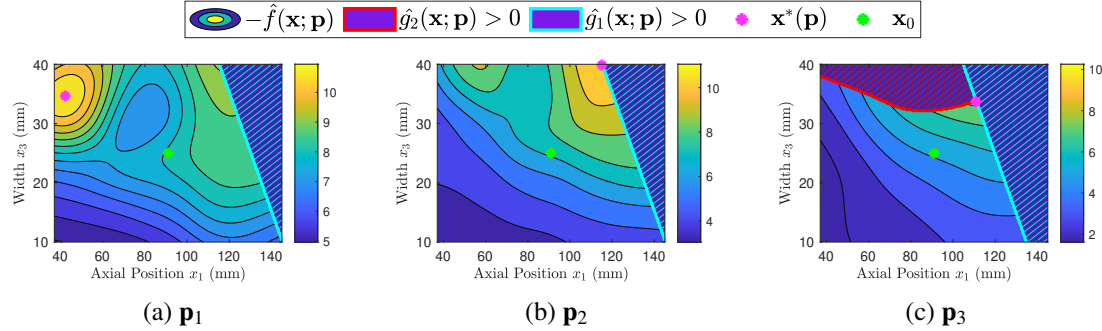


Figure 4–5: Three sample parametric optimal designs;  $x_0$  denotes the baseline design

latin hypercube search was used during the search step. A progressive barrier approach was used for handling constraints [92]. This choice of algorithm is motivated by the discussion in Section 2.7.

As described earlier, LHSs are used to sample the design and parameter spaces defined by the bounds and ranges of the design variables and parameters, respectively (see Tables 4–1 and 4–2).

For our numerical investigations, the design optimization problem is solved for 1200 LH samples of the parameter space to obtain a set of parametric optimal design solutions. Up to 900 samples are used as a training set for the KS model, while the remaining 300 are reserved for use as a validation set to check the order-based error.

The effect of the parameters on the optimizer is illustrated by 3 sample results shown in Figure 4–5 (see Table 4–3).

These 3 samples have been chosen to include one interior optimal design (Figure 4–5a), one boundary optimal design with one active constraint ((Figure 4–5b), and one boundary optimal design with two active constraints (Figure 4–5c). The optimizers obtained by sampling the parameter space are used to construct a convex hull to quantify the

Table 4–3: Sample optimization problem results

Result	Units	Parameters								
		<b>p<sub>1</sub></b>			<b>p<sub>2</sub></b>			<b>p<sub>3</sub></b>		
		$P_{\text{load}}$ (MPa)	$T_m$ (°C)	$W_{\text{total}}$ (mm)	$P_{\text{load}}$ (MPa)	$T_m$ (°C)	$W_{\text{total}}$ (mm)	$P_{\text{load}}$ (MPa)	$T_m$ (°C)	$W_{\text{total}}$ (mm)
		1.87	1,400	155	2.08	1,400	155	2.3973	1,427	145
$x_1^*$	mm		42.2			115.1			110.9	
$x_2^*$	mm		10.0			9.0			8.8	
$x_3^*$	mm		34.7			39.9			33.7	
$P_{\text{laser}}^*$	W		3,500			3,770			3,991	
$g_1(\mathbf{x}^*)$	mm		-78.1			0 (active)			0 (active)	
$g_2(\mathbf{x}^*)$	°C		-393			-381			0 (active)	
$f(\mathbf{x}^*)$	-		-11			-11			-8	

size of the set of parametric optimal designs. The qhull algorithm was used to construct the 4-dimensional polygon (polytope) characterizing the convex hull [93].

#### 4.2.3 Scalable optimal design results

Of the 900 parametric optimal designs obtained by solving the optimization problem for different parameter values, 592 samples were used to construct a response surface that can predict a parametric optimal design for other parameter values. As explained in Section 4.1.4, the order-based error relative to a validation set was minimized to determine the number of training samples. The kernel bandwidth ( $\lambda$ ) was determined to be 0.71. This result is shown in Figure 4–7.

Designs meeting scalability requirements in the parameter space are identified using the scalability constraint in Section 4.1.3. The monotonicity vector is defined as  $\mathbf{m} = [0 \ 1 \ 1 \ 0]^T$  for the variables in Table 4–1. The change agent vector is defined as  $\mathbf{n} = [1 \ -1 \ -1]^T$ . As an illustrative example, the two-dimensional projections of the parameter space for the optimal width design variable are depicted in Figure 4–6.

## 4.2. APPLICATION EXAMPLE: AEROENGINE COMPONENT REMANUFACTURING

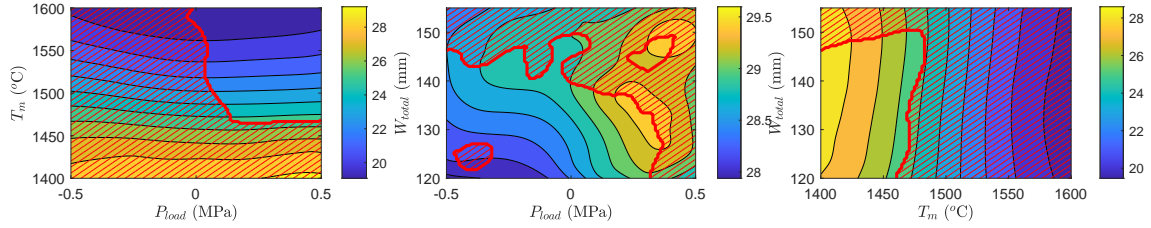


Figure 4–6: Projections of the optimal width design variable  $\hat{x}_3^*$  with non-scalable regions of the parameter space hatched

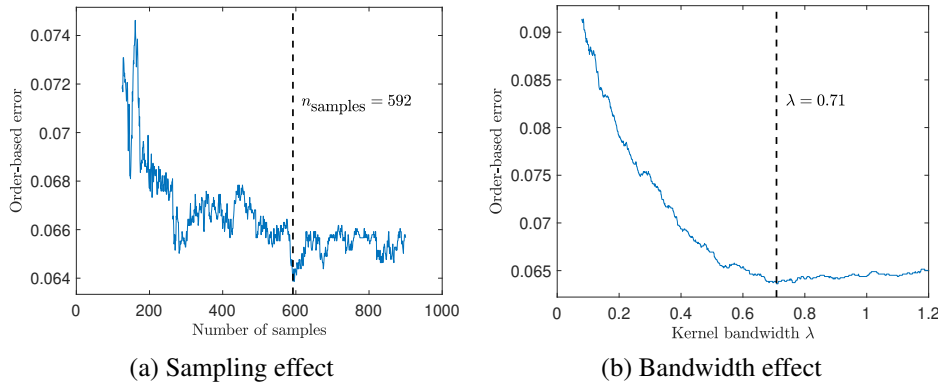


Figure 4–7: Effect of number of training points and kernel bandwidth on order-based error

The scalability transition rule results in pockets within the parameter space that can be mapped back to design space by evaluating the optimizer response surface within these pockets. The parameter space is sampled using a full factorial grid and designs meeting the scalability constraint are tabulated and projected on the design space in Figure 4–8a.

The convex hull formed by the scalable optimal designs is considerably smaller in volume than that formed by the set of parametric optimal designs.

The set of scalable optimal designs can be enlarged to include more designs by relaxing some of the scalability constraints. We relax all the constraints with respect to the thickness design variable  $x_2$  by setting the monotonicity with respect to  $x_2$  to 0. The

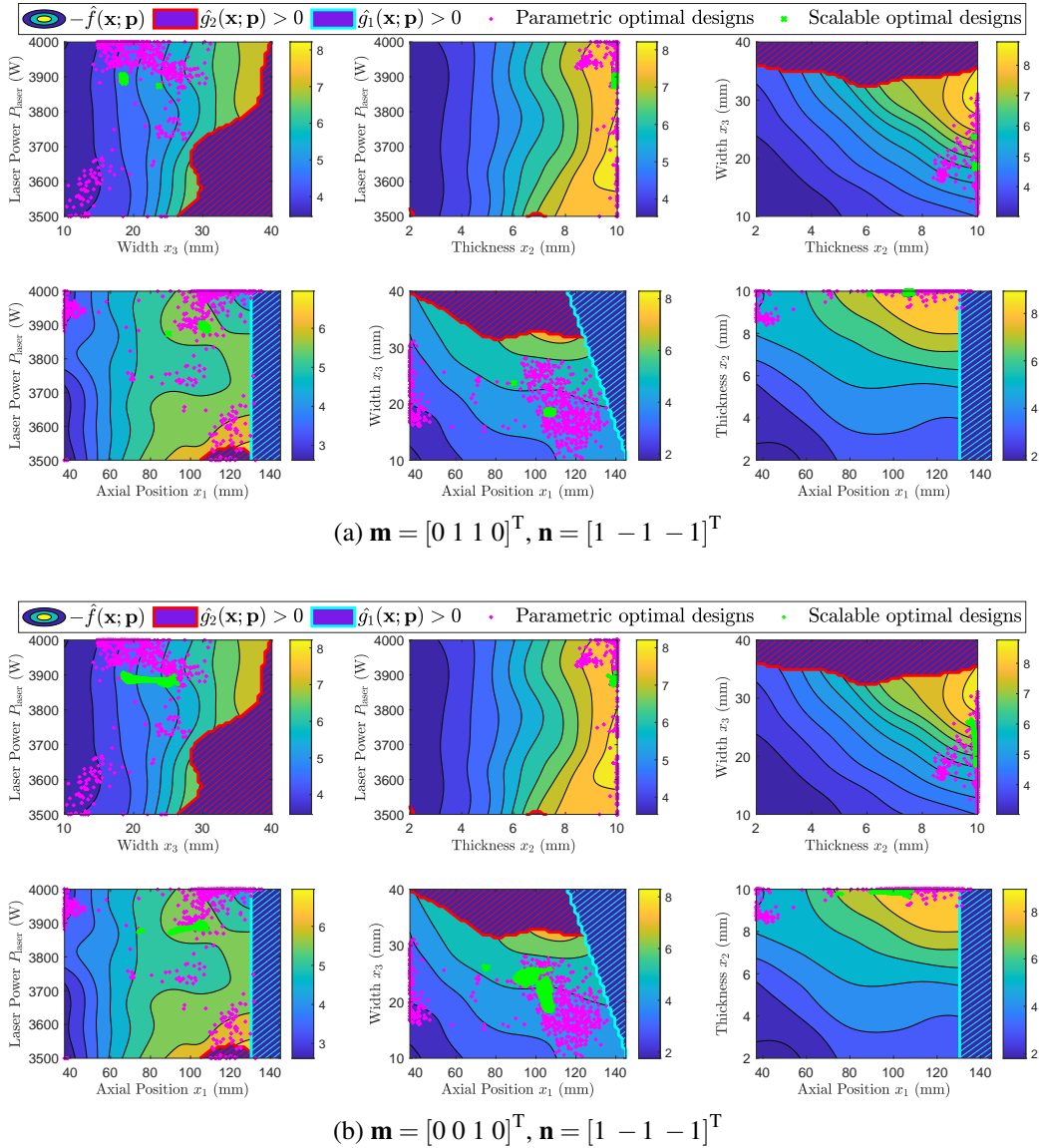


Figure 4–8: Safety factor in the feasible design space as a function of design variables for different monotonicity vectors

monotonicity vector becomes  $\mathbf{m} = [0 \ 0 \ 1 \ 0]^T$ . The result of this relaxation is shown in

Figure 4–8b.

## 4.2. APPLICATION EXAMPLE: AEROENGINE COMPONENT REMANUFACTURING

Adhering to scalability constraints allows designers the flexibility to scale designs as parameters evolve even after commitment by considering remanufacturing scenarios. Figure 4–6 shows this scenario as the contours of  $\hat{x}_3^*$  increase in value for any vector contained within the change agent hyperoctant as defined by  $\mathbf{n}$ .

### **4.2.4 Design set variability and comparison**

Having generated the feasible design set, the set of parametric optimal designs, and the set of scalable optimal designs for the TRS remanufacturing example, some comparisons can be made. Several metrics exist in the literature for comparing the variability of a design solution set generated by parametric optimal design tools such as those formulated in this thesis. The volume of the convex hull provides a good perception of design variability provided that there are sufficient points to construct the polytope characterizing the convex hull [94]. The convex hull volume was used to compare the reduction in the design sets as our method was applied to the TRS example. The lower and upper bounds (LB and UB, respectively) of the ranged set containing each solution set are also found. They are used to compute the volume of the bounding hyper-rectangle. The hyper-rectangle volume provides a benchmark against the ranged set representation used for previous SBD studies [53, 58, 38, 39, 34].

Table 4–4 summarizes the results of this comparison. It can be seen that a significant reduction of the design space was caused by each set-based filter step of our method. This is because smaller values for the laser power  $P_{\text{laser}}$  and thickness  $x_2$  resulted in consistently suboptimal designs with respect to performance. However, among the scalable designs many featured axial positions ( $x_1$ ) and widths ( $x_3$ ) near the upper and lower bounds for each variable respectively. This is due the positive monotonicity of the volume with respect

Table 4–4: Design space comparison results

Quantity	Feasible design space		Set of parametric optimal designs		Scalable design set			
					$\mathbf{m} = [0 \ 1 \ 1 \ 0]^T$	$\mathbf{m} = [0 \ 0 \ 1 \ 0]^T$		
	LB	UB	LB	UB	$\mathbf{n} = [1 \ -1 \ -1]^T$	$\mathbf{n} = [1 \ -1 \ -1]^T$	LB	UB
$x_1$	37	145	37	136	88.9	108.6	73.7	108.7
$x_2$	2	10	8.4	10	9.8	9.9	9.6	9.9
$x_3$	10	40	10.3	31.1	18.3	23.7	18.3	26.4
$P_{\text{laser}}$	3500	4000	3500	4000	3874	3904	3869	3907
$V_{\text{hyper-rectangle}}$	1		0.13		0.0016		0.0025	
$V_{\text{convhull}}$	0.77		0.028		$6.3 \times 10^{-9}$		$1.04 \times 10^{-5}$	
Relative volume	77%		2.8%		$6.3 \times 10^{-7}\%$		0.00104%	

to  $x_3$ . Such designs have the greatest potential for scalability. The relative volume of the convex hull to that of the design space is calculated in the last row of the table. The design space volume was normalized to 1 for ease of comparison. Feasible solutions comprised about three fourths of the design space (77%). The parametric optimal design solutions comprised only 2.8%. The scalable solutions obtained for  $\mathbf{m} = [0 \ 1 \ 1 \ 0]^T$  and  $\mathbf{m} = [0 \ 0 \ 1 \ 0]^T$  comprised  $6.3 \times 10^{-7}\%$  and 0.00104% of the design space, respectively. While these proportions may seem small, they are significant in size in the considered 4-dimensional design space. For comparison, the volume of the hyper-rectangle enclosing the design sets was also calculated since most of the surveyed set-based design methods used hyper-rectangles to prescribe their solution sets. The design variable bounds were normalized relative to the upper and lower bounds of the design space and corresponding volume was computed by finding the product of the length of the “edges” of the hyper-rectangle. It can be seen that the hyper-rectangle overestimates the volume of the design

sets due to its inability to capture the arbitrary shape of the different design sets shown in Figure 4–8.

The results of this application example demonstrate the usefulness of the transition rule formulated in this chapter for providing scalable remanufacturing design solutions for a range of design requirements. By accommodating variability in the design stage and incorporating flexible design principles, future potential losses in raw material and manufacturing effort are alleviated by avoiding disposal and replacement scenarios. Even previously commissioned components can be scaled by our method as shown in this chapter by carefully designing the remanufactured additions to the component. This will ensure continued scalability of the component in the future.

### 4.3 Computational cost

The method presented involves the computational cost of constructing the surrogate model used for solving the parametric optimization problem given by Equation (4.1). The remainder of the method given by Algorithms 1 and 2 depends on using the surrogate model for making predictions in the design and parameter spaces and incurs relatively low computational cost. A breakdown of the computational cost for obtaining the set of scalable optimal designs for the TRS remanufacturing example is shown in Table 4–5. It can be seen that obtaining surrogate models for the design requirements (objective  $\hat{f}(\mathbf{x}; \mathbf{p})$  and constraint functions  $\hat{\mathbf{g}}(\mathbf{x}; \mathbf{p})$ ) amounts for 89% of the computational cost and scales with the number of samples needed depending on the dimensionality of the problem. The total cost of 40.9 days is justified for problems such as the ones discussed in this thesis due to the relatively long lifecycle of aerospace components which spans decades. The potential benefits of extending the useful lifecycles of aerospace components by a few

Table 4–5: Breakdown of total computational cost

Algorithm	Step	function evaluations	evaluation time	iterations	iteration time	total time
<b>1</b>	inputs	1492	35 min	-	-	36.3 days
	step 6	-	-	1200	320 s	4.4 days
	sub-step 7	≈160	2 s	1	320 s	
<b>2</b>	step 3	-	-	20000	0.84 s	4.7 Hrs
	sub-step 4-8	≈140	6 ms	1	0.84 s	
<b>Total cost</b>			40.9 days			

years via remanufacturing outweigh the computational cost of our method. However, the same cannot be said for problems involving the design of products with short lead times and frequently changing requirements (such as patient-specific medical equipment).

#### 4.4 Summary

This chapter presented a set-based design method that utilizes surrogate-assisted numerical optimization, post-optimality analysis, and monotonicity-driven transition rules related to additive or subtractive manufacturing to generate a set of scalable optimal designs. This method can be used either for considering several different alternative solutions during initial design stages where requirements are still open-ended or, in combination with remanufacturing, to implement redesigns that can satisfy changed requirements, extending thus the useful lifetime of components and systems.

An application example was used to demonstrate the method for the remanufacturing design of an aeroengine component: a set of parametric optimal design solutions was generated and scalable design solutions were successfully extracted. Since we are only considering a finite, albeit large, amount of designs, we used convex hulls to quantify

approximately the cardinality of the sets in order to make relative comparisons among them.

The scalability assessment assumed monotonicity of component volume in the considered design variables, which is not uncommon in many engineering design and remanufacturing problems. Nevertheless, the scalability assessment presented here may be extendable to include nonmonotonic variables by performing localized monotonicity assessments in the design space.

We defined scalability in terms of volume of material added during remanufacturing. Equation (4.14) is a specific case of scalability where remanufacturing by AM or subtractive manufacturing is being considered. However, scalability does not necessarily depend on manufacturing constraints exclusively. There are other effects that could be considered for general remanufacturing problems such as cost, tooling, and assembly. These effects can be accommodated by our framework for identifying scalable designs by defining the appropriate functions in terms of the Jacobian components to substitute the constraint function given by Equation (4.14) in Algorithm 2.

This work enables design changes by remanufacturing through the derived transition rules. The formulated optimization problem is driven by thermomechanical performance requirements that impact its useful lifetime and how it can be extended.

The framework presented by this chapter addressed the problem of designing a product for remanufacturing due to a change in requirements. However, the changes in requirements that have been considered so far are based on the current state of the component being remanufactured and its desired state after the requirement change is implemented. In practice, requirement changes occur several times throughout a product's lifecycle or

development process. Decisions about the optimal remanufacturing design strategy should incorporate past and current knowledge about the state of the component and its requirements. This helps designers address future changes in the requirements that are not immediately apparent.

This chapter only considers incorporating scalability and flexibility by proxy in product design to mitigate changing requirements. Alternatively, designs can incorporate design margins to passively absorb changing requirements. This is an example of robust design. The following chapter investigates a tool for strategically allocating both design flexibility and robustness to address changing requirements by the use of design margins.

## Chapter 5

### Design margin quantification and optimization

This chapter describes a novel design tool for quantifying the level of overdesign in a product via the notion of excess and buffer which constitute the design margins. These definitions are quantified in a multi-dimensional parameter space using rigorous mathematical tools. Design margins determine the product's capacity for absorbing change and therefore its robustness. However, excessive margins result in overdesign and severe operational costs.

We therefore develop a design method for strategically allocating design margins without compromising the product's reliability and ability to meet uncertain requirements.

The method in this chapter is demonstrated using an application example from the industry for the remanufacturing of a TRS. The thermomechanical model described in Section 3.1 along with the load case in Section 3.2.2 is used to define the design variables and changing parameters involved in the remanufacturing design problem. Remanufacturing is performed by AM using laser DED. The design space considered in this problem is finite since the decision variables are categorical. This kind of problem was chosen to show importance of high level conceptual decisions on the performance of a design as requirements change gradually.

We begin by defining the method for obtaining the set-based solutions for arbitrary design and parameter spaces in Section 5.1. We then demonstrate the method for the

remanufacturing of the TRS in Section 5.2. We present the corresponding results in Section 5.3. We provide some insights and conclusions about the uses and limitations of the developed framework in Section 5.5.

## 5.1 Method

We consider a product design problem where requirements change several times throughout the product's lifecycle or development process. In this chapter, we will refer to these two time periods as the product cycle for conciseness. Requirements changes occur after a defined period of time (referred to as an epoch) has elapsed.

A decision regarding product redesign is made at the beginning of each epoch depending on a number of factors. The factors driving these decisions include capability, buffer, excess, and reliability. We will formally define these terms.

### 5.1.1 Relevant design metrics

The parameter space in which our design metrics are defined is the set of values assumed by the changing parameters driving the requirements and feasibility criteria. The parameters vector  $\mathbf{p} = [p_1 \ p_2 \ \cdots \ p_n]^T$  is defined in the multi-dimensional parameter space  $\mathbf{p} \in \mathbb{R}^n$ , where  $n$  is the number of changing parameters.

The feasibility criteria are formulated as constraints that the design must satisfy  $\mathbf{t} - \mathbf{g}_f(\mathbf{p}) \leq 0$ , where  $\mathbf{t}$  is a vector of threshold values that the constraint function  $\mathbf{g}_f(\mathbf{p})$  must exceed. Unlike requirements, feasibility constraints are fixed throughout the product cycle. Capability is defined as the set of possible values of a design parameter for which feasibility is maintained [26]:

$$C = \{\mathbf{p} \in \mathbb{R}^n \mid \mathbf{t} - \mathbf{g}_f(\mathbf{p}) \leq 0\}. \quad (5.1)$$

We represent requirements using a joint probability density function (PDF)  $F_{\mathbf{X}}(\mathbf{p})$ [51, 95–97]. Knowing the capability of a design and the corresponding requirement joint PDF we can calculate reliability in terms of the probability that the design satisfies the requirement [98, 99]:

$$\mathbb{P}(\mathbf{p} \in C) = \frac{\int_{C \cap R} F_{\mathbf{X}}(\mathbf{p}) d\mathbf{p}}{\int_R F_{\mathbf{X}}(\mathbf{p}) d\mathbf{p}}. \quad (5.2)$$

$R$  in the denominator is the requirement set defined by the set of parameter values that yield significant probability density values from the joint PDF used.

The requirement set  $R$  for a uniform PDF is given by

$$F_{\mathbf{X}}(\mathbf{p}) = \begin{cases} \frac{1}{\prod_{j=1}^n |b_j - a_j|} & \text{for } \mathbf{a} \leq \mathbf{p} \leq \mathbf{b}, \\ 0 & \text{for } \mathbf{p} < \mathbf{a} \text{ or } \mathbf{p} > \mathbf{b} \end{cases}, \quad (5.3)$$

where  $\mathbf{a}$  and  $\mathbf{b}$  are the lower and upper bound vectors, respectively. The requirement set  $R$  comprises the values of  $\mathbf{p}$  that lie within the bounds  $\mathbf{a}$  and  $\mathbf{b}$ :

$$R = \{\mathbf{p} \in \mathbb{R}^n \mid \mathbf{a} \leq \mathbf{p} \leq \mathbf{b}\}. \quad (5.4)$$

The Gaussian joint PDF is given by

$$F_{\mathbf{X}}(\mathbf{p}) = \frac{\exp\left(-\frac{1}{2}(\mathbf{p} - \boldsymbol{\mu})^T \boldsymbol{\Sigma}^{-1} (\mathbf{p} - \boldsymbol{\mu})\right)}{\sqrt{(2\pi)^n |\boldsymbol{\Sigma}|}}, \quad (5.5)$$

where  $\boldsymbol{\mu}$  is the mean vector and  $\boldsymbol{\Sigma}$  is the covariance matrix. In this chapter, we assume that parameters are uncorrelated. This results in a diagonal covariance matrix given by  $\boldsymbol{\Sigma} = \text{diag}(\boldsymbol{\sigma})$ , where  $\boldsymbol{\sigma}$  is the standard deviation vector. In the denominator of Equation (5.5),

$|\Sigma| \equiv \det \Sigma \equiv \prod_{j=1}^n \sigma_j$ . The requirement set  $R$  is defined as the values of  $\mathbf{p}$  that result in a probability density level greater than that at the  $3\sigma$  isocontour of a Gaussian  $F_{\mathbf{X}}(\mathbf{p})$ .

The requirement set  $R$  is defined as the values of  $\mathbf{p}$  that result in a probability density level greater than that at the  $3\sigma$  isocontour of a Gaussian  $F_{\mathbf{X}}(\mathbf{p})$

$$R = \left\{ \mathbf{p} \in \mathbb{R}^n \mid F_{\mathbf{X}}(\mathbf{p}) \geq F_{\mathbf{X}}(\boldsymbol{\mu} + [3\sigma_1 \ 0 \ \cdots \ 0]^T) \right\}. \quad (5.6)$$

This is because the probability that a random parameter value sampled from a Gaussian PDF lies outside the  $3\sigma$  isocontour is small ( $< 0.3\%$ ). Note that  $F_{\mathbf{X}}(\boldsymbol{\mu} + [3\sigma_1 \ 0 \ \cdots \ 0]^T) \equiv F_{\mathbf{X}}(\boldsymbol{\mu} + [0 \ 3\sigma_2 \ \cdots \ 0]^T) \equiv F_{\mathbf{X}}(\boldsymbol{\mu} + [0 \ 0 \ \cdots \ 3\sigma_n]^T)$  since they all lie on the  $3\sigma$  isocontour.

We use Monte Carlo integration to approximate the integrals in Equation (5.2). Monte Carlo integration based on Latin hypercube (LH) sampling has the advantage of scaling well with dimensionality of the problem [100, 101], while importance sampling can be used in the case of a Gaussian PDF to enhance the accuracy of the approximation [96, 98, 102]. The Monte Carlo approximation is given by

$$\mathbb{P}(\mathbf{p} \in C) \approx \frac{\sum_{i=1}^{|C \cap R|} F_{\mathbf{X}}(\mathbf{p}_i)}{\sum_{i=1}^{|R|} F_{\mathbf{X}}(\mathbf{p}_i)}. \quad (5.7)$$

We use a two-dimensional parameter space to illustrate the calculation of the reliability represented by  $\mathbb{P}(\mathbf{p} \in C)$  as shown in Figure 5–1. Only the Monte Carlo samples that lie within the set  $C$  (shown in green) are evaluated by  $F_{\mathbf{X}}(\mathbf{p})$  and summed to compute the numerator of Equation (5.7). All the Monte Carlo samples shown in Figure 5–1 are evaluated by  $F_{\mathbf{X}}(\mathbf{p})$  and summed to compute the denominator of Equation (5.7).

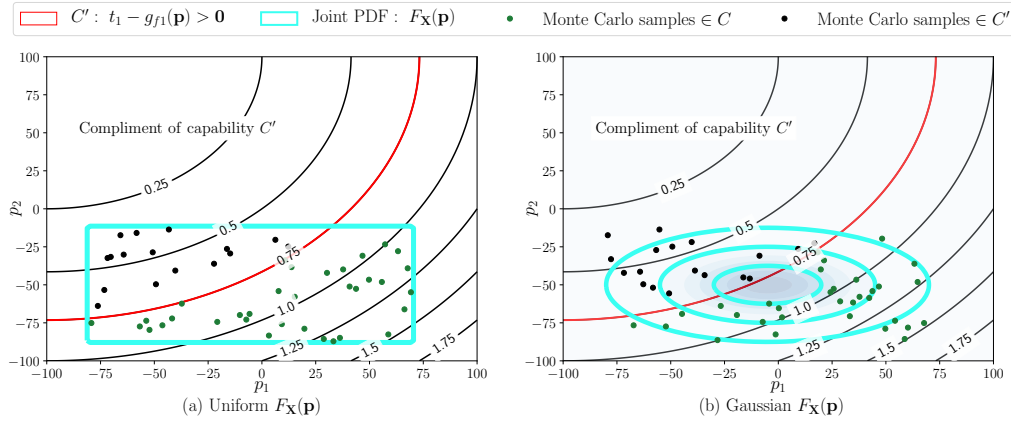


Figure 5–1: Contours of feasibility constraint  $g_{f1}(\mathbf{p})$  in the two-dimensional parameter space for uniform (left) and Gaussian (right) PDFs

We can now define buffer in the parameter space as the portion of the capability of a design reserved for changes in requirements [26]. In other words, the buffer set is defined as the intersection of sets  $C$  and  $R$

$$B = \{\mathbf{p} \in \mathbb{R}^n \mid \mathbf{p} \in (C \cap R)\}. \quad (5.8)$$

Excess is defined as the portion of the parameter space reserved for possible future changes in the requirements [26]. This is reflected by the set of parameter values that lie within the capability set  $C$  but not within the requirement set (given by its compliment  $R'$ ). Mathematically this is expressed as follows

$$E = \{\mathbf{p} \in \mathbb{R}^n \mid \mathbf{p} \in (C \cap R')\}. \quad (5.9)$$

Note that  $B \cup E = C$ .

The sets  $R$ ,  $E$ , and  $B$  are shown in Figure 5–2 for the two-dimensional parameter space example.

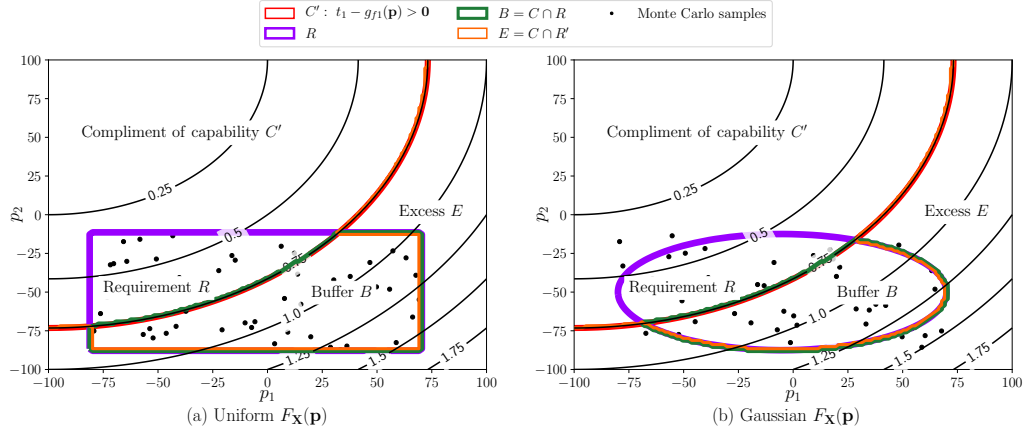


Figure 5–2: Buffer and excess relative to a feasibility constraint  $g_{f1}(\mathbf{p})$  in the two-dimensional parameter space for uniform (left) and Gaussian (right) PDFs

We are particularly interested in minimizing excess during the product redesign cycle.

We estimate excess using the volume of the set  $E$

$$V_E \approx \frac{1}{N} \sum_{i=1}^N H(\mathbf{p}_i), \text{ where } H(\mathbf{p}_i) = \begin{cases} 1 & \text{if } \mathbf{p}_i \in E \\ 0 & \text{otherwise} \end{cases}, \quad (5.10)$$

where  $N$  is the number of samples from the parameter space used for the integration. We can use the reliability calculation and the volume of the requirement set  $R$  to estimate the volume of the set  $E$  indirectly.

The volume of  $R$  can be computed analytically for a uniform or Gaussian distribution using the corresponding hyper-rectangle or hyper-ellipsoid, respectively:

$$V_R = \begin{cases} \prod_{j=1}^n |b_j - a_j| & \text{if } F_{\mathbf{X}}(\mathbf{p}) \text{ is uniform} \\ \frac{\pi^2}{32} \prod_{j=1}^n |b_j - a_j| & \text{if } F_{\mathbf{X}}(\mathbf{p}) \text{ is Gaussian} \end{cases}. \quad (5.11)$$

We can then estimate the volume of set  $C$  similarly:

$$V_C \approx \frac{1}{N} \sum_{i=1}^N H(\mathbf{p}_i), \text{ where } H(\mathbf{p}_i) = \begin{cases} 1 & \text{if } \mathbf{p}_i \in C \\ 0 & \text{otherwise} \end{cases}. \quad (5.12)$$

The reliability approximates the percentage of  $R$  in  $C$  and can be used as a proxy for the volume of  $C \cap R$  such that  $V_{C \cap R} \approx \mathbb{P}(\mathbf{p} \in C) \times V_R$ .  $V_E$  can now be approximated using

$$V_E \approx V_C - \mathbb{P}(\mathbf{p} \in C) \times V_R. \quad (5.13)$$

Having defined all the required design metrics, we can formulate an optimization problem to minimize excess subject to reliability constraints. We first set the context of the optimization problem in terms of an epoch-era analysis [36] to simulate changing requirements throughout the product cycle.

### 5.1.2 Epoch-era analysis for product redesign

We consider the redesign of component as time progresses through its development and lifecycle. At every epoch in the product cycle, the designer must make redesign decisions. The set of redesign choices is defined as the set of non-negative integers  $\mathcal{D} = \{0, 1, 2, \dots, q\}$ . In practice, the set of redesign choices is derived from a finite number of feasible design alternatives that the designer wishes to include in their decision-making. Chaining multiple choices together results in a design arc defined as

$$\mathbf{D} = [D_1 \ D_2 \ \dots \ D_o] \quad (5.14)$$

with possible choices  $D_d \in \mathcal{D}^o$ , where  $1 \leq o \leq q + 1$ . The maximum number of redesign choices  $q + 1$  dictates the maximum number of possible design arc combinations where no

choice is repeated twice. For example, consider a case where there are  $q + 1 = 3$  redesign choices given by  $\mathcal{D} = \{0, 1, 2\}$ . If  $o = 1$  then we have three possible design arcs:  $\mathbf{D} = [0]$ ,  $\mathbf{D} = [1]$ , and  $\mathbf{D} = [2]$ . For  $o = 2$ , 6 additional design arcs can be obtained by permuting any 2 choices from  $\mathcal{D}$ . Similarly, another 6 design arcs can be obtained for  $o = 3$  by permutating all three choices in set  $\mathcal{D}$ . A total of 15 design arcs can be obtained from  $\mathcal{D} = \{0, 1, 2\}$ .

These enumerations comprise a set of possible design arcs given by  $\Omega_D$ . The cardinality of  $\Omega_D$  for a different number of redesign choices  $q + 1$  is given by

$$\Omega_D = \sum_{o=1}^{q+1} {}^{q+1}P_o, \quad (5.15)$$

where  ${}^{q+1}P_o$  is the number of ways for obtaining an ordered subset of  $o$  elements from a set of  $q + 1$  elements.

We define a product cycle with  $m$  number of epochs. We assume that the number of epochs is given a priori by the number of design revisions that a product encounters during its cycle. A decision vector  $S \in \mathcal{S}^m$  is defined, where  $S_k$  is the decision at epoch  $k$  and  $\mathcal{S}$  is the set of possible decisions. In this chapter, we consider discrete redesign choices only. A non-negative integer value from the set  $\mathcal{S}$  implies a redesign choice. A value of  $-1$  implies no redesign is performed at the current epoch. This means that  $\mathcal{S} = \{-1, 0, 1, 2, \dots, q\}$ , where  $q + 1$  is the number of available redesign choices.

The vector of all the decisions taken throughout the product cycle is referred to as the decision arc and is defined as

$$\mathbf{S} = [S_1 \ S_2 \ \dots \ S_m]. \quad (5.16)$$

The set of possible decision arcs that can be generated from the set of possible decisions  $S$  may be restricted by constraints. A feasible decision arc cannot contain repeated choices. For example, the decision arc  $\mathbf{S} = [0 \ -1 \ 0 \ -1 \ 1 \ 3]$  is infeasible since the choice 0 was repeated twice. Furthermore, the first decision cannot be empty, i.e.  $S_1 \neq -1$ . This is because a decision arc must begin with some sort of design. These restrictions make computing the cardinality of the set of possible decision arcs  $\Omega_S$  challenging. However, the cardinality of  $\Omega_S$  is given by a finite positive integer similar to  $\Omega_D$  in Equation (5.15).

A corresponding design arc can be extracted from the decision arc by removing all negative elements from  $\mathbf{S}$  to obtain  $\mathbf{D} = [0 \ 2 \ 1 \ 3]$ .

For each epoch  $k$ , a design arc can be extracted by excluding values from  $\mathbf{S}$  that are equal to  $-1$ . The vector  $\mathbf{D}_k = [D_1 \ D_2 \ \dots \ D_o]$  represents this design arc at epoch  $k$  where the elements of  $\mathbf{D}$  are non-negative integers and  $o$  is the number of non-negative integers in  $\mathbf{S}_k = [S_1 \ S_2 \ \dots \ S_k]$  up to the current epoch  $k$ . E.g., for a problem with  $m = 6$  epochs and the decision arc

$$\mathbf{S} = [0 \ -1 \ 2 \ -1 \ 1 \ 3],$$

the following  $m = 6$  design arcs can be extracted

$$\text{epoch } k = 1 : \mathbf{D}_1 = [0]$$

$$\text{epoch } k = 2 : \mathbf{D}_2 = [0]$$

$$\text{epoch } k = 3 : \mathbf{D}_3 = [0 \ 2]$$

$$\text{epoch } k = 4 : \mathbf{D}_4 = [0 \ 2]$$

$$\text{epoch } k = 5 : \mathbf{D}_5 = [0 \ 2 \ 1]$$

$$\text{epoch } k = 6 : \mathbf{D}_6 = [0 \ 2 \ 1 \ 3].$$

It follows that a design arc cannot feature repeated elements due to the uniqueness of the positive decision arc elements. Each design arc has a unique capability set  $C_k$ .

We now define the requirement arc as a vector of joint PDFs that has  $m$  elements, where each element corresponds to a different epoch  $k$  with a requirement joint PDF  $F_{Xk}(\mathbf{p})$ :

$$\mathbf{R} = [F_{X1}(\mathbf{p}) \ F_{X2}(\mathbf{p}) \ \cdots \ F_{Xm}(\mathbf{p})]. \quad (5.17)$$

The reliability at epoch  $k$  (quantified by  $\mathbb{P}_k(\mathbf{p} \in C_k)$ ) can be calculated from  $C_k$  (derived from  $\mathbf{D}_k$ ) and the requirement joint PDF  $F_{Xk}(\mathbf{p})$ :

$$\mathbf{P}(\mathbf{p} \in \mathbf{C}) = [\mathbb{P}_1(\mathbf{p} \in C_1) \ \mathbb{P}_2(\mathbf{p} \in C_2) \ \cdots \ \mathbb{P}_m(\mathbf{p} \in C_m)], \quad (5.18)$$

where  $\mathbf{C}$  is the vector of capability sets  $\mathbf{C} = [C_1 \ C_2 \ \cdots \ C_m]$ .

At each epoch, a reliability threshold  $P_k$  is defined to yield a vector of reliability thresholds defined as

$$\mathbf{P}_{th} = [P_1 \ P_2 \ \cdots \ P_m]. \quad (5.19)$$

The volume of the excess set  $V_{Ek}$  at epoch  $k$  can be calculated from  $C_k$  and the requirement joint PDF  $F_{Xk}(\mathbf{p})$  using Equations (5.9) and (5.13). The cumulative excess for a given decision arc can be formulated as

$$E_c = \sum_{k=1}^m V_{Ek}. \quad (5.20)$$

In addition to the decision arc  $\mathbf{S}$ , a fixed design concept  $c_t \in \mathcal{C}$  is defined. The concept type  $c_t$  is selected at the very beginning of the epoch-era analysis and does not change throughout epochs. The choice of  $c_t$  dictates the list of redesign choices available for the remainder of the product cycle.  $\mathcal{C}$  is the set of concept choices whose elements are all

non-negative integers. This means that  $\mathcal{C} = \{0, 1, 2, \dots, r\}$ , where  $r + 1$  is the number of available concept choices.

Each concept type  $C_t$  has a set of redesign options  $\mathcal{D}_t$  with  $q + 1$  redesign choices attached to it. Accordingly, each concept type  $c_t$  will have a set of possible design arcs  $\Omega_{Dt}$  and a set of possible decision arcs  $\Omega_{St}$ . The combination of a concept and design arc  $\{c, \mathbf{D}\}$  will be referred to as a design arc in this chapter for conciseness. Similarly, the combination of a concept and a decision arc  $\{c, \mathbf{S}\}$  will be referred to as a decision arc.

The cardinality of the set of possible design arcs  $\Omega_{cD}$  can be obtained by summing up the cardinalities of all sets  $\Omega_{Dt}$  for a given set of concept choices  $\mathcal{C}$ :

$$\beta = |\Omega_{cD}| = \sum_{t=0}^r |\Omega_{Dt}|, \quad (5.21)$$

where  $|\Omega_{Dt}|$  can be obtained from Equation (5.15) given the number of redesign choices  $q + 1$  for each concept. The set of possible design arcs represents the feasible design space, defined as

$$\Omega_{cD} = \left\{ \{c, \mathbf{D}\}_1, \{c, \mathbf{D}\}_2, \dots, \{c, \mathbf{D}\}_\beta \right\}. \quad (5.22)$$

We now formulate an optimization problem for choosing the optimal concept  $c$  and decision arc  $\mathbf{S}$  such that cumulative excess  $E_c$  is minimized subject to reliability constraints:

$$\underset{\{c, \mathbf{S}\} \in \Omega_{cS}}{\text{minimize}} \quad f(c, \mathbf{S}; \mathbf{R}) = E_c = \sum_{k=1}^m V_{Ek}(c, \mathbf{D}_k; F_{\mathbf{X}k}(\mathbf{p})) \quad (5.23)$$

$$\text{subject to } \mathbf{g}(c, \mathbf{S}; \mathbf{R}) = \mathbf{P}_{th} - \mathbf{P}(\mathbf{p} \in \mathbf{C}) \leq \mathbf{0},$$

where  $\Omega_{cS}$  denotes the set of all feasible decision arcs.

We also define a second optimization problem to simulate the effect of accumulating costs that can be incurred throughout a product's lifecycle (since we focus on aerospace

applications in this thesis, we consider the cumulative weight of the decision arc to be a proxy of cumulative costs such as fuel [103]):

$$\begin{aligned} \underset{\{c, \mathbf{S}\} \in \Omega_{cS}}{\text{minimize}} \quad & f(c, \mathbf{S}) = W_c = \sum_{k=1}^m W_k(c, \mathbf{D}_k) \\ \text{subject to} \quad & \mathbf{g}(c, \mathbf{S}; \mathbf{R}) = \mathbf{P}_{th} - \mathbf{P}(\mathbf{p} \in \mathbf{C}) \leq \mathbf{0}. \end{aligned} \quad (5.24)$$

Minimizing the cumulative excess is equivalent to minimizing an equally weighted sum of all excesses for all epochs. The designer may substitute the objective functions in Equations (5.24) and (5.23) with a weighted sum of excess or cost to place emphasis on a particular epoch during the development process.

The optimization problems are solved for a given requirement arc that is generated by random sampling techniques at the start of the product cycle. If the problem is solved in real-time as requirements are updated progressively, a nonanticipativity constraint can be added to the problem to include requirements up to and including the current epoch  $k$  [44].

The problems in Equations (5.23) and (5.24) are solved using the mixed variable optimization variant of the MADS algorithm provided by the NOMAD software package [77]. This implementation of MADS allow users to specify categorical constraints via an extended poll subroutine and is called during the search step [104, 105].

The solutions of the problems given by Equations (5.23) and Equations (5.24) depend on the requirement arc. Requirements are subject to change; therefore, we adopt a set-based design strategy to address such requirement changes.

### 5.1.3 Set-based design to mitigate changing requirements

Our set-based design strategy involves sampling requirement arcs  $\mathbf{R}$  from the set of possible requirement arcs  $\Omega_R = \{\mathbf{R}_1, \mathbf{R}_2, \dots, \mathbf{R}_s\}$  with  $s = |\Omega_R|$ . A sample  $\mathbf{R}_w$  involves populating the requirement arc with joint PDFs at each epoch  $k$  by selecting a joint PDF from the set of possible joint PDFs  $\mathcal{R} = \{F_{\mathbf{X}1}(\mathbf{p}), F_{\mathbf{X}2}(\mathbf{p}), \dots, F_{\mathbf{X}v}(\mathbf{p})\}$ , where  $v$  is the number of joint PDF choices.

Populating the set  $\mathcal{R}$  is based on the designer's experience and previous knowledge in requirements. E.g., if requirements are expected to become well-defined over time around a certain value in the parameter space, then a matrix of mean vectors  $\mathbf{M} = [\mu_1, \mu_2, \dots, \mu_e]^T$  and a matrix of standard deviation vectors  $\Sigma = [\sigma_1, \sigma_2, \dots, \sigma_e]^T$  can be obtained by interpolating between the initial and final states for each type of joint PDF. An example of this kind of interpolation search strategy is shown in Figure 5–3 for the same 2D example used in Section 5.1.1.

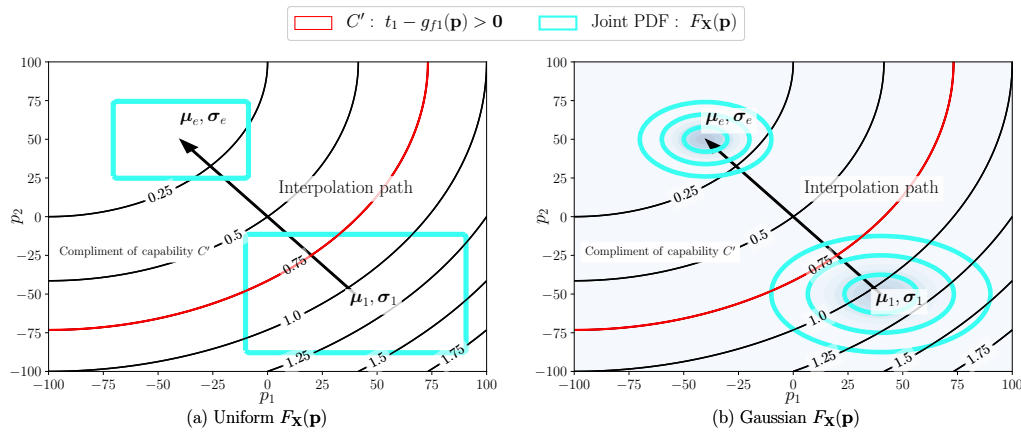


Figure 5–3: Contours of feasibility constraint  $g_{f1}(\mathbf{p})$  in the 2 dimensional parameter space for different types of requirement PDFs

The set of possible requirement arcs  $\Omega_R$  spans every possible combination of the joint PDFs (their type, mean, and standard deviation) and has a cardinality given by

$$v = e \times e \times |\mathcal{T}| \text{ and}$$

$$s = |\Omega_R| = m^v, \text{ respectively.}$$

Note that a small increase in the number of joint PDF types would cause the cardinality of  $\Omega_R$  to increase rapidly since interpolation levels would have to increase as well. For practical reasons, only the first few elements of  $\Omega_R$  will be used during the set-based design analysis and  $s$  will be capped at  $10^5$  samples. The rationale behind these choices is explained in Section 5.3.

The first set-based solution is obtained by solving the optimization problem in Equation (5.23) for every requirement arc sample  $\mathbf{R}_w$ . The corresponding optimal design arc  $\mathbf{D}^*$  can be extracted from the optimal decision arc  $\mathbf{S}^*$  to obtain the solution  $\mathbf{x}^*(\mathbf{R}_w) = \{c^*, \mathbf{D}^*\}(\mathbf{R}_w)$ . This is done in order to compare the overdesign levels across different design arcs rather than different decision arcs.

The set of parametric optimal design arcs with respect to excess is defined as

$$S_E^* = \{\mathbf{x}^*(\mathbf{R}_1), \mathbf{x}^*(\mathbf{R}_2) \cdots, \mathbf{x}^*(\mathbf{R}_s)\}. \quad (5.25)$$

We track the number of times a specific design arc  $\{c, \mathbf{D}\}_\lambda$  appears as the solution to the parametric optimization problem in  $S_E^*$  via a design optimality vector defined as

$$\mathbf{N}_E = [n_{E1} \ n_{E2} \ \cdots \ n_{E\beta}], \quad (5.26)$$

where  $n_{E\lambda}$  is equal to the number of times design arc  $\{c, \mathbf{D}\}_\lambda \in \Omega_{cD}$  is repeated in  $S_E^*$ . The top  $\alpha$  design arcs with the largest  $n_{E\lambda}$  values are selected as the set-based solution

representing the best performing design arcs in terms of minimizing overdesign:

$$S_E = \{\{c, \mathbf{D}\}_{E1}, \{c, \mathbf{D}\}_{E2} \dots, \{c, \mathbf{D}\}_{E\alpha}\}. \quad (5.27)$$

The rationale for selecting  $\alpha$  will be described in the context of the application example presented in this chapter.

where the subscript  $E1, E2, \dots, E\alpha$  indicates that the corresponding base is ordered by frequency in the set of parametric optimal solutions with respect to excess  $S_E^*$ .

The same procedure is repeated for the optimization problem in Equation (5.24) to obtain the second set-based solution comprising the best performing design arcs in terms of minimizing weight throughout the product cycle:

$$S_W = \{\{c, \mathbf{D}\}_{W1}, \{c, \mathbf{D}\}_{W2} \dots, \{c, \mathbf{D}\}_{W\alpha}\}. \quad (5.28)$$

The pseudo-algorithm in Algorithm 3 summarizes the above described method for obtaining the sets of optimal design arcs with respect to excess or weight.

The third set-based solution is the robust design set. We define robustness of a design arc by the number of design arcs satisfied from the set  $\Omega_R$ . We evaluate the feasibility of each design arc  $\{c, \mathbf{D}\}_\lambda$  sampled from the set of possible design arcs in Equation (5.22) with respect to every requirement arc  $\mathbf{R}_w$  in  $\Omega_R$ .

We generate all the possible decision arcs for a given design arc  $\{c, \mathbf{D}\}_\lambda$  by randomly inserting the  $-1$  decisions into the design arc vector until it has the same number of elements as the number of epochs  $m$ . We show this using an example. Consider the design

---

**Algorithm 3:** Pseudo-algorithm for obtaining the set of optimal design arcs  $S_E$ 


---

**Input:** Set of possible requirement arcs  $\Omega_R$ , Set of possible design arcs  $\Omega_{cD}$

**Output:**  $S_E$

- 1 Initialize  $S_E^* = \emptyset$
  - 2 Initialize design optimality vector  $\mathbf{N}_E = [n_{E1}, n_{E2}, \dots, n_{E\beta}] = \mathbf{0}$
  - 3 **for**  $w = 1, 2, \dots, s$  **do**
  - 4     Solve the parametric optimization problem in Equation (5.23) to obtain optimal decision arc  $\mathbf{x}_S^*(\mathbf{R}_w) = \{c^*, \mathbf{S}^*\}(\mathbf{R}_w)$
  - 5     Obtain optimal design arc from optimal decision arc by eliminating  $-1$  components of  $\mathbf{S}^*$  to obtain  $\mathbf{x}^*(\mathbf{R}_w) = \{c^*, \mathbf{D}^*\}(\mathbf{R}_w)$
  - 6     Augment  $S_E^* \leftarrow S_E^* \cup \{\mathbf{x}^*(\mathbf{R}_w)\}$
  - 7     Find the unique index  $\lambda$  corresponding to  $\{c^*, \mathbf{D}^*\}$  in  $\Omega_{cD}$
  - 8     Award design arc  $n_{E\lambda} \leftarrow n_{E\lambda} + 1$
  - 9 Sort design optimality vector  $\mathbf{N}_E$  in descending order
  - 10 Select top  $\alpha$  design arcs with largest values  $n_{E\lambda}$  to obtain set of optimal designs
- $$S_E = \{\{c, \mathbf{D}\}_{E1}, \{c, \mathbf{D}\}_{E2}, \dots, \{c, \mathbf{D}\}_{E\alpha}\}$$
- 

arc  $\{c = 1, \mathbf{D} = [2 \ 0 \ 1]\}$ . The possible decision arcs are

$$\{c = 1, \mathbf{S} = [2 \ -1 \ -1 \ -1 \ 0 \ 1]\}$$

$$\{c = 1, \mathbf{S} = [2 \ -1 \ -1 \ 0 \ -1 \ 1]\}$$

$$\{c = 1, \mathbf{S} = [2 \ -1 \ -1 \ 0 \ 1 \ -1]\}$$

$$\{c = 1, \mathbf{S} = [2 \ -1 \ 0 \ -1 \ 1 \ -1]\}$$

$$\{c = 1, \mathbf{S} = [2 \ -1 \ 0 \ 1 \ -1 \ -1]\}$$

$$\{c = 1, \mathbf{S} = [2 \ 0 \ -1 \ 1 \ -1 \ -1]\}$$

$$\{c = 1, \mathbf{S} = [2 \ 0 \ 1 \ -1 \ -1 \ -1]\},$$

yielding the set of decision arcs with  $\zeta = 7$  elements

$$S_{cD} = \{\{c, \mathbf{S}\}_1, \{c, \mathbf{S}\}_2, \dots, \{c, \mathbf{S}\}_7\}. \quad (5.29)$$

Feasibility in terms of reliability is checked for every possible decision arc  $\{c, \mathbf{S}\}_\gamma$  for a given  $\{c, \mathbf{D}\}_\lambda$  and requirement arc  $\mathbf{R}_w$  using  $\mathbf{g}(c_\gamma, \mathbf{S}_\gamma; \mathbf{R}_w) = \mathbf{P}_{th} - \mathbf{P}(\mathbf{p} \in \mathbf{C}) \leq \mathbf{0}$ . If any of the decision arcs in set  $S_{cD}$  satisfy all the reliability constraints then the corresponding design arc  $\{c, \mathbf{D}\}_\lambda$  is considered feasible. We track the number of requirement arcs satisfied by design arc  $\{c, \mathbf{D}\}_\lambda$  through a robustness vector defined as

$$\mathbf{N}_R = [n_{R1} \ n_{R2} \ \cdots \ n_{R\beta}] , \quad (5.30)$$

where  $n_{R\lambda}$  is equal to the number of requirement arcs  $\mathbf{R}_w \in \Omega_R$  satisfied by design arc  $\{c, \mathbf{D}\}_\lambda \in \Omega_{cD}$ . The top  $\alpha$  design arcs with the largest  $n_{R\lambda}$  values are considered as the robust design set:

$$S_R = \{\{c, \mathbf{D}\}_{R1}, \{c, \mathbf{D}\}_{R2}, \dots, \{c, \mathbf{D}\}_{R\alpha}\}, \quad (5.31)$$

The final set-based solution is the flexible design set. All possible design arcs in set  $\Omega_{cD}$  are ranked in terms of filtered outdegree, defined as the number of possible design arcs that can be obtained from the current design arc by adding exactly one redesign choice that is not an element of the current design arc. The filtered outdegree for a design arc  $\{c, \mathbf{D}\}_\lambda$  having  $o$  elements and  $q + 1$  redesign choices is equal to

$$O_{F_\lambda} = q - o. \quad (5.32)$$

The top  $\alpha$  design arcs in terms of filtered outdegree are considered as the flexible design set:

$$S_F = \{\{c, \mathbf{D}\}_{F1}, \{c, \mathbf{D}\}_{F2}, \dots, \{c, \mathbf{D}\}_{F\alpha}\}. \quad (5.33)$$

The pseudo-algorithm in Algorithm 4 summarizes the above described method for obtaining the sets of robust and flexible design arcs.

**Algorithm 4:** Pseudo-algorithm for obtaining the sets of robust  $S_R$  and flexible  $S_F$  design arcs

**Input:** Set of possible requirement arcs  $\Omega_R$ , Set of possible design arcs  $\Omega_{cD}$   
**Output:**  $S_R, S_F$

- 1 Initialize design robustness vector  $\mathbf{N}_R = [n_{R1}, n_{R2}, \dots, n_{R\beta}] = \mathbf{0}$
- 2 Initialize design flexibility vector  $\mathbf{N}_F = [O_{F_1}, O_{F_2}, \dots, O_{F_\beta}] = \mathbf{0}$
- 3 **for**  $\lambda = 1, 2, \dots, \beta$  **do**
- 4     Enumerate possible decision arcs from  $\{c, \mathbf{D}\}_\lambda$  to obtain the set  
 $S_{cD} = \{\{c, \mathbf{S}\}_1, \{c, \mathbf{S}\}_2, \dots, \{c, \mathbf{S}\}_\zeta\}$
- 5     **for**  $w = 1, 2, \dots, s$  **do**
- 6         **for**  $\gamma = 1, 2, \dots, \zeta$  **do**
- 7             **if**  $\mathbf{g}(c_\gamma, \mathbf{S}_\gamma; \mathbf{R}_w) \leq \mathbf{0}$  **then**
- 8                 Award design arc  $n_{R\lambda} \leftarrow n_{R\lambda} + 1$
- 9                 **break**
- 10     Compute filtered outdegree for  $\{c, \mathbf{D}\}_\lambda$  using  $O_{F_\lambda} = q - o$
- 11     Update design flexibility vector with  $O_{F_\lambda}$
- 12     Sort design robustness vector  $\mathbf{N}_R$  in descending order
- 13     Select top  $\alpha$  design arcs with largest values  $n_{R\lambda}$  to obtain set of robust design arcs  $S_R = \{\{c, \mathbf{D}\}_{R1}, \{c, \mathbf{D}\}_{R2}, \dots, \{c, \mathbf{D}\}_{R\alpha}\}$
- 14     Sort design flexibility vector  $\mathbf{N}_F$  in descending order
- 15     Select top  $\alpha$  design arcs with largest values  $O_{F_\lambda}$  to obtain set of flexible design arcs  $S_F = \{\{c, \mathbf{D}\}_{F1}, \{c, \mathbf{D}\}_{F2}, \dots, \{c, \mathbf{D}\}_{F\alpha}\}$

Figure 5–4 depicts the flowdiagram of our method for obtaining the set-based solutions  $S_E, S_W, S_R$ , and  $S_F$ . We will now describe the tradespace used to visualize and compare these solution sets.

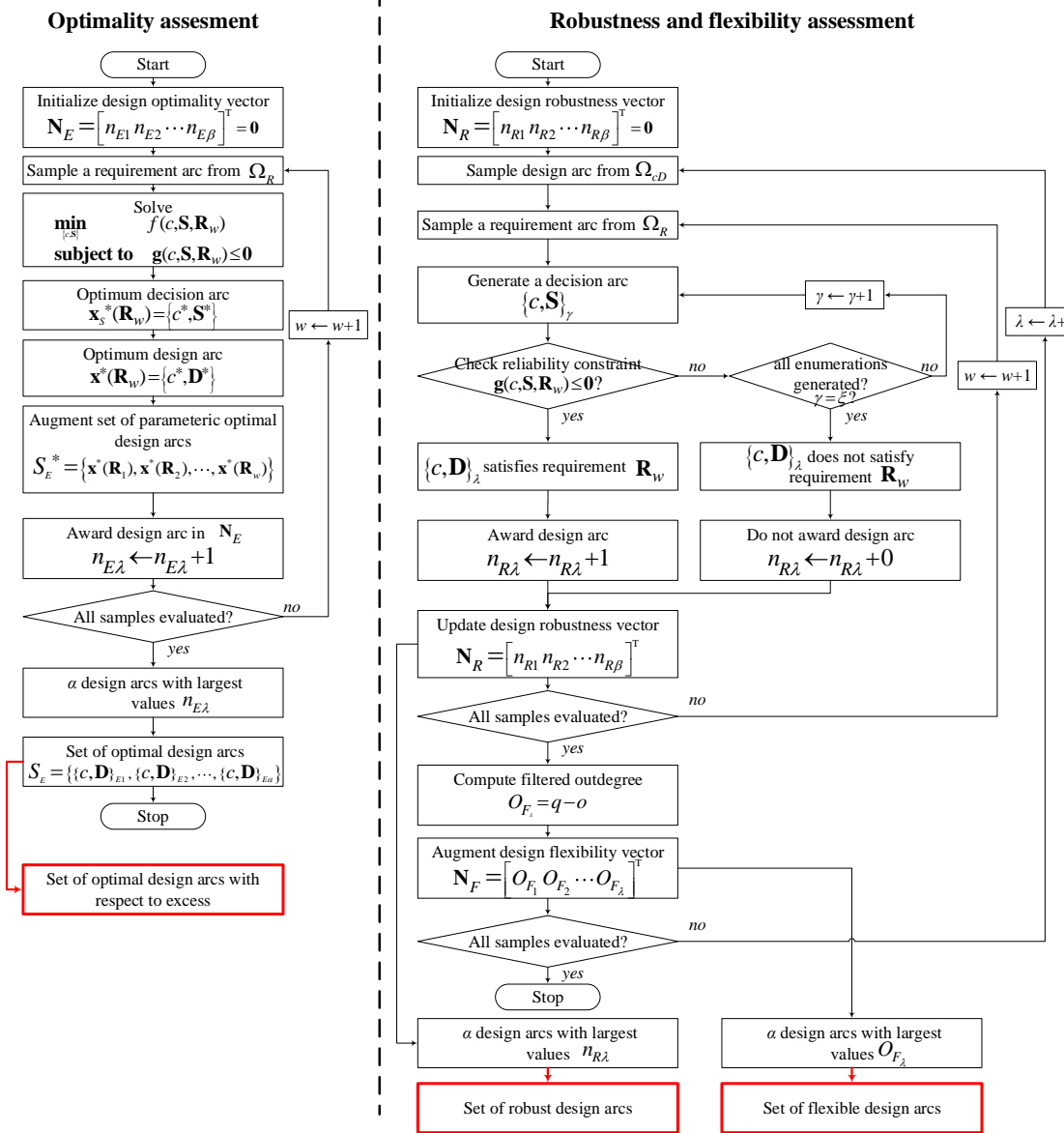


Figure 5–4: Flowdiagram of method for generating set-based solutions

pare these solution sets.

### 5.1.4 Tradespace exploration for comparing solution sets

A tradespace can be constructed by plotting the volume of the capability set  $V_c$ , against the weight of each design arc. The volume of capability set is chosen as the utility since it is independent of the requirement joint PDF. This allows for a fair comparison between different design arcs. The design arcs in sets  $S_E, S_W, S_R$ , and  $S_F$  are also projected on the same tradespace to compare their relative position and size. The Pareto front for such a tradespace can be approximated by solving the bi-objective problem

$$\underset{\{c, \mathbf{D}\} \in \Omega_{cD}}{\text{minimize}} \quad [-V_c(c, \mathbf{D}) \quad W(c, \mathbf{D})]. \quad (5.34)$$

The positioning of sets  $S_E, S_W, S_R$ , and  $S_F$  relative to the Pareto set obtained by solving the problem in Equation (5.34) provides a measure for the dominance of each design set.

## 5.2 Application

We demonstrate the importance of minimizing excess in aerospace structural component design by applying our method to the design of a turbine rear structure (TRS). The TRS is remanufactured using AM to increase the stiffness of the outer casing in response to changing requirements (temperature loads). The TRS can undergo multiple redesigns as given by a decision arc during its product cycle. We will now describe the available stiffener designs.

### 5.2.1 Stiffener deposition on TRS outercasing

Stiffeners deposited on the outer casing of the TRS involve the application of heat to the outer casing (the substrate) to deposit material on its surface. The application of large heat fluxes to the surface of a structure causes residual distortion that persists after the removal of the heat source. This residual distortion affects the structural performance

of the structure when loads are applied during operation. As a result, the residual stresses experienced by the TRS due to the deposition of a stiffener must be quantified prior to any structural analysis.

The residual stress tensors that persist after removal of the equivalent heat flux are stored and applied during the analysis of the thermal load case.

There are several stiffener geometries available to the designer of the TRS given by the set of possible design arcs  $\Omega_{cD}$ . We draw inspiration from commonly used standard stiffener designs to generate concepts and design choices [106]. The design space consists of three possible deposition concepts  $C = \{0, 1, 2\}$ . Concept  $c = 0$  is a “wavy” stiffener that has three redesign choices  $D_0 = \{0, 1, 2\}$ . Concept  $c = 1$  is a “hatched” stiffener that has five redesign choices  $D_1 = \{0, 1, 2, 3, 4\}$ . Concept  $c = 2$  is a “tubular” stiffener that has four redesign choices  $D_2 = \{0, 1, 2, 3\}$ . We illustrate these concepts and their respective design choices in Figure 5–5.

We compute the cardinality of the set  $\Omega_{cD}$  using Equations (5.15) and (5.21) for this problem as follows:

$$\text{concept } c_0 : |\Omega_{D0}| = 15$$

$$\text{concept } c_1 : |\Omega_{D1}| = 325$$

$$\text{concept } c_2 : |\Omega_{D2}| = 64$$

$$\beta = |\Omega_{cD}| = 15 + 325 + 64 = 404.$$

We now describe the analysis steps for obtaining the capability of a given stiffener design arc as a function of the thermal temperature loads.

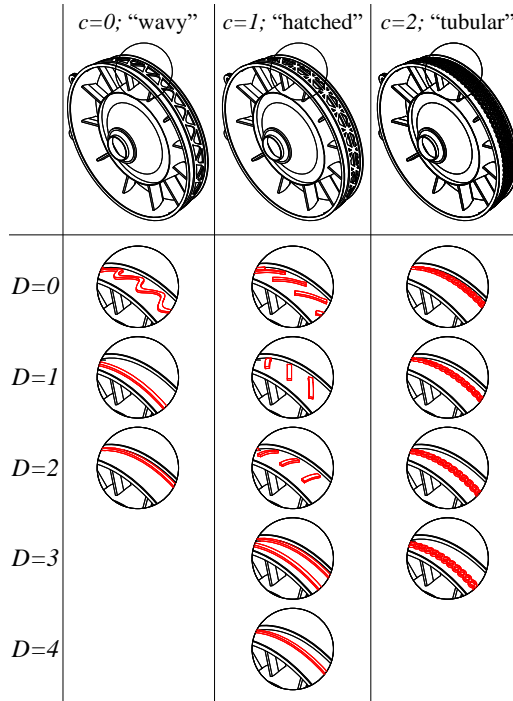


Figure 5–5: Illustration of possible concepts and redesign choices for TRS stiffener

### 5.2.2 Loadcase description

The changing temperature loads in Figure 3–6b are used to specify the vector of changing parameters  $\mathbf{p} = [T_1 \ T_2 \ T_3 \ T_4]^T$ .

We constrain our study to a parameter space defined by

$$\mathbf{p} \in \{\mathbf{p} : \mathbf{p}_{\text{nominal}} - \mathbf{p}_{\text{deviation}} \leq \mathbf{p} \leq \mathbf{p}_{\text{nominal}} + \mathbf{p}_{\text{deviation}}\},$$

where  $\mathbf{p}_{\text{nominal}} = [350 \ 425 \ 410 \ 580]^T$  and  $\mathbf{p}_{\text{deviation}} = [100 \ 100 \ 100 \ 100]^T$ .

In this chapter, we assume that there is no correlation between these temperature loads. This is because environmental factors such as the atmospheric temperature are

independent of the exhaust temperature. This allows us to assume that the requirement PDFs defined in Section 5.1.1 feature diagonal covariance matrices.

The TRS design is constrained by a safety factor (equal to 2.8) against low-cycle fatigue failure or yielding, whichever occurs first. The thermal load case is cycled and is used to compute the expected fatigue life of the TRS using low-cycle fatigue calculations described in Section 3.2.3.

The structural analysis is performed using a FE simulation model which is computationally expensive. As a result, for every design arc in  $\Omega_{cD}$ , we build a surrogate model for computing  $n_{\text{safety}}(\mathbf{p})$ . The surrogate is built using data obtained from the simulation model for 25 Latin hypercube samples of the parameter space for every design in  $\Omega_{cD}$ . This resulted in  $25 \times 404 = 10100$  samples for the surrogate. For this particular problem, the sampling was sufficient to capture the effect of increasing the internal temperature loads ( $T_2, T_3$ , and  $T_4$ ) on decreasing  $n_{\text{safety}}$  due to the expansion of the outer casing of the TRS. We use an open source surrogate model library to build and optimize the hyperparameters of an ensemble of surrogates [84].

Mathematically, we formulate the constraint on the safety factor as

$$t_1 - \hat{g}_{f1}(\mathbf{p}) \leq 0. \quad (5.35)$$

We visualize this constraint in the 4-dimensional parameter space for a few example design arcs in Section 5.3.1.

### 5.2.3 Loadcase requirements

Having defined the 4-dimensional parameter space, we now define the joint PDFs and the corresponding requirement arcs that can be constructed from them.

While we consider only two types ( $\mathcal{T} = \{\text{uniform}, \text{Gaussian}\}$ ), any distribution can be used in our method.

All design metrics and requirements are scaled between 0 and 1. This helps when making comparisons between different design arcs in terms of hypervolume of sets with 0 being the minimum possible hypervolume and 1 being the maximum possible hypervolume.

We use  $e = 5$  interpolation levels to obtain  $\mathbf{M}$  and  $\Sigma$ . The initial mean and standard deviation vectors are  $\boldsymbol{\mu}_1 = [0.15 \ 0.80 \ 0.80 \ 0.85]^T$  and  $\boldsymbol{\sigma}_1 = [0.1875 \ 0.125 \ 0.125 \ 0.1875]^T$ , respectively. The final mean and standard deviation vectors are  $\boldsymbol{\mu}_5 = [0.85 \ 0.20 \ 0.20 \ 0.15]^T$  and  $\boldsymbol{\sigma}_5 = [0.375 \ 0.250 \ 0.250 \ 0.375]^T$ , respectively. As a result, the matrix of interpolated mean and standard deviation vectors is

$$\mathbf{M} = \begin{bmatrix} \boldsymbol{\mu}_1^T \\ \boldsymbol{\mu}_2^T \\ \boldsymbol{\mu}_3^T \\ \boldsymbol{\mu}_4^T \\ \boldsymbol{\mu}_5^T \end{bmatrix} = \begin{bmatrix} 0.15 & 0.80 & 0.80 & 0.85 \\ 0.325 & 0.65 & 0.65 & 0.675 \\ 0.5 & 0.5 & 0.5 & 0.5 \\ 0.675 & 0.35 & 0.35 & 0.325 \\ 0.85 & 0.20 & 0.20 & 0.15 \end{bmatrix}$$

and

$$\Sigma = \begin{bmatrix} \boldsymbol{\sigma}_1^T \\ \boldsymbol{\sigma}_2^T \\ \boldsymbol{\sigma}_3^T \\ \boldsymbol{\sigma}_4^T \\ \boldsymbol{\sigma}_5^T \end{bmatrix} = \begin{bmatrix} 0.1875 & 0.125 & 0.125 & 0.1875 \\ 0.234375 & 0.15625 & 0.15625 & 0.234375 \\ 0.28125 & 0.1875 & 0.1875 & 0.28125 \\ 0.328125 & 0.21875 & 0.21875 & 0.328125 \\ 0.375 & 0.250 & 0.250 & 0.375 \end{bmatrix},$$

respectively.

We consider a remanufacturing design problem with  $m = 6$  epochs. The number of choices  $v$  for  $\mathcal{R} = \{F_{\mathbf{X}1}(\mathbf{p}), F_{\mathbf{X}2}(\mathbf{p}), \dots, F_{\mathbf{X}v}(\mathbf{p})\}$  and the cardinality  $s$  for  $\Omega_R$  are

$$v = e \times e \times |\mathcal{T}| = 5 \times 5 \times 2 = 50 \text{ and}$$

$$s = |\Omega_R| = m^v = 6^{50}, \text{ respectively.}$$

Only the first few elements of  $\Omega_R$  will be used during the set-based design analysis and  $s$  will be capped at  $10^5$  samples. This is because the set-based solutions stabilize and do not change after sampling  $4 \times 10^4$  requirement arc samples.

While we chose the following reliability threshold vector for this example

$$\mathbf{P}_{th} = [0.01 \ 0.1 \ 0.3 \ 0.3 \ 0.8 \ 0.9]^T,$$

a design engineer can test and react to different lifecycle scenarios by adjusting the reliability threshold.

All problem sets, parameters, and constants are summarized in Table 5–1.

### 5.3 Results and discussion

We initiate the solution of the remanufacturing design problem by obtaining the capability set for every design arc in the set  $\Omega_{cD}$ . We begin by investigating a few selected design arcs from  $\Omega_{cD}$ . We then solve a single optimization problem to minimize excess for a given requirement arc from the set  $\Omega_R$ . We then present the set-based results for the problem using a tradespace.

Table 5–1: Example sets, parameters, and constants

Set/parameter/constant	Notation	Units	Value
Set of concept choices	$C$	-	$\{0, 1, 2\}$
Set of deposit choices for concept 0	$\mathcal{D}_0$	-	$\{0, 1, 2\}$
Set of deposit choices for concept 1	$\mathcal{D}_1$	-	$\{0, 1, 2, 3, 4\}$
Set of deposit choices for concept 2	$\mathcal{D}_2$	-	$\{0, 1, 2, 3\}$
Cardinality of design arcs	$\beta$	-	404
Number of epochs	$m$	-	6
Interpolation levels	$e$	-	5
Set of PDF types	$\mathcal{T}$	-	{"Uniform", "Gaussian"}
PDF initial mean	$\mu_1$	-	$[0.15 \ 0.80 \ 0.80 \ 0.85]^T$
PDF initial standard deviation	$\sigma_1$	-	$[0.1875 \ 0.125 \ 0.125 \ 0.1875]^T$
PDF final mean	$\mu_e$	-	$[0.85 \ 0.20 \ 0.20 \ 0.15]^T$
PDF final standard deviation	$\sigma_e$	-	$[0.375 \ 0.250 \ 0.250 \ 0.375]^T$
Reliability threshold	$P_{th}$	-	$[0.01 \ 0.1 \ 0.3 \ 0.3 \ 0.8 \ 0.9]^T$
Number of PDFs	$v$	-	50
Number of requirement arc samples	$s$	-	$10^5$
Nacelle temperature	$T_1$	°C	$300 \pm 100$
Tailcone temperature	$T_2$	°C	$400 \pm 100$
Rotor temperature	$T_3$	°C	$450 \pm 100$
Gas surface temperature	$T_4$	°C	$600 \pm 100$
Laser power	$P_{laser}$	W	3806
Laser beam radius	$r_l$	mm	14.2
Scanning speed	$u$	mm/s	5.0
Stiffener height	$S_{height}$	mm	10.0
Laser penetration depth	$D_p$	mm	5.0
Number of deposition layers	$n_d$	-	2
Threshold low-cycle fatigue safety factor	$t_1$	-	2.8

### 5.3.1 Example for calculating the design properties of a given design arc

We use two design arcs from the set  $\Omega_{cD}$  to visualize feasible space, capability and reliability in two-dimensional projections of the four-dimensional parameter space in Figure 5–6. The design arcs and their filtered outdegree, weight, and hypervolume of capability are reported in Table 5–2.

We can observe that the addition of one more deposit to the design arc  $\{c = 1, \mathbf{D} = [1, 2, 4]\}$  increases its performance in terms of capability and reliability. However, this

Table 5–2: Results obtained for example design arcs

Index	Design arc	Filtered outdegree	Weight	PDF mean vector	PDF standard deviation vector	PDF type	Reliability	Set volume		
$\lambda$	$\{c, \mathbf{D}\}$	$O_F$	$W$	$\boldsymbol{\mu}$	$\boldsymbol{\sigma}$	$t$	$\mathbb{P}(\mathbf{p} \in C)$	$V_R$	$V_E$	$V_C$
109	$\{c = 1, \mathbf{D} = [1, 2, 4]\}$	2	13.9 kg	$\begin{bmatrix} 0.375 \\ 0.5 \\ 0.5 \\ 0.625 \end{bmatrix}$	$\begin{bmatrix} 0.375 \\ 0.125 \\ 0.125 \\ 0.375 \end{bmatrix}$	“Uniform”	0.3089	0.0352	0.529	0.540
110	$\{c = 1, \mathbf{D} = [1, 2, 4, 0]\}$	1	18.5 kg	$\begin{bmatrix} 0.375 \\ 0.5 \\ 0.5 \\ 0.625 \end{bmatrix}$	$\begin{bmatrix} 0.375 \\ 0.125 \\ 0.125 \\ 0.375 \end{bmatrix}$	“Uniform”	0.759	0.0352	0.856	0.883

comes at the cost of an additional 4.6 kg of weight, reduced filtered outdegree, and an additional excess (0.327 and 0.335 for uniform and Gaussian PDFs, respectively). The choice of design arc for a given requirement arc is driven by the need to maintain reliability while minimizing excess.

Chen et al. use capability indices to quantify reliability of a design [49]. While there are similarities between their approach and ours for estimating reliability, there are some notable differences. Their calculation of reliability is based on estimating the moments of a normal PDF that is assumed to govern the feasibility criteria (referred to as performance) in the presence of changing parameters (referred to as noise variables). Reliability (referred to as capability index) is computed as the distance from the expected value of feasibility to the nearest requirement bound (upper or lower bound) normalized by  $3\sigma$ . Our approach differs due to its ability to directly relate changing parameters to the feasibility criteria

via a response surface. Reliability is then estimated for arbitrary requirement PDFs using Monte Carlo integration.

We will apply epoch-era analysis and numerical optimization to solve related design decision problems.

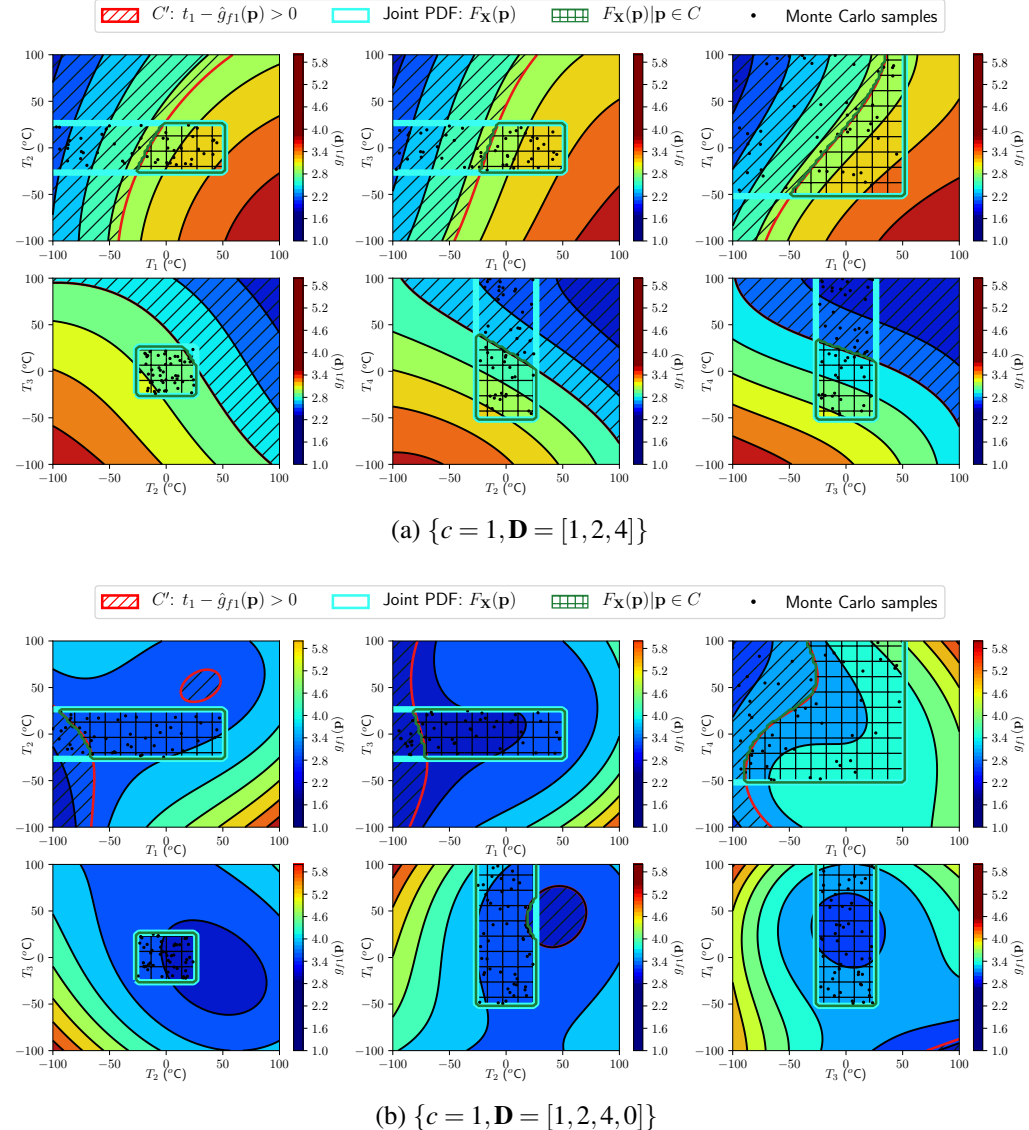


Figure 5–6: 2D projections of isocontours of safety factor in the parameter space

### 5.3.2 Combinatorial optimization with respect to a requirement arc

We solve the problem given by Equation (5.23) using a mixed variable programming version of MADS [77]. The requirement arc  $\mathbf{R}_w$  used for this problem is given in Table 5–3.

Table 5–3: Requirement arc  $\mathbf{R}_w$

PDF Index $F_X \in \mathcal{R}$	PDF mean vector $\mu$				PDF interval vector $\sigma$				PDF type $t$
	0.5	0.5	0.5	0.5	0.1875	0.125	0.125	0.1875	
$F_{X36}$	[0.5 0.5 0.5 0.5]				[0.1875 0.125 0.125 0.1875]				"Gaussian"
$F_{X50}$	[0.85 0.2 0.2 0.15]				[0.375 0.25 0.25 0.375]				"Gaussian"
$F_{X1}$	[0.15 0.8 0.8 0.85]				[0.1875 0.125 0.125 0.375]				"uniform"
$F_{X46}$	[0.85 0.2 0.2 0.15]				[0.1875 0.125 0.125 0.1875]				"Gaussian"
$F_{X13}$	[0.5 0.5 0.5 0.5]				[0.28125 0.1875 0.1875 0.28125]				"uniform"
$F_{X31}$	[0.325 0.65 0.65 0.675]				[0.1875 0.125 0.125 0.1875]				"Gaussian"

We plot the results from various decision arcs across epochs in Figure 5–7. The first decision arc,  $\{c = 1, \mathbf{S} = [2, 1, -1, -1, 0, -1]\}$  (shown in red) does not satisfy the reliability constraint as shown in Figure 5–7a. This is because at epoch  $k = 3$  the reliability of the corresponding design arc  $\{c = 1, \mathbf{D} = [2, 1]\}$  is almost 0. No redesign occurred at epoch  $k = 3$  when it was needed to increase the reliability of the design arc above the threshold.

We investigate another decision arc  $\{c = 1, \mathbf{S} = [4, 1, 0, 2, -1, 3]\}$  (shown in green) that achieves very high reliability throughout all epochs. However, this comes at the cost of increased cumulative excess (green shaded area in Figure 5–7b) relative to that of the first decision arc (red shaded area).

We solve the optimization problem given by Equation (5.23) to get the third decision arc  $\{c = 1, \mathbf{S} = [4, 1, 0, 2, -1, 3]\}$  (shown in blue) which is optimal in terms of minimizing excess. This decision arc has lower reliability relative to the second decision arc (shown in

green) but lower cumulative excess and therefore less overdesign. We provide the values of the objective function and reliability constraints for all three decision arcs in Table 5–4.

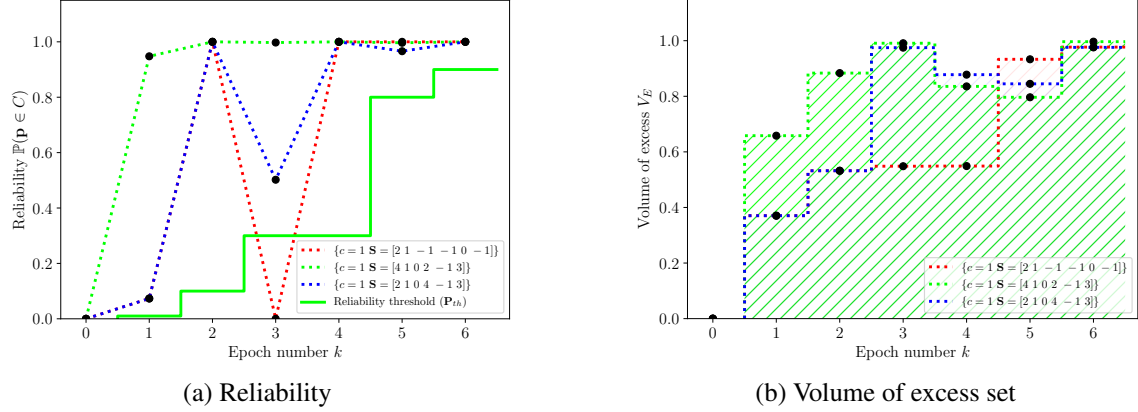


Figure 5–7: Visualization of decision arcs

Finally, the example in this section shows that the order of redesign steps can have a significant impact on the reliability and level of overdesign throughout epochs. The second and third decision arcs contain the same redesign choices but in different order. The differences between them in terms of reliability and cumulative excess reflect the importance of choosing the right order of redesign operations when considering multiple epochs.

We will now solve similar optimization problems for every requirement arc in the set  $\Omega_R$  to obtain a set-based solution.

### 5.3.3 Set-based design and tradespace exploration

We solve an optimization problem similar to the one in Section 5.3.2 for every requirement arc in  $\Omega_R$  to obtain the set of parametric optimal design arcs when optimizing for cumulative excess ( $S_E^*$ ) and cumulative weight ( $S_W^*$ ). We plot the frequency of each

Table 5–4: Results obtained for example decision arcs

Index	Decision arc $\{c, \mathbf{S}\}$	Objective value $f(c, \mathbf{S}; \mathbf{R})$	Reliability constraints $\mathbf{g}(c, \mathbf{S}; \mathbf{R})$	Design arc $\{c, \mathbf{D}\}$
1	$\{c = 1,$ $\mathbf{S} = [2, 1, -1, -1, 0, -1]\}$	3.91	$\begin{bmatrix} -0.063 \\ -0.9 \\ 0.3 \\ -0.7 \\ -0.2 \\ -0.1 \end{bmatrix}$	$\{c = 1,$ $\mathbf{D} = [2, 1, 0]\}$
2	$\{c = 1,$ $\mathbf{S} = [4, 1, 0, 2, -1, 3]\}$	5.16	$\begin{bmatrix} -0.94 \\ -0.9 \\ -0.70 \\ -0.7 \\ -0.20 \\ -0.1 \end{bmatrix}$	$\{c = 1,$ $\mathbf{D} = [4, 1, 0, 2, 3]\}$
3	$\{c = 1,$ $\mathbf{S} = [2, 1, 0, 4, -1, 3]\}$	4.58	$\begin{bmatrix} -0.063 \\ -0.9 \\ -0.20 \\ -0.7 \\ -0.17 \\ -0.1 \end{bmatrix}$	$\{c = 1,$ $\mathbf{D} = [2, 1, 0, 4, 3]\}$

design arc in  $S_E^*$  and  $S_W^*$  and normalize it by the cardinality  $\beta$  of set  $\Omega_R$  to obtain the histograms shown in Figure 5–8.

We also evaluated the flexibility and robustness of each design arc in  $\Omega_{cD}$  using the method in Figure 5–4 and Algorithm 4. We present the set of design arcs ordered with respect to robustness and flexibility in Figures 5–9a and 5–9b, respectively.

We select the top  $\alpha = 10$  design arcs in Figure 5–8 as our set of optimal design arcs for  $S_E$  and  $S_W$ . In practice,  $\alpha$  is constrained by the designers' ability to concurrently develop and analyze the selected set of design arcs. For example, development time and cost may limit the designers to a maximum of 10 designs that can be concurrently developed at any given time during development. Furthermore, the 10th design arc in  $S_E$  and  $S_W$  given by

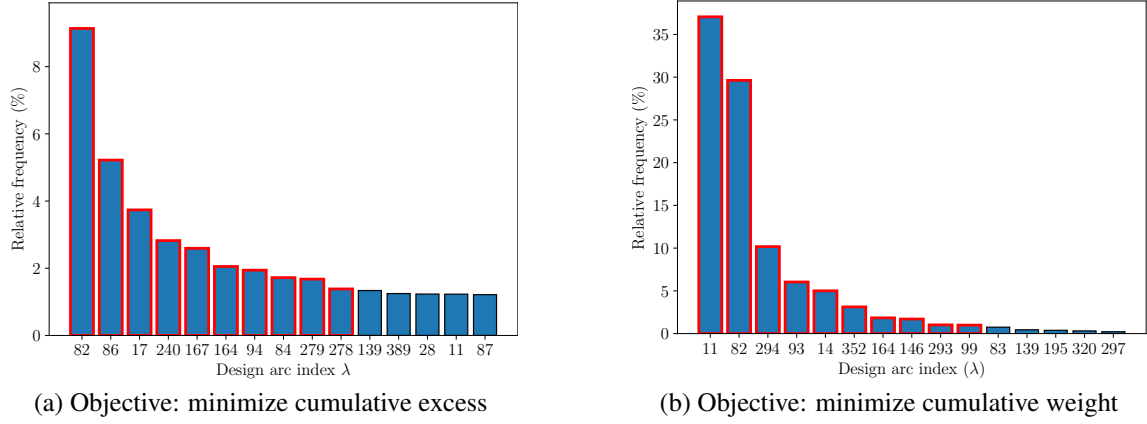


Figure 5–8: Distribution of design arcs in optimization driven set-based solutions

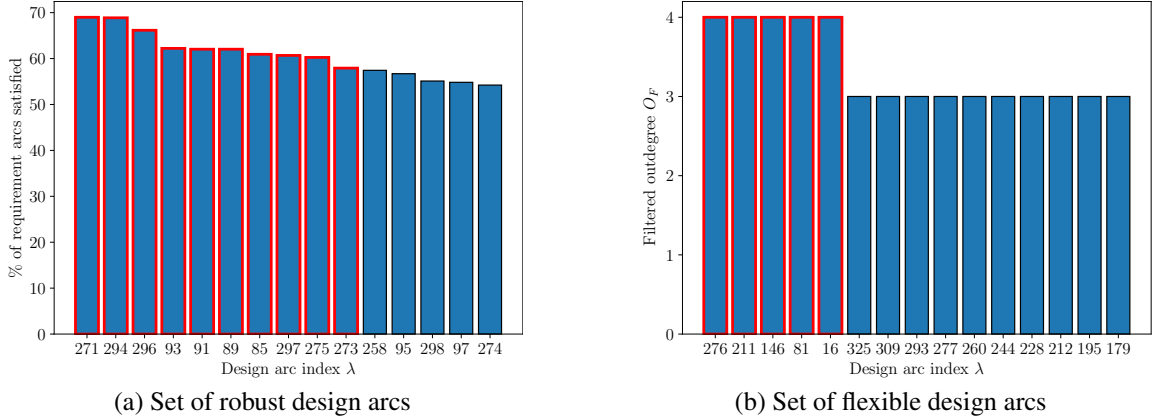


Figure 5–9: Distribution of design arcs in set-based solutions

$\lambda = 278$  and  $\lambda = 99$ , respectively is representative of the lower ranking design arcs since they all have comparable frequencies.

A similar rationale is used for obtaining the set of robust design arcs  $S_R$ . Only  $\alpha = 5$  design arcs are used to construct the flexible set-based solution  $S_F$  since we focus on those designs with maximum possible filtered outdegree  $O_F = 4$ .

The sets  $S_E$ ,  $S_W$ ,  $S_R$ , and  $S_F$  are visualized on a tradespace. This tradespace is described by a utility (given by the volume of the capability set  $V_c$ ) and cost (given by the weight  $W$ ) and is shown in Figure 5–10. The Pareto front for the tradespace is obtained by solving the problem in Equation (5.34).

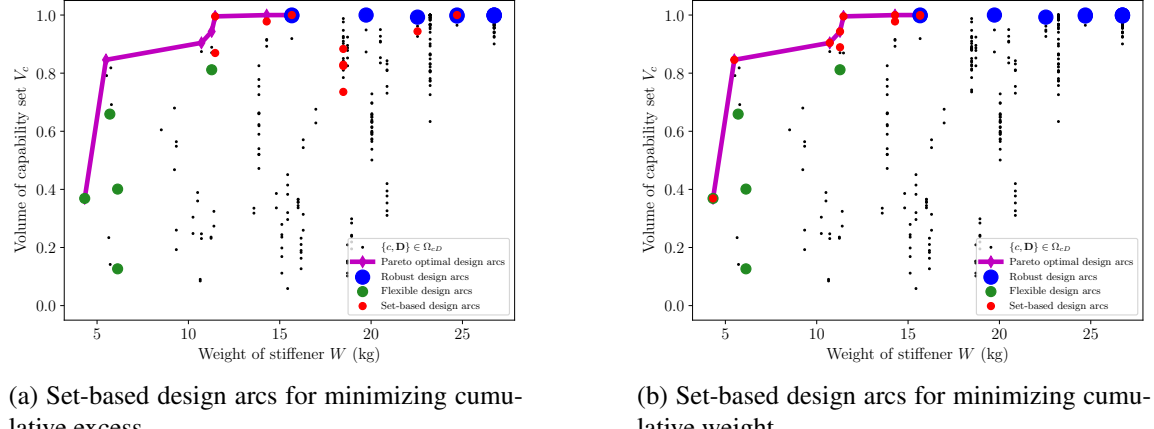


Figure 5–10: Tradespace of set-based design arcs

From the tradespace, we can draw several insights. The flexible set-based solution minimizes cost but also minimizes utility. In contrast, the robust design set maximizes utility but also maximizes the cost. The set-based solution obtained by optimization with respect to excess or weight balances utility with cost. The weight-optimized set-based solution has a larger spread than the excess-optimized solution. We quantify the size of the set-based solutions by their convex hulls. We use the convex hull to calculate three metrics: the area spanned by the set, location of the set given by its centroid and proximity to the Pareto front given by the distance from the centroid to the nearest Pareto point [94]. We report these convex hull metrics in Table 5–5.

Table 5–5: Set-based solution comparison

Quantity	Set of feasible design arcs $\Omega_{cD}$		Set of robust design arcs $S_R$		Set of flexible design arcs $S_F$		Set of optimal design arcs $S_E$		Set of optimal design arcs $S_W$	
Coordinates	$W$	$V_c$	$W$	$V_c$	$W$	$V_c$	$W$	$V_c$	$W$	$V_c$
Lower	4.32	0.059	15.66	0.992	4.32	0.127	11.47	0.736	4.32	0.369
Upper	26.74	1.00	26.74	1.00	11.28	0.812	24.70	1.00	15.66	1.00
Set centroid	14.02	0.533	22.34	0.998	6.86	0.516	16.35	0.920	11.15	0.868
$V_{\text{hyper-rectangle}}$	1		0.0038		0.226		0.166		0.339	
$V_{\text{convhull}}$	0.758		0.0026		0.092		0.104		0.126	
$\%V_{\text{feasible}}$	75.8%		0.26%		9.2%		10.4%		12.6%	
$D_{\text{Pareto}}$	0.421		0.298		0.172		0.0904		0.0432	

We can see that the set of optimal design arcs with respect to cumulative excess  $S_E$  occupies 10.4% of the objective space which is comparable to that occupied by the set of flexible design arcs  $S_F$  and greater than that occupied by the set of robust design arcs  $S_R$ . The set of optimal design arcs with respect to cumulative weight  $S_W$  occupies 12.6% which is comparable to the volume of  $S_E$ . Furthermore, we can see that the sets of optimal design arcs  $S_E$  and  $S_W$  are close to the Pareto front, which is expected since these sets aim to balance robustness with flexibility which are indirectly related to capability and weight.

Although there are a lot of commonalities between sets  $S_E$  and  $S_W$ , there are some notable differences. Set  $S_E$  favors designs that have higher capability when compared to  $S_W$  as given by the  $V_c$  coordinate of their centroids of 0.920 and 0.868, respectively. The discrepancy between the two sets is due to the fact that weight, or in more general cases, cost does not necessarily translate to excess. For example two designs of identical weight may have different excesses due to differences in the placement of the stiffener. It is therefore important that the designers carefully select their desired metric for optimization in the problem given by Equation (5.23).

We aim to analyze the top 6 designs in sets  $S_E$  and  $S_W$  in Figure 5–8 by using the reduced tradespace shown in Figure 5–11. We also display the geometry of the deposits that belong to these designs in Tables 5–6 and 5–7.

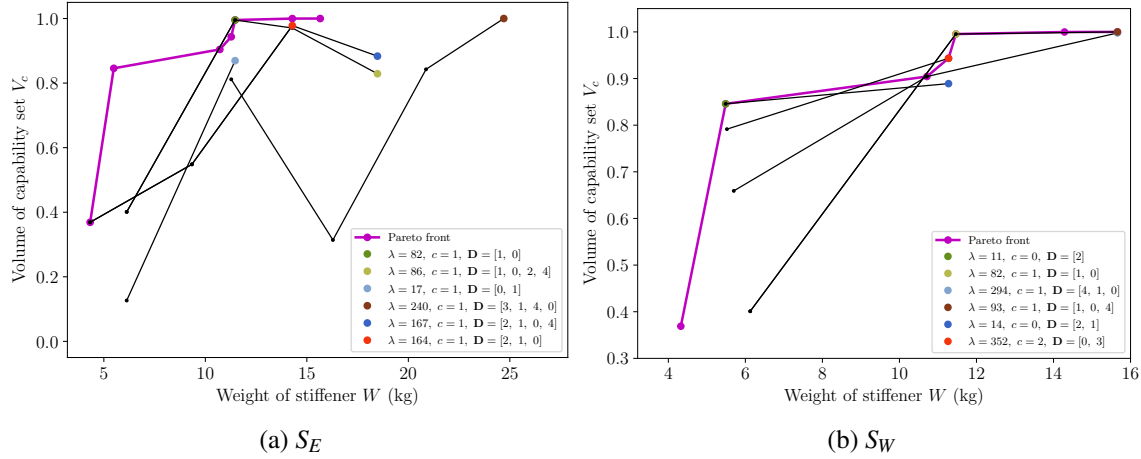


Figure 5–11: Reduced tradespace of solutions in sets  $S_E$  and  $S_W$

Figure 5–11a and Table 5–6 show that the top 6 designs in  $S_E$  share the same concept  $c = 1$ . The top two designs ( $\lambda = 82$  and  $\lambda = 86$ ) share the first two deposit choices  $D_1 = 1$  and  $D_2 = 0$ . The runner-up design ( $\lambda = 86$ ) adds two additional deposits to the top ranked design ( $\lambda = 82$ ). From Figure 5–11a, it can be seen that the addition of two more deposits to the top ranked design reduced the capability  $V_c$ . This is because of the overstiffening of the TRS outer casing by the addition of more stiffeners. This overstiffening reduced the fatigue life of the outer casing by inducing concentrated tensile stresses in the unreinforced gaps between the stiffener deposits. The third ranked design ( $\lambda = 17$ ) is identical in geometry to the top ranked designs as seen in Table 5–6 but has the order of the deposit choices interchanged. The discrepancy between  $\lambda = 17$  and  $\lambda = 82$  is due to the difference in thermomechanical effect of depositing  $D_1 = 0$  first instead of  $D_1 = 1$ .

Similar observations can be made for set  $S_W$  in Figure 5–11b. However, the top performing design belonged to concept  $c = 0$  while the 6th ranked design belonged to concept  $c = 2$ . Furthermore, the number of deposits used for any given design arc did not exceed  $o = 3$ . In contrast,  $S_E$  featured many designs with  $o = 4$ . The fewer number of deposits in  $S_W$  can be attributed to the preference of the algorithm for minimizing weight above all. Another difference between  $S_W$  and  $S_E$  is that most designs in  $S_W$  are Pareto optimal as given by the proximity metric in Table 5–5.  $S_W$  has a Pareto proximity metric of 0.0432 units which is smaller than the value of 0.0904 units belonging to  $S_E$ . This is due to the reasons explained earlier regarding the discrepancy between weight and excess.

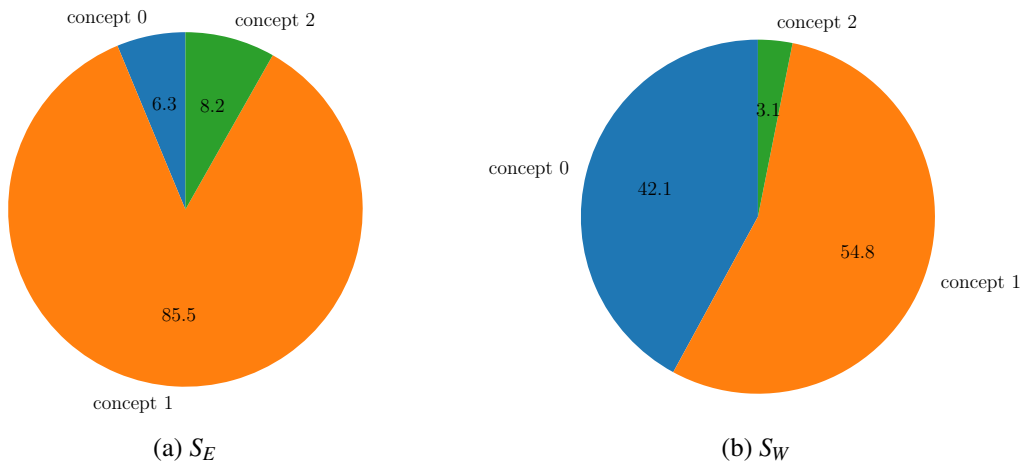


Figure 5–12: Distribution of concepts in sets  $S_E$  and  $S_W$

We analyze the the distribution of the concept choices  $c$  within the set  $S_E$  in Figure 5–12a. We can see that concept choice  $c = 1$  dwarfs the other two concept choices. This is because the “hatched” concept has deposit choices with relatively high capability and

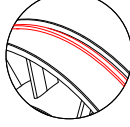
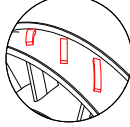
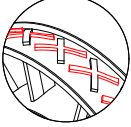
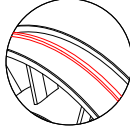
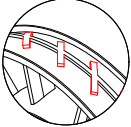
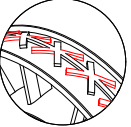
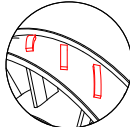
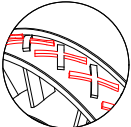
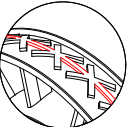
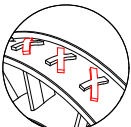
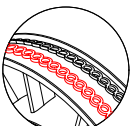
Table 5–6: Top performing design arcs in  $S_E$ 

Design arc Index	concept	1st deposit	2nd deposit	3rd deposit	4th deposit
$\lambda$	$c$	$D_1$	$D_2$	$D_3$	$D_4$
82	1				
86	1				
17	1				
240	1				
167	1				
164	1				

excess. The discontinuous stiffener design featured by its various deposits provided sufficient reinforcement without overstiffening the outer casing. This contrasts the deposit choices available to the "wavy" and "tubular" stiffener concepts which are continuous.

We also look at the distribution of concept choices  $c$  within the set  $S_W$  in Figure 5–12b. The concept choices  $c = 0$  and  $c = 1$  are comparable in terms of frequency within the set. This is because both concepts contain deposit choices that are low in weight. Since the

Table 5–7: Top performing design arcs in  $S_W$ 

Design arc Index	concept	1st deposit	2nd deposit	3rd deposit
$\lambda$	$c$	$D_1$	$D_2$	$D_3$
11	0			
82	1			
294	1			
93	1			
14	1			
352	2			

optimization objective for set  $S_W$  is weight, the low-weight deposit choices within these concepts are equally preferred.

We then analyze the distribution of the first choice  $D_1$  in the design arcs within the set  $S_E$ . This distribution is shown in Figure 5–13a. We can see from this distribution that the redesign choice  $D_1 = 1$  is chosen most frequently due the high capability  $V_c$  of this deposit choice and its children. The third most common design choice is  $D_1 = 0$ , which is comparable in frequency to  $D_1 = 2$ . However, it should be noted that committing to

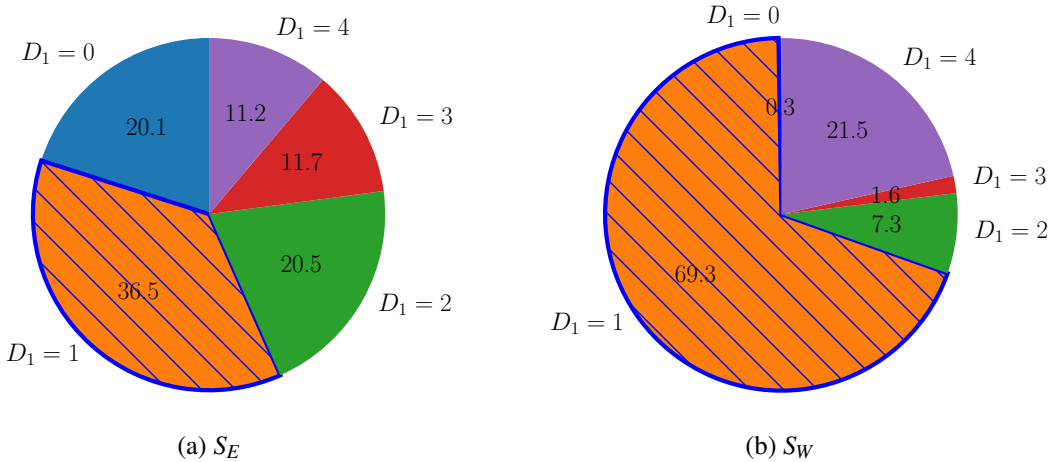


Figure 5–13: Distribution of first deposit  $D_1$  when concept  $c = 1$  is selected in sets  $S_E$  and  $S_W$

$D_1 = 0$  restricts the designers' choices later in the product's cycle. Figure 5–11a shows that  $\lambda = 17$  is the only possible design arc with  $D_1 = 0$ . This is in contrast to  $D_1 = 1$  that can be used to obtain two different design arcs  $\lambda = 82$  and  $\lambda = 86$ . These additional insights obtained by close examination of the tradespace can be beneficial as opposed to picking the most obvious result from Figure 5–13.

The tools developed in this chapter can help designers make informed decisions about the sequence of redesign choices during a product cycle. These insights are particularly useful for determining the first redesign choice when uncertainty and the number of possible choices are high.

#### 5.4 Computational cost

As explained in Section 5.2.2 a surrogate model for  $n_{\text{safety}}(\mathbf{p})$  is built using 10100 samples to estimate capability, reliability, and excess in the parameter space for feasible design arcs. Algorithms 3 and 4 were used with lookup tables that return the excess and

Table 5–8: Breakdown of total computational cost for obtaining surrogate models

Task	function evaluations	evaluation time	iterations	iteration time	total time
Surrogate $n_{\text{safety}}(\mathbf{p})$	10100	10 min	-	-	70.1 days
Lookup table	$6.06 \times 10^8$	1 ms	20200	30 s	
Compute $V_C$	10000	1 ms	1	10 s	
Compute $V_E$	10000	1 ms	1	10 s	7.01 days
Compute $\mathbb{P}(\mathbf{p} \in C)$	10000	1 ms	1	10 s	
<b>Total cost</b>				77.1 days	

reliability for every design arc  $\{c, \mathbf{D}\} \in \Omega_{CD}$  and requirement PDF  $F_{\mathbf{X}} \in \mathcal{R}$  to avoid re-computing them during parametric optimization. This results in  $404 \times 50 = 20,200$  excess and reliability values that need to be computed using Monte Carlo integration before exercising the algorithms in this chapter. Table 5–8 shows a breakdown of the computational cost for obtaining the lookup table.

A breakdown of the computational cost of Algorithms 3 and 4 is shown in Table 5–9. It can be concluded that obtaining the surrogate model for the feasibility criterion  $n_{\text{safety}}(\mathbf{p})$  incurs the most computational cost of 70.1 days as opposed to 9.9 days for excersing the algorithms in this chapter. The total computational cost incurred for obtaining solutions to the example in this chapter is 87 days. This is significantly greater than the cost incurred by finding scalable solutions to the problem in Chapter 4 (40.7 days). However, the methods in this chapter provide solutions for multiple epochs as opposed to a single design revision. This means that the methods presented could potentially provide more added value to the component through multiple life extensions.

Table 5–9: Breakdown of total computational cost for Chapter 5 algorithms

Algorithm	Step	function evaluations	evaluation time	iterations	iteration time	total time
3	step 3	-	-	100000	5 s	2.89 days
	sub-step 4	≈500	5 ms	1	2.5 s	
4	step 3	-	-	404	25 min	7.01 days
	sub-step 4-9	≈ $3 \times 10^5$	5 ms	1	25 min	
<b>Total cost</b>				9.90 days		

## 5.5 Summary

We presented a set-based design tool for generating optimal redesign sequences for a product as its lifecycle or development process progresses. Design arcs are obtained by solving an optimization problem to minimize excess subject to reliability constraints that depend on changing requirements.

We developed a tool for quantifying the level of excess in a design when multiple changing parameters are considered simultaneously. The areas of the multi-dimensional parameter space related to design capability, requirements, excess, or buffer are identified by means of sets, and their volume is obtained using Monte Carlo integration.

By minimizing the volume of the excess set for a particular design and requirement, overdesign costs are mitigated. We model changing parameters by means of requirement arcs. The optimization problem is solved for each requirement arc to obtain a set of corresponding design arcs.

Tradespace exploration is then used to visualize the set of optimal design arcs and compare it to sets of flexible and robust design arcs. It was shown that our approach results in a set of design arcs that balance flexibility with robustness. An examination

of the frequency of each design choice within the set of optimal design arcs provides designers with useful insights about the best approach at the early stages of the product's lifecycle or development process when uncertainty is high and decisions have a lasting impact on the product's performance for the remainder of its lifecycle.

The work in this chapter extends the approach used in Chapter 4 to include problems where multiple changes in requirements may occur. This is represented by the requirement arcs discussed in this chapter. Furthermore, robustness in addition to flexibility was quantified and used as a design metric in this chapter.

In the next chapter, we discuss the use of stochastic optimization algorithms for obtaining sets of design solutions when changing parameters govern the design optimization problem. Such approaches can help address the need for extensive exploration of the parameter space or the set of possible requirements (given by  $\Omega_R$ ) by reducing the number of needed function evaluations. We show how such approaches can substitute parts of the algorithms that have been developed in this chapter and Chapter 4.

## Chapter 6

### Managing uncertain requirements by means of stochastic optimization

This chapter explores the use of state-of-the-art stochastic optimization algorithms for managing uncertain requirements in design problems. We show how a set of design solutions can be obtained from the models defined in Chapter 3 via a stochastic version of MADS, StoMADS [107]. StoMADS returns a set of candidate solutions for a given stochastic programming problem which makes it an ideal choice for set-based design.

The method described in this chapter can help simplify the algorithms introduced in Chapters 4 and 5 by eliminating the steps involved in searching for a set of parametric optimal solutions.

#### 6.1 Method

Consider the optimization problem defined in Section 4.1.2 in Equation (4.1). The objectives and constraints are a function of uncertain parameters  $\mathbf{p}$ . In this section we denote the uncertain parameters by random variables  $\mathbf{P} = [P_1, P_2, \dots, P_m]$  (not to be confused with the reliability vector defined in Chapter 5). The objective and constraints functions in Equation (4.1) are deterministic in nature. By replacing the uncertain parameters with their random counterparts, the objective and constraint functions become stochastic

$$\begin{aligned} & \underset{\mathbf{x}}{\text{minimize}} \quad \hat{f}(\mathbf{x}) \text{ where } \hat{f}(\mathbf{x}) = \mathbb{E}_{\mathbf{P}} [\hat{f}_{\mathbf{P}}(\mathbf{x})] \\ & \text{subject to} \quad \hat{\mathbf{g}}(\mathbf{x}) \leq \mathbf{0} \text{ where } \hat{\mathbf{g}}(\mathbf{x}) = \mathbb{E}_{\mathbf{P}} [\hat{\mathbf{g}}_{\mathbf{P}}(\mathbf{x})], \end{aligned} \tag{6.1}$$

where  $\mathbb{E}_{\mathbf{P}}$  denotes the expectation with respect to the vector of random variables  $\mathbf{P}$ .  $\hat{f}_{\mathbf{P}}(\mathbf{x})$  and  $\hat{\mathbf{g}}_{\mathbf{P}}(\mathbf{x})$  denote the stochastic version of the surrogate models for the engineering design problem being solved.

$\hat{f}_{\mathbf{P}}(\mathbf{x})$  and  $\hat{\mathbf{g}}_{\mathbf{P}}(\mathbf{x})$  are obtained from their deterministic counterparts  $\hat{f}(\mathbf{x}; \mathbf{p})$  and  $\hat{\mathbf{g}}(\mathbf{x}; \mathbf{p})$  by randomly sampling the components of the parameters vector  $\mathbf{p}$  from a joint PDF  $F_{\mathbf{X}}(\mathbf{p})$ . In this chapter, we use a uniform distribution for the joint PDF although other distributions can be used depending on the problem.

The optimization problem in Equation (6.1) is solved via StoMADS to obtain a set of candidate solutions for the optimizer  $\mathbf{X}^* = \{\mathbf{x}_1^*, \mathbf{x}_2^*, \dots, \mathbf{x}_w^*\}$ .

We demonstrate the capabilities of StoMADS by solving a TRS remanufacturing problem where uncertain parameters are involved.

## 6.2 Example

We investigate the deposition of a circumferential stiffener on the outer casing of a TRS (shown in Figure 3–1) subject to 4 uncertain temperature loads (shown in Figure 3–6b). We formulate the problem as

$$\begin{aligned} & \underset{\mathbf{x}}{\text{minimize}} \quad \hat{f}(\mathbf{x}; \mathbf{p}) = -n_{\text{safety}}(\mathbf{x}; T_1, T_2, T_3, T_4) \\ & \text{subject to} \quad g_{\text{linear}}(\mathbf{x}) = x_3 + x_1 - W_{\text{total}} \leq 0, \end{aligned} \tag{6.2}$$

where  $\mathbf{x} = [x_1, x_2, x_3]^T$ . The objective function is obtained from a surrogate model for the safety factor  $n_{\text{safety}}(\mathbf{x}; \mathbf{p})$ , where the inputs are the stiffener dimensions  $x_1, x_2$ , and  $x_3$  and temperature loads  $T_1, T_2, T_3$ , and  $T_4$ .

The design variables for this problem govern the circumferential stiffener geometry (given by  $x_1, x_2$ , and  $x_3$ ). The uncertain parameters for this problem are the 4 temperature

loads experienced by the TRS ( $T_1, T_2, T_3$ , and  $T_4$ ). We extract the relevant design variables and parameters from Table 3–2 and list them in the tables below.

Table 6–1: Design variables  $\mathbf{x}$ 

Design variable	Notation	Units	Lower bound	Upper bound
Stiffener axial position	$x_1$	mm	37	145
Stiffener thickness	$x_2$	mm	2	10
Stiffener width	$x_3$	mm	10	40

Table 6–2: Relevant model parameters and constants

Parameter/constant	Notation	Units	Value
Uncertain parameters $\mathbf{p}$			
Nacelle temperature	$T_1$	°C	$300 \pm 100$
Tailcone temperature	$T_2$	°C	$400 \pm 100$
Rotor temperature	$T_3$	°C	$450 \pm 100$
Gas surface temperature	$T_4$	°C	$600 \pm 100$
Constant parameters			
Laser Power	$P_{\text{laser}}$	W	3806
Laser beam radius	$r_l$	mm	14.2
Scanning speed	$V$	mm/s	5.0
Laser penetration depth	$D_p$	mm	5.0
Substrate base width	$W_{\text{total}}$	mm	155

The design problem in Equation (6.2) is transformed to its stochastic counterpart by randomly sampling the uncertain parameters from a uniform distribution

$$\begin{aligned} & \underset{\mathbf{x}}{\text{minimize}} \quad \mathbb{E}_{\mathbf{P}} [\hat{f}_{\mathbf{P}}(\mathbf{x})] \\ & \text{subject to} \quad g_{\text{linear}}(\mathbf{x}) = x_3 + x_1 - W_{\text{total}} \leq 0, \end{aligned} \tag{6.3}$$

where  $\mathbf{x} = [x_1, x_2, x_3]^T$ ,  $\mathbf{P} = [T_1, T_2, T_3, T_4]^T$ , and  $\hat{f}_{\mathbf{P}}(\mathbf{x})$  is the stochastic version of the objective. The random vector  $\mathbf{P}$  has its components sampled from a uniform distribution. The constraint remains unchanged since it does not involve uncertain parameters.

Before solving the problem in Equation (6.3), we perform Monte Carlo simulation on the stochastic objective function to determine the effect of the design variables on the expected value of the objective.

### 6.2.1 Monte Carlo simulation of stochastic objective function

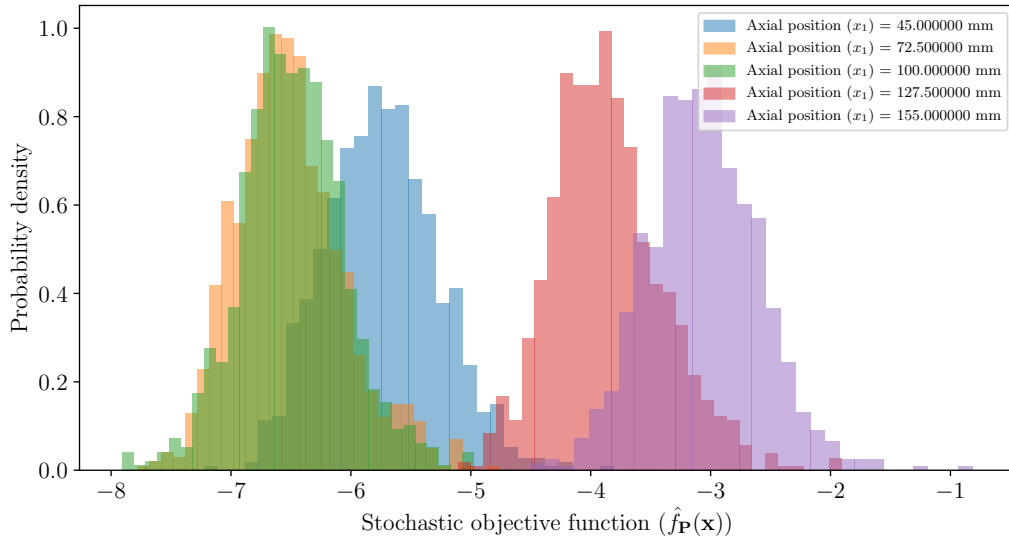
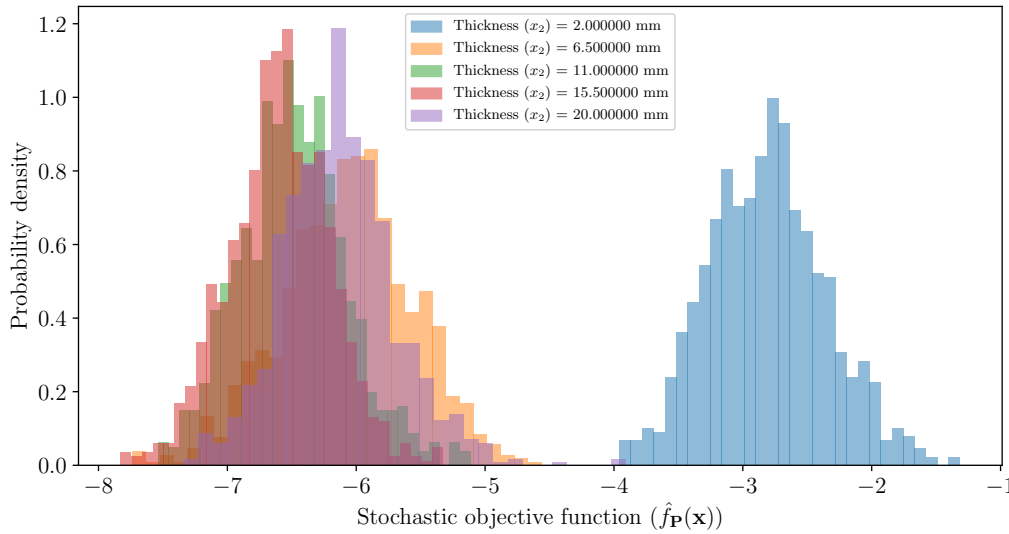
For each design variable in  $\mathbf{x}$ , we vary one variable at a time while holding the others fixed at their nominal values as given by Table 6–1. The stochastic objective function is called 1000 times for a given combination of variables while randomly sampling the design parameters in  $\mathbf{P}$  from a uniform distribution. The upper and lower bound for the uniform distribution that each random parameter  $P_m$  follows is given by Table 6–2.

The results of the Monte Carlo simulation are visualized in Figure 6–1. From these results, it can be seen that the expectation of the stochastic objective function  $\mathbb{E}_{\mathbf{P}} [\hat{f}_{\mathbf{P}}(\mathbf{x})]$  as given by the mean of the 1000 samples for each run is dependant on the variables in  $\mathbf{x}$ . It can be seen that  $\mathbb{E}_{\mathbf{P}} [\hat{f}_{\mathbf{P}}(\mathbf{x})]$  is maximized in the range  $72.5 \leq x_1 \leq 100$  and at  $x_2 \approx 15$  and  $x_3 \approx 87.5$ .

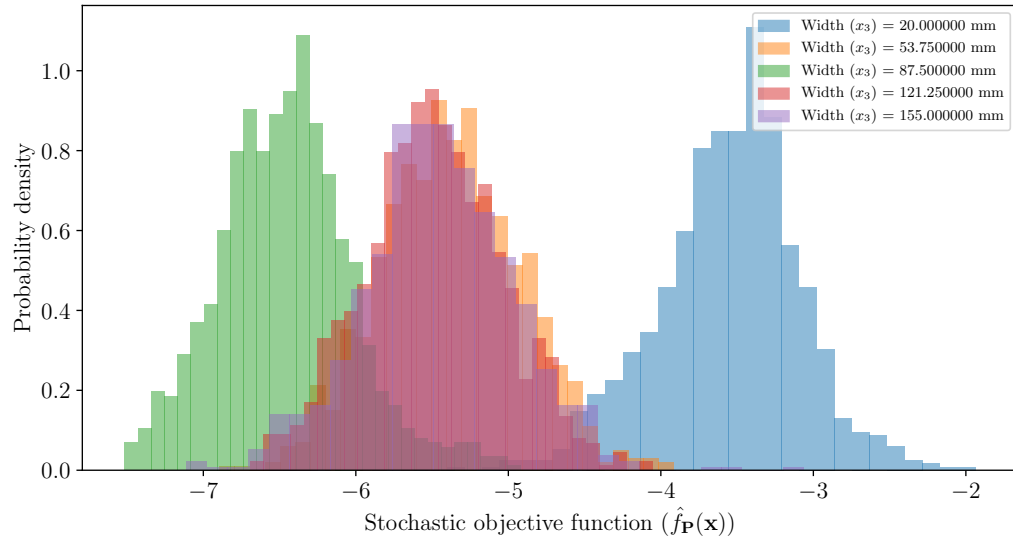
### 6.2.2 StoMADS results for stochastic optimization problem

We solved the problem in Equation (6.3) using StoMADS–PB to obtain a set of solutions. This algorithm is a version of StoMADS where constraints are handled by the progressive barrier approach [92].

The problem is also solved using the deterministic version of the algorithm NOMAD in order to be used as a benchmark for the quality of the solutions obtained via StoMADS–PB [90].

(a) Effect of  $x_1$ ,  $x_2 = 6$  mm,  $x_3 = 25$  mm(b) Effect of  $x_2$ ,  $x_1 = 91$  mm,  $x_3 = 25$  mmFigure 6–1: Monte Carlo simulation of  $\hat{f}_P(\mathbf{x})$  using 1000 samples

It is recommended by the developers of StoMADS–PB to set the maximum number of blackbox evaluations parameter of the algorithm to `max_bb_eval =  $(n + 1) \times 1000$` , where  $n$  is the number of variables. As a result, 4000 iterations were used with StoMADS–PB.

(c) Effect of  $x_3$ ,  $x_1 = 91$  mm,  $x_2 = 6$  mmFigure 6-1: Monte Carlo simulation of  $\hat{f}_P(\mathbf{x})$  using 1000 samples (cont.)

The best four solutions in terms of the expectation of the objective function are listed in Table 6-3. In order to compute the expectation, a Monte Carlo simulation was performed for each of the solutions obtained in Table 6-3. The results of the Monte Carlo simulation are shown in Figure 6-2.

It can be seen from Table 6-3 that the StoMADS-PB algorithm performs better than the NOMAD algorithm when comparing the expected value of the objective function at the optimizer. Only StoMADS-PB candidate solution 2 underperformed in terms of the expectation of the objective function relative to the NOMAD solution. Furthermore it can be seen that the constraint was inactive for the best performing candidate solution. It should also be noted that although the NOMAD algorithm is deterministic, running the problem with the same initial conditions and algorithm parameters will yield a variety of solutions due to the stochastic nature of the objective function.

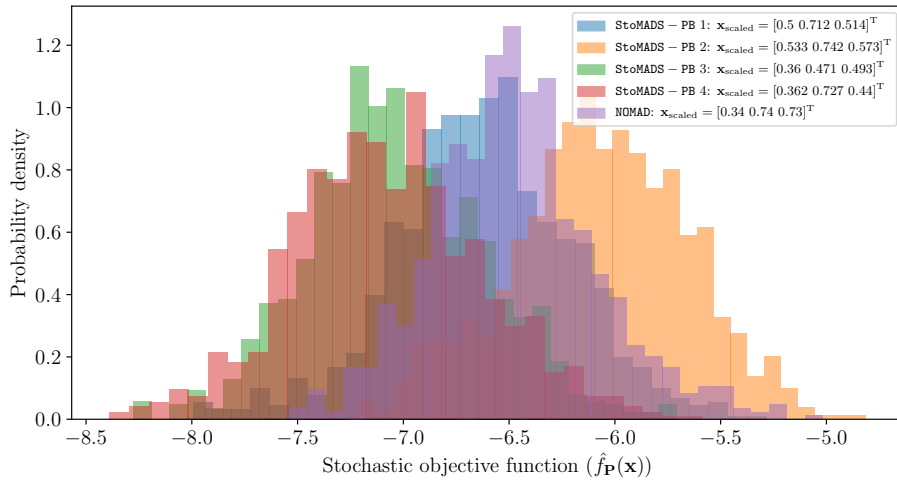


Figure 6–2: Monte Carlo simulation results of StoMADS–PB and NOMAD solutions

Table 6–3: TRS optimization problem results

Solution No.	Axial Position	Thickness	Width	Objective		Constraint $g_{\text{linear}}(\mathbf{x})$
	$x_1$	$x_2$	$x_3$	$\hat{f}_{\mathbf{P}}(\mathbf{x})$	Variance	
				$\mathbb{E}_{\mathbf{P}}[\hat{f}_{\mathbf{P}}(\mathbf{x})]$	$\sigma^2$	
Algorithm: StoMADS–PB						
1	100.0	14.8	89.4	-6.63	0.417	-11.58
2	103.6	15.4	97.4	-6.07	0.417	-0.0004
3	84.6	10.5	86.5	-7.03	0.415	-29.9
4	84.8	15.1	79.4	-7.08	0.447	-36.8
Algorithm: NOMAD						
1	82.4	15.3	118.6	-6.48	0.389	-0.05

We will now summarize the implications of this approach for obtaining set-based solutions in relation to the set-based design approaches that have been developed in this thesis.

### 6.3 Summary

This chapter presented an alternative strategy for solving parametric optimization problems. Rather than sampling the parameter space and solving the optimization problem for a given sample of parameter values, StoMADS can be used to directly obtain a set of solutions with an equivalent stochastic objective and constraint functions where the parameters are sampled from their respective random distributions.

The approach presented in this chapter can be used to improve Algorithms 1 and 3. Solving the problem in Equation (6.1) can substitute steps 1 through 10 in Algorithm 1. However, the solution to the problem in Equation (6.1) only outputs the optimizer values in the design space. Corresponding parameter values cannot be obtained since they are intrinsic to the stochastic version of the objective and constraint functions. The set of optimizers and their corresponding parameter values are needed by Algorithm 1 to construct a response surface in the parameter space.

However, the approach in this chapter can substitute steps 3 through 6 within Algorithm 3 by randomly selecting requirement arcs from  $\Omega_R$  in the stochastic version of the problem. The requirement arc corresponding to each solution in  $S_E^*$  is not needed since only the frequency of the design arcs is needed to isolate the set-based solution. However, the development version of StoMADS is restricted to optimization problems with continuous variables and needs to be further developed to include mixed variable programming problems such as those in Chapter 5.

The approach presented in this chapter can prove useful to designers who are accustomed to more traditional design practices involving point-based design. This is because

StoMADS has a similar interface to most available deterministic design optimization approaches that output a single design solution.

## **Chapter 7**

### **Conclusions**

This thesis presented a framework for managing problems involving changing requirements and parameters. The developed framework is based on the use of parametric design optimization to exhaustively explore multi-dimensional design and parameter spaces and is distinguished by the following features.

- It manages an instantaneous or gradual change in design requirements.
- It constructs surrogate models of expensive engineering models to mitigate the computational cost of exploring the design and parameter space.
- It utilizes rigorous derivative-free optimization tools for exploring multi-dimensional design and parameter space without the need for gradients or their approximation.
- It provides sets of design solutions represented by response surfaces or convex hulls for multi-dimensional continuous or discrete design spaces respectively.
- Provides a mathematical formulation for qualitative design characteristics such as flexibility, scalability, and excess.

A total of four algorithms were developed, demonstrated, and applied to multiple application examples featuring the remanufacturing design of a TRS with different design variables, design space types (continuous or categorical), and varying requirements change scenarios (instantaneous or gradual).

A method for mapping between design and parameter space using response surfaces was provided in Algorithm 1. A scalability constraint was formulated as part of Algorithm 2 and demonstrated using the TRS application example. These two algorithms are combined to identify a set of scalable optimal designs in the parameter space of a design problem when an instantaneous change in requirements occurs. The algorithms provided a relatively small albeit varied set of scalable design solutions for the TRS application example. This set of solutions is useful for reducing the design space to a manageable set of solutions for further development and detailed analysis.

A third algorithm was developed to manage a cascade of requirement changes at discrete times in a product's lifecycle or development cycle. As part of Algorithm 3, three design metrics were quantified mathematically. They allow designers to quantify the capability, buffer, and excess embedded in a design. The mathematical formulation of these design metrics is novel and allows them to be quantified in a multi-dimensional parameter space where multiple parameters may change simultaneously. The algorithm favors designs that minimize cost or excess throughout the product's cycle. The TRS application example for demonstrating this algorithm featured a categorical design space governed by a finite set of possible design choices. The resulting set-based solution obtained by this algorithm was displayed on a tradespace.

The fourth and final algorithm, Algorithm 4 was used to obtain robust and flexible design sets using tools and definitions from the literature that were adapted for a gradual change in requirements. The algorithm was also applied to the categorical TRS application example and its resulting sets were superpositioned on the same tradespace used to visualize the set-based solution obtained by minimizing excess. The tradespace revealed

that utilizing design optimization can help balance the amount of robustness and flexibility in a design, a problem which is difficult to address in the early stages of the product cycle due to the relatively high uncertainty during this time period.

Finally, we proposed some stochastic optimization tools that can be used to substitute parts of Algorithms 1 and 3 to make managing design and parameter spaces with relatively large dimensionality more tractable.

To the best of our knowledge, Algorithms 2 and 3, their metrics, and constraints are novel and are a first attempt at a systematic approach for managing a wide range of requirement change scenarios that are frequently encountered in the industry.

## 7.1 Recommendations for future work

In this thesis, we considered continuous or categorical design spaces independently. A framework for solving problems involving mixed variable design spaces is needed to identify the most efficient design combinations possible.

Although we have provided a varied set of tools for quantifying design changeability, the cost of change must be considered when implementing the change in order to satisfy the definition of changeability [35].

Although we consider the cumulative weight as a proxy for lifecycle cost, this definition is not sufficient and more advanced lifecycle modeling tools should be used for computing cost [35]. This relates directly to the lifecycle of the component and its importance to circular economy principles. A changeability cost threshold must be observed by designers when making remanufacturing decisions [36].

Future studies could also focus on other product recovery activities along the innermost circles of a CE such as repair and reuse as they may preserve valuable resources

more efficiently than remanufacturing. Nevertheless, these options need not be mutually exclusive.

The PDFs used to model the uncertain requirements in this thesis assume that the parameters governing them are not correlated. Such correlations can be easily modeled using a covariance matrix as part of the requirement formulation to involve more general scenarios.

Importance sampling was used to make the management of a large number of requirement change scenarios more tractable. More advanced sampling techniques can be used to make the parametric studies used in this thesis more efficient. One such approach was demonstrated in Chapter 6.

The algorithms were designed to accommodate a wide range of optimization and search methods for managing different kinds of design problems. Application of the algorithms to different design problems featuring similar definitions of scalability, buffer, and excess but with different search methods used in lieu of MADS would provide more insight on the effectiveness of MADS within the developed framework.

The metrics developed in this thesis such as scalability could be generalized for other design problems where manufacturing constraints are not the only concern governing the scalability. The concept of the Jacobian provides a powerful tool for understanding the effect of changing parameters on design variables and could be used to cover a wide range of redesign scenarios in practice.

Building on the methods developed in this thesis, should allow designers to make decisions in the early stages of the product's development process or lifecycle when innovation potential is at its highest.

## Bibliography

- [1] B. S. Blanchard and W. J. Fabrycky. *Systems engineering and analysis*. Prentice Hall International, Englewood Cliffs N.J., 2nd edition, 1981. ISBN 9780138808402.
- [2] C. Peterson, R. K. Paasch, P. Ge, and T. G. Dietterich. Product innovation for interdisciplinary design under changing requirements. In *Proceedings of the International Conference on Engineering Design*, pages 861–862, Paris, 2007.
- [3] The Boeing design change process, 2013. URL <https://787updates.newairplane.com/Design-Change-Process/The-Boeing-Design-Change-Process>. Visited 2019-06-13.
- [4] C. Eckert, P. J. Clarkson, and W. Zanker. Change and customisation in complex engineering domains. *Research in Engineering Design*, 15(1):1–21, 2004. ISSN 09349839. doi:[10.1007/s00163-003-0031-7](https://doi.org/10.1007/s00163-003-0031-7).
- [5] D. Ullman. *The mechanical design process*. McGraw-Hill. McGraw-Hill Education, 2009. ISBN 9780072975741.
- [6] Ellen Macarthur Foundation. Towards the circular economy: Opportunities for the consumer goods sector. 2, 2013. ISSN 10881980. doi:[10.1162/108819806775545321](https://doi.org/10.1162/108819806775545321).
- [7] S. Matos and J. Hall. Integrating sustainable development in the supply chain: The case of life cycle assessment in oil and gas and agricultural biotechnology. *Journal*

- of Operations Management*, 25(6):1083–1102, 2007. ISSN 02726963.
- [8] J. Neto, G. Walther, J. Bloemhof, J. Van Nunen, and T. Spengler. From closed-loop to sustainable supply chains: The WEEE case. *International Journal of Production Research*, 48(15):4463–4481, 2010. ISSN 00207543.
- [9] M. Lieder and A. Rashid. Towards circular economy implementation: A comprehensive review in context of manufacturing industry. *Journal of Cleaner Production*, 115:36–51, 2016. ISSN 09596526.
- [10] Ellen Macarthur Foundation. Towards the circular economy: An economic and business rationale for an accelerated transition. 1, 2013. ISSN 10881980.  
doi:[10.1162/108819806775545321](https://doi.org/10.1162/108819806775545321).
- [11] P. Goodall, E. Rosamond, and J. Harding. A review of the state of the art in tools and techniques used to evaluate remanufacturing feasibility. *Journal of Cleaner Production*, 81:1–15, 2014. ISSN 09596526.
- [12] W. Ijomah, C. McMahon, G. Hammond, and S. Newman. Development of robust design-for-remanufacturing guidelines to further the aims of sustainable development. *International Journal of Production Research*, 45(18-19):4513–4536, 2007. ISSN 00207543.
- [13] J. Liu and Y. Ma. Sustainable design-oriented level set topology optimization. *Journal of Mechanical Design*, 139(1), 2016. ISSN 1050-0472.
- [14] B. Mahadevan, D. Pyke, and M. Fleischmann. Periodic review, push inventory policies for remanufacturing. *European Journal of Operational Research*, 151(3):536–551, 2003. ISSN 03772217.

- [15] P. Golinska, M. Kosacka, R. Mierzwiak, and K. Werner-Lewandowska. Grey decision making as a tool for the classification of the sustainability level of remanufacturing companies. *Journal of Cleaner Production*, 105:28–40, 2015. ISSN 09596526.
- [16] L. Van-Thao, H. Paris, and G. Mandil. Using additive and subtractive manufacturing technologies in a new remanufacturing strategy to produce new parts from End-of-Life parts. In *Proceedings of the 22ème Congrès Français de Mécanique*, pages 1–8, 2015. doi:[10.13140/RG.2.1.2442.3129](https://doi.org/10.13140/RG.2.1.2442.3129).
- [17] C. Song, X. Guan, Q. Zhao, and Y. Ho. Machine learning approach for determining feasible plans of a remanufacturing system. *IEEE Transactions on Automation Science and Engineering*, 2(3):262–275, 2005. ISSN 15455955.
- [18] Y. Koren, X. Gu, F. Badurdeen, and I. Jawahir. Sustainable living factories for next generation manufacturing. In *Procedia Manufacturing*, volume 21, pages 26–36, 2018.
- [19] W. L. Ijomah. Addressing decision making for remanufacturing operations and design-for-remanufacture. *International Journal of Sustainable Engineering*, 2(2):91–102, 2009. ISSN 19397038. doi:[10.1080/19397030902953080](https://doi.org/10.1080/19397030902953080).
- [20] M. Lindahl, E. Sundin, J. Östlin, and M. Björkman. Concepts and definitions for product recovery Analysis and clarification of the terminology used in academia and industry. In *Innovation in Life Cycle Engineering and Sustainable Development*, pages 123–138. Springer Netherlands, Dordrecht, 2007.
- [21] M. Thierry, M. Salomon, J. Van Nunen, and L. Van Wassenhove. Strategic issues in product recovery management. *California Management Review*, 37(2):114–136,

1995. ISSN 0008-1256.
- [22] Remanufacturing Industries Council. Specifications for the process of remanufacturing. *ANSI/RIC001.1-2016*, 2017. URL <https://webstore.ansi.org/Standards/ANSI/ANSIRIC0012016>.
- [23] E. Fricke and A. P. Schulz. Design for changeability (DfC): Principles to enable changes in systems throughout their entire lifecycle. *Systems Engineering*, 8(4): 342–359, 2005. ISSN 10981241. doi:[10.1002/sys.20039](https://doi.org/10.1002/sys.20039).
- [24] R. De Neufville and S. Scholtes. *Flexibility in engineering design*. MIT Press, 2011. ISBN 9780262016230.
- [25] K. Alhandawi, P. Andersson, M. Panarotto, O. Isaksson, and M. Kokkolaras. Scalable set-based design optimization and remanufacturing for meeting changing requirements. *Journal of Mechanical Design*, 143(2), 2020. ISSN 1050-0472. doi:[10.1115/1.4047908](https://doi.org/10.1115/1.4047908).
- [26] C. Eckert, O. Isaksson, and C. Earl. Design margins: A hidden issue in industry. *Design Science*, 5:e9, 2019. ISSN 2053-4701. doi:[10.1017/dsj.2019.7](https://doi.org/10.1017/dsj.2019.7).
- [27] D. Long and S. Ferguson. A case study of evolvability and excess on the B-52 stratofortress and F/A-18 hornet. In *Proceedings of the ASME International Design Engineering Technical Conferences and Computers and Information in Engineering Conference*, volume 4. American Society of Mechanical Engineers (ASME), 2017. ISBN 9780791858165. doi:[10.1115/DETC2017-68287](https://doi.org/10.1115/DETC2017-68287).
- [28] R. G. Cooper. Perspective: The stage-gates® idea-to-launch process - Update, what's new, and NexGen systems. *Journal of Product Innovation Management*, 25(3):213–232, 2008. ISSN 07376782. doi:[10.1111/j.1540-5885.2008.00296.x](https://doi.org/10.1111/j.1540-5885.2008.00296.x).

- [29] H. L. Mcmanus, M. G. Richards, A. M. Ross, and D. E. Hastings. A framework for incorporating "ilities" in tradespace studies. In *Proceedings of the AIAA SPACE 2007 Conference & Exposition*, 2007. doi:[10.2514/6.2007-6100](https://doi.org/10.2514/6.2007-6100).
- [30] J. M. Wilson, C. Piya, Y. C. Shin, F. Zhao, and K. Ramani. Remanufacturing of turbine blades by laser direct deposition with its energy and environmental impact analysis. *Journal of Cleaner Production*, 80:170–178, 2014. ISSN 09596526. doi:[10.1016/j.jclepro.2014.05.084](https://doi.org/10.1016/j.jclepro.2014.05.084).
- [31] Y. Tang, K. Mak, and Y. Zhao. A framework to reduce product environmental impact through design optimization for additive manufacturing. *Journal of Cleaner Production*, 137:1560–1572, 2016. ISSN 09596526.
- [32] K. Xing, M. Belusko, L. Luong, and K. Abhary. An evaluation model of product upgradeability for remanufacture. *International Journal of Advanced Manufacturing Technology*, 35(1-2):1–14, 2007. ISSN 02683768. doi:[10.1007/s00170-006-0698-9](https://doi.org/10.1007/s00170-006-0698-9).
- [33] M. Kwak and H. Kim. Market positioning of remanufactured products with optimal planning for part upgrades. *Journal of Mechanical Design*, 135(1), 2013. ISSN 10500472. doi:[10.1115/1.4023000](https://doi.org/10.1115/1.4023000).
- [34] E. S. Suh, O. L. De Weck, and D. Chang. Flexible product platforms: Framework and case study. *Research in Engineering Design*, 18(2):67–89, 2007. ISSN 09349839. doi:[10.1007/s00163-007-0032-z](https://doi.org/10.1007/s00163-007-0032-z).
- [35] L. Lawand, K. Alhandawi, M. Panarotto, P. Andersson, O. Isaksson, and M. Kokkolaras. A lifecycle cost-driven system dynamics approach for considering

- additive re-manufacturing or repair in aero-engine component design. In *Proceedings of the International Conference on Engineering Design*, volume 2019-August, pages 1343–1352. Cambridge University Press, 2019. doi:[10.1017/dsi.2019.140](https://doi.org/10.1017/dsi.2019.140).
- [36] A. Ross, D. Rhodes, and D. E. Hastings. Defining changeability: Reconciling flexibility, adaptability, scalability, modifiability, and robustness for maintaining system lifecycle value. *Systems Engineering*, 11(3):246–262, 2008. ISSN 10981241.
- [37] M. W. P. Tackett, C. A. Mattson, and S. M. Ferguson. A model for quantifying system evolvability based on excess and capacity. *Journal of Mechanical Design*, 136(5), 2014. ISSN 10500472. doi:[10.1115/1.4026648](https://doi.org/10.1115/1.4026648).
- [38] A. Olewnik, T. Brauen, S. Ferguson, and K. Lewis. A framework for flexible systems and its implementation in multiattribute decision making. *Journal of Mechanical Design*, 126(3), 2004. ISSN 10500472. doi:[10.1115/1.1701874](https://doi.org/10.1115/1.1701874).
- [39] H. Liu, W. Chen, M. J. Scott, and K. Qureshi. Determination of ranged sets of design specifications by incorporating design-space heterogeneity. *Engineering Optimization*, 40(11):1011–1029, 2008. ISSN 0305215X. doi:[10.1080/03052150802378558](https://doi.org/10.1080/03052150802378558).
- [40] C. F. Rehn, S. S. Pettersen, S. O. Erikstad, and B. E. Asbjørnslett. Investigating tradeoffs between performance, cost and flexibility for reconfigurable offshore ships. *Ocean Engineering*, 147:546–555, 2018. ISSN 00298018. doi:[10.1016/j.oceaneng.2017.11.004](https://doi.org/10.1016/j.oceaneng.2017.11.004).
- [41] L. Viscito and A. Ross. Quantifying flexibility in tradespace exploration: Value-weighted filtered outdegree. In *Proceedings of the AIAA SPACE 2009 Conference & Exposition*, Pasadena, California, 2009. American Institute of Aeronautics and

- Astronautics. ISBN 978-1-60086-980-8. doi:[10.2514/6.2009-6561](https://doi.org/10.2514/6.2009-6561).
- [42] S. Rapp, R. Chinnam, N. Doerry, A. Murat, and G. Witus. Product development resilience through set-based design. *Systems Engineering*, 21(5):490–500, 2018. ISSN 15206858. doi:[10.1002/sys.21449](https://doi.org/10.1002/sys.21449).
- [43] M. J. Chalupnik, D. C. Wynn, and P. J. Clarkson. Comparison of ilities for protection against uncertainty in system design. *Journal of Engineering Design*, 24(12): 814–829, 2013. ISSN 09544828. doi:[10.1080/09544828.2013.851783](https://doi.org/10.1080/09544828.2013.851783).
- [44] M. A. Cardin, Q. Xie, T. S. Ng, S. Wang, and J. Hu. An approach for analyzing and managing flexibility in engineering systems design based on decision rules and multistage stochastic programming. *IIE Transactions*, 49(1):1–12, 2017. ISSN 24725862. doi:[10.1080/0740817X.2016.1189627](https://doi.org/10.1080/0740817X.2016.1189627).
- [45] M. A. Cardin and J. Hu. Analyzing the tradeoffs between economies of scale, time-value of money, and flexibility in design under uncertainty: study of centralized versus decentralized waste-to-energy systems. *Journal of Mechanical Design*, 138 (1), 2016. ISSN 10500472. doi:[10.1115/1.4031422](https://doi.org/10.1115/1.4031422).
- [46] S. Ferguson, K. Lewis, A. Siddiqi, and O. L. De Weck. Flexible and reconfigurable systems: Nomenclature and review. In *Proceedings of the ASME International Design Engineering Technical Conferences and Computers and Information in Engineering Conference*, volume 6 PART A, pages 249–263, 2007. ISBN 0791848027. doi:[10.1115/DETC2007-35745](https://doi.org/10.1115/DETC2007-35745).
- [47] B. Yannou, T. W. Simpson, and R. R. Barton. Towards a conceptual design explorer using metamodeling approaches and constraint programming. In *Proceedings of the ASME International Design Engineering Technical Conferences and Computers*

- and Information in Engineering Conference*, volume 2 PART A of *International Design Engineering Technical Conferences and Computers and Information in Engineering Conference*, pages 605–614, 2003. doi:[10.1115/detc2003/dac-48766](https://doi.org/10.1115/detc2003/dac-48766).
- [48] C. Small, G. S. Parnell, E. Pohl, S. R. Goerger, M. Cilli, and E. Specking. Demonstrating set-based design techniques: an unmanned aerial vehicle case study. *Journal of Defense Modeling and Simulation*, pages 1–17, 2019. ISSN 1557380X. doi:[10.1177/1548512919872822](https://doi.org/10.1177/1548512919872822).
- [49] W. Chen, T. W. Simpson, J. K. Allen, and F. Mistree. Satisfying ranged sets of design requirements using design capability indices as metrics. *Engineering Optimization*, 31(5):615–619, 1999. ISSN 0305215X. doi:[10.1080/03052159908941389](https://doi.org/10.1080/03052159908941389).
- [50] P. L. Cross and M. Mulford. Realizing collaborative systems design for missile seekers by combining design margin analysis with multi-disciplinary optimization. *Concurrent Engineering Research and Applications*, 23(3):226–235, 2015. ISSN 15312003. doi:[10.1177/1063293X15586837](https://doi.org/10.1177/1063293X15586837).
- [51] D. Villanueva, R. T. Haftka, and B. V. Sankar. Accounting for future redesign to balance performance and development costs. *Reliability Engineering and System Safety*, 124:56–67, 2014. ISSN 09518320. doi:[10.1016/j.ress.2013.11.013](https://doi.org/10.1016/j.ress.2013.11.013).
- [52] E. Z. Cansler, S. B. White, S. M. Ferguson, and C. A. Mattson. Excess identification and mapping in engineered systems. *Journal of Mechanical Design*, 138(8), 2016. ISSN 10500472. doi:[10.1115/1.4033884](https://doi.org/10.1115/1.4033884).
- [53] A. Qureshi, J. Dantan, J. Bruyere, and R. Bigot. Set-based design of mechanical systems with design robustness integrated. *International Journal of Product Development*, 19(1/2/3):64, 2014. ISSN 1477-9056.

- [54] E. Kerga, M. Rossi, M. Taisch, and S. Terzi. A serious game for introducing set-based concurrent engineering in industrial practices. *Concurrent Engineering Research and Applications*, 22(4):333–346, 2014. ISSN 15312003.
- [55] D. Sobek II, A. Ward, and J. Liker. Toyota’s principles of set-based concurrent engineering. *MIT Sloan Management Review*, 40(2):67–83, 1999. ISSN 0019848X.
- [56] C. Levandowski, M. Michaelis, and H. Johannesson. Set-based development using an integrated product and manufacturing system platform. *Concurrent Engineering Research and Applications*, 22(3):234–252, 2014. ISSN 15312003.
- [57] J. Carlson and J. Doyle. Highly optimized tolerance: Robustness and design in complex systems. *Physical Review Letters*, 84(11):2529–2532, 2000. ISSN 10797114.
- [58] Y. Nahm and H. Ishikawa. Representing and aggregating engineering quantities with preference structure for set-based concurrent engineering. *Concurrent Engineering Research and Applications*, 13(2):123–133, 2005. ISSN 1063293X.
- [59] G. Gventer and R. Haftka. Using response surface methodology in fuzzy set based design optimization. *Structural Optimization*, 18:1–12, 1999. ISSN 02734508.
- [60] J. Kizer and D. Mavris. Set-based design space exploration enabled by dynamic constraint analysis. In *Proceedings of the 29th congress of the international council of the aeronautical sciences*, 2014.
- [61] D. Shahan and C. Seepersad. Bayesian network classifiers for set-based collaborative design. *Journal of Mechanical Design*, 134(7), 2012. ISSN 10500472.
- [62] P. Backlund, D. Shahan, and C. Seepersad. Classifier-guided sampling for discrete variable, discontinuous design space exploration: Convergence and computational performance. *Engineering Optimization*, 47(5):579–600, 2015. ISSN 10290273.

- [63] D. Rosen. A set-based design method for material-geometry structures by design space mapping. In *Proceedings of the ASME International Design Engineering Technical Conferences and Computers and Information in Engineering Conference*, pages 1–11, 2015. doi:[10.1115/DETC2015-46760](https://doi.org/10.1115/DETC2015-46760).
- [64] P. Ge, S. Lu, and S. Bukkapatnam. Supporting negotiations in the early stage of large-scale mechanical system design. *Journal of Mechanical Design*, 127(6), 2005. ISSN 10500472.
- [65] G. Taguchi. *System of experimental design: Engineering methods to optimize quality and minimize cost*. UNIPUB/Kraus International Publications, 1987. ISBN 0527916218.
- [66] J. Landahl, C. Levandowski, H. Johannesson, and O. Isaksson. Assessing producibility of product platforms using set-based concurrent engineering. In *Transdisciplinary Engineering: Crossing Boundaries*, volume 4, pages 35–44, 2016. ISBN 9781614997023.
- [67] J. Wang and J. Terpenny. Interactive evolutionary solution synthesis in fuzzy set-based preliminary engineering design. *Journal of Intelligent Manufacturing*, 14(2):153–167, 2003. ISSN 09565515.
- [68] N. Doerry, M. Earnesty, C. Weaver, J. Banko, J. Myers, D. Browne, M. Hopkins, and S. Balestrini. Using set-based design in concept exploration. *NAME Chesapeake Section Technical Meeting, Army Navy Country Club*, 1(V):1–8, 2014.
- [69] R. Malak, J. Aughenbaugh, and C. Paredis. Multi-attribute utility analysis in set-based conceptual design. *CAD computer Aided Design*, 41(3):214–227, 2009. ISSN 00104485.

- [70] G. Avigad and A. Moshaiov. Set-based concept selection in multi-objective problems: Optimality versus variability approach. *Journal of Engineering Design*, 20(3):217–242, 2009. ISSN 09544828.
- [71] S. W. Miller, M. A. Yukish, and T. W. Simpson. Design as a sequential decision process: A method for reducing design set space using models to bound objectives. *Structural and Multidisciplinary Optimization*, 57(1):305–324, 2018. ISSN 16151488. doi:[10.1007/s00158-017-1756-7](https://doi.org/10.1007/s00158-017-1756-7).
- [72] S. Hannapel and N. Vlahopoulos. Implementation of set-based design in multidisciplinary design optimization. *Structural and Multidisciplinary Optimization*, 50(1):101–112, 2014. ISSN 16151488.
- [73] T. Athan and P. Papalambros. A note on weighted criteria methods for compromise solutions in multi-objective optimization. *Engineering Optimization*, 27(2):155–176, 1996. ISSN 0305215X.
- [74] C. Audet and W. Hare. *Derivative-free and blackbox optimization*. Springer International Publishing, 2017. ISBN 978-3-319-68912-8. doi:[10.1007/978-3-319-68913-5](https://doi.org/10.1007/978-3-319-68913-5).
- [75] X. Du, W. Chen, and Y. Wang. Most probable point-based methods. In *Extreme statistics in nanoscale memory design*, pages 179–202. Springer US, 2010. doi:[10.1007/978-1-4419-6606-3\\_7](https://doi.org/10.1007/978-1-4419-6606-3_7).
- [76] D. Lehký, O. Slowik, and D. Novák. Reliability-based design: Artificial neural networks and double-loop reliability-based optimization approaches. *Advances in Engineering Software*, 117:123–135, mar 2018. ISSN 18735339. doi:[10.1016/j.advengsoft.2017.06.013](https://doi.org/10.1016/j.advengsoft.2017.06.013).

- [77] M. A. Abramson, C. Audet, J. W. Chrissis, and J. G. Walston. Mesh adaptive direct search algorithms for mixed variable optimization. *Optimization Letters*, 3(1):35–47, 2009. ISSN 18624472. doi:[10.1007/s11590-008-0089-2](https://doi.org/10.1007/s11590-008-0089-2).
- [78] T. Mukherjee, W. Zhang, and T. DebRoy. An improved prediction of residual stresses and distortion in additive manufacturing. *Computational Materials Science*, 126:360–372, 2017. ISSN 09270256. doi:[10.1016/j.commatsci.2016.10.003](https://doi.org/10.1016/j.commatsci.2016.10.003).
- [79] V. D. Manvatkar, A. A. Gokhale, G. Jagan Reddy, A. Venkataramana, and A. De. Estimation of melt pool dimensions, thermal cycle, and hardness distribution in the laser-engineered net shaping process of austenitic stainless steel. *Metallurgical and Materials Transactions A: Physical Metallurgy and Materials Science*, 42(13):4080–4087, 2011. ISSN 10735623. doi:[10.1007/s11661-011-0787-8](https://doi.org/10.1007/s11661-011-0787-8).
- [80] D. Rosenthal. *The theory of moving sources of heat and its application to metal treatments*, volume 68. Transactions of the American Society of Mechanical Engineers, 1946.
- [81] J. Goldak, A. Chakravarti, and M. Bibby. A new finite element model for welding heat sources. *Metallurgical Transactions B*, 15(2):299–305, 1984. ISSN 03602141. doi:[10.1007/BF02667333](https://doi.org/10.1007/BF02667333).
- [82] A. H. Nickel, D. M. Barnett, and F. B. Prinz. Thermal stresses and deposition patterns in layered manufacturing. *Materials Science and Engineering A*, 317(1-2):59–64, 2001. ISSN 09215093. doi:[10.1016/S0921-5093\(01\)01179-0](https://doi.org/10.1016/S0921-5093(01)01179-0).
- [83] R. G. Budynas, J. K. Nisbett, and J. E. Shigley. *Shigley's mechanical engineering design*. McGraw-Hill Education, New York, 10th edition, 2015.

- [84] B. Talgorn, C. Audet, S. Le Digabel, and M. Kokkolaras. Locally weighted regression models for surrogate-assisted design optimization. *Optimization and Engineering*, 19(1):213–238, 2018. ISSN 15732924.
- [85] S. Lophaven, H. Nielsen, and J. Søndergaard. *DACE - a matlab kriging toolbox, version 2.0.* 2002. URL <http://www.omicron.dk/dace/dace.pdf>. Visited 2019-05-06.
- [86] C. Audet, M. Kokkolaras, S. Le Digabel, and B. Talgorn. Order-based error for managing ensembles of surrogates in mesh adaptive direct search. *Journal of Global Optimization*, 70(3):645–675, 2018. ISSN 15732916.
- [87] J. Sobiesczanski-Sobieski, J. Barthelemyy, and K. Riley. Sensitivity of optimum solutions to problem parameters. *AIAA Journal*, 20(9):1291–1299, 1982. ISSN 0001-1452. doi:[10.2514/3.51191](https://doi.org/10.2514/3.51191).
- [88] M. McKay, R. Beckman, and W. Conover. A comparison of three methods for selecting values of input variables in the analysis of output from a computer code. *Technometrics*, 21(2):239–245, 1979.
- [89] J. Loeppky, J. Sacks, W. Welch, and W. Welch. Choosing the sample size of a computer experiment: A practical guide. *Technometrics*, 51(4):366–376, 2009. doi:[10.1198/TECH.2009.08040](https://doi.org/10.1198/TECH.2009.08040).
- [90] S. Le Digabel. Algorithm 909. *ACM Transactions on Mathematical Software*, 37(4):1–15, 2011. ISSN 00983500.
- [91] C. Audet and J. E. Dennis. Mesh adaptive direct search algorithms for constrained optimization. *SIAM Journal on Optimization*, 17(1):188–217, 2006. ISSN 10526234. doi:[10.1137/040603371](https://doi.org/10.1137/040603371).

- [92] C. Audet and J. E. Dennis. A progressive barrier for derivative-free nonlinear programming. *SIAM Journal on Optimization*, 20(1):445–472, 2009. ISSN 1052-6234. doi:[10.1137/070692662](https://doi.org/10.1137/070692662).
- [93] C. Barber, D. Dobkin, and H. Huhdanpaa. The quickhull algorithm for convex hulls. *ACM Transactions on Mathematical Software*, 22(4):469–483, 2002. ISSN 00983500.
- [94] N. Brown and C. Mueller. Quantifying diversity in parametric design: A comparison of possible metrics. *Artificial Intelligence for Engineering Design, Analysis and Manufacturing*, 33(1):40–53, 2019. ISSN 14691760.
- [95] H. J. Pradlwarter, M. F. Pellissetti, C. A. Schenk, G. I. Schuëller, A. Kreis, S. Fransen, A. Calvi, and M. Klein. Realistic and efficient reliability estimation for aerospace structures. *Computer Methods in Applied Mechanics and Engineering*, 194(12-16):1597–1617, 2005. ISSN 00457825. doi:[10.1016/j.cma.2004.05.029](https://doi.org/10.1016/j.cma.2004.05.029).
- [96] D. M. Frangopol and K. Maute. Life-cycle reliability-based optimization of civil and aerospace structures. *Computers and Structures*, 81(7):397–410, 2003. ISSN 00457949. doi:[10.1016/S0045-7949\(03\)00020-8](https://doi.org/10.1016/S0045-7949(03)00020-8).
- [97] S. Zhu, H. Huang, R. Smith, V. Ontiveros, L. He, and M. Modarres. Bayesian framework for probabilistic low cycle fatigue life prediction and uncertainty modeling of aircraft turbine disk alloys. *Probabilistic Engineering Mechanics*, 34:114–122, 2013. ISSN 02668920. doi:[10.1016/j.probengmech.2013.08.004](https://doi.org/10.1016/j.probengmech.2013.08.004).
- [98] A. F. Shahraki and R. Noorossana. Reliability-based robust design optimization: A general methodology using genetic algorithm. *Computers & Industrial Engineering*, 74:199–207, 2014. ISSN 03608352. doi:[10.1016/j.cie.2014.05.013](https://doi.org/10.1016/j.cie.2014.05.013).

- [99] C. Bucher. *Computational analysis of randomness in structural mechanics*. CRC Press, 2009. ISBN 9780415403542.
- [100] P. E. Magnusen, R. J. Bucci, A. J. Hinkle, J. R. Brockenbrough, and H. J. Konish. Analysis and prediction of microstructural effects on long-term fatigue performance of an aluminum aerospace alloy. *International Journal of Fatigue*, 19(93):275–283, 1997. ISSN 01421123. doi:[10.1016/S0142-1123\(97\)00044-3](https://doi.org/10.1016/S0142-1123(97)00044-3).
- [101] M. Zhang, W. Gou, L. Li, X. Wang, and Z. Yue. Multidisciplinary design and optimization of the twin-web turbine disk. *Structural and Multidisciplinary Optimization*, 53(5):1129–1141, 2016. ISSN 16151488. doi:[10.1007/s00158-015-1373-2](https://doi.org/10.1007/s00158-015-1373-2).
- [102] M. Kleiber, J. Knabel, and J. Rojek. Response surface method for probabilistic assessment of metal forming failures. *International Journal for Numerical Methods in Engineering*, 60(1):51–67, 2004. ISSN 00295981. doi:[10.1002/nme.954](https://doi.org/10.1002/nme.954).
- [103] B. Thomsen, M. Kokkolaras, T. Måansson, and O. Isaksson. Quantitative assessment of the impact of alternative manufacturing methods on aeroengine component lifting decisions. *Journal of Mechanical Design*, 139(2), 2016. ISSN 1050-0472. doi:[10.1115/1.4034883](https://doi.org/10.1115/1.4034883).
- [104] M. A. Abramson. Mixed variable optimization of a load-bearing thermal insulation system using a filter pattern search algorithm. *Optimization and Engineering*, 5(2): 157–177, 2004. ISSN 1389-4420. doi:[10.1023/b:opte.0000033373.79886.54](https://doi.org/10.1023/b:opte.0000033373.79886.54).
- [105] M. A. Abramson, T. J. Asaki, J. E. Dennis, K. R. O'Reilly, and R. L. Pingel. Quantitative object reconstruction using abel transform X-ray tomography and mixed variable optimization. *SIAM Journal on Imaging Sciences*, 1(3):322–342, 2008. ISSN 19364954. doi:[10.1137/08071380X](https://doi.org/10.1137/08071380X).

- [106] U.S. Army Materiel Command. *Engineering design handbook: Automotive series-bodies and hulls*. 1970. ISBN 3153304432.
- [107] C. Audet, K. J. Dzahini, M. Kokkolaras, and S. Le Digabel. Stomads: Stochastic blackbox optimization using probabilistic estimates, 2019. URL <https://arxiv.org/abs/1911.01012>.